[redacted]

MARTIN MARIETTA ENERGY SYSTEMS LIBRARIES
3 4456 0352994 7

ORNL-1214
Progress
9a

AEC RESEARCH AND DEVELOPMENT REPORT

LABORATORY RECORDS
1954

PHYSICS OF SOLIDS INSTITUTE

QUARTERLY PROGRESS REPORT

FOR PERIOD ENDING OCTOBER 31, 1951

DECLASSIFIED
CLASSIFICATION CHANGED TO:
BY AUTHORITY OF: AEC-7-12-60
BY: M. Bowman 8/26/60

CENTRAL RESEARCH LIBRARY
DOCUMENT COLLECTION
LIBRARY LOAN COPY
DO NOT TRANSFER TO ANOTHER PERSON
If you wish someone else to see this document, send in name with document and the library will arrange a loan.

OAK RIDGE NATIONAL LABORATORY
OPERATED BY
CARBIDE AND CARBON CHEMICALS COMPANY
A DIVISION OF UNION CARBIDE AND CARBON CORPORATION
UCC
POST OFFICE BOX P
OAK RIDGE, TENNESSEE

[redacted]

[redacted]

ORNL-1214

This document consists of 79 pages.
Copy 9 of 149 . Series A.

Contract No. W-7405-eng-26

METALLURGY DIVISION

J. H. Frye, Jr., Director

PHYSICS OF SOLIDS INSTITUTE QUARTERLY PROGRESS REPORT

For Period Ending October 31, 1951

D. S. Billington, Acting Director

Edited by

D. S. Billington and J. T. Howe

DATE ISSUED:

JUN 11 1952

OAK RIDGE NATIONAL LABORATORY
Operated by
CARBIDE AND CARBON CHEMICALS COMPANY
A Division of Union Carbide and Carbon Corporation
Post Office Box P
Oak Ridge, Tennessee

[redacted]

MARTIN MARIETTA ENERGY SYSTEMS LIBRARIES

3 4456 0352994 7

[redacted]

[redacted]

ORNL-1214
Progress

INTERNAL DISTRIBUTION

1. G. T. Felbeck (C&CCC)
2-3. Chemistry Library
4. Physics Library
5. Biology Library
6. Health Physics Library
7. Metallurgy Library
8-9. Training School Library
10. Reactor Experimental Engineering Library
11-14. Central Files
15. C. E. Center
16. C. E. Larson
17. W. B. Humes (K-25)
18. L. B. Emlet (Y-12)
19. A. M. Weinberg
20. E. H. Taylor
21. E. J. Murphy
22. E. D. Shipley
23. D. S. Billington
24. F. C. VonderLage
25. R. C. Briant
26. J. A. Swartout
27. S. C. Lind
28. F. L. Steahly
29. A. H. Snell
30. A. Hollaender
31. M. T. Kelley
32. G. H. Clewett
33. K. Z. Morgan
34. J. S. Felton
35. A. S. Householder
36. C. S. Harrill
37. C. E. Winters
38. D. W. Cardwell
39. E. M. King
40. G. P. Keim
41. L. K. Jetter
42. E. J. Boyle
43. W. D. Manly
44. C. D. Susano
45. B. S. Borie
46. R. J. Gray
47. E. E. Stansbury
48. G. P. Smith
49. J. E. Cunningham
50. E. C. Miller
51. A. Brasunas
52. A. G. H. Andersen
53. J. O. Betterton, Jr.
54. R. B. Oliver
55. P. Patriarca
56. T. H. Blewitt
57. J. H. Crawford, Jr.
58. W. E. Taylor
59. O. Sisman
60. C. W. Keilholtz
61. J. T. Howe
62. R. H. Kernohan
63. S. E. Dismuke
64. J. C. Wilson
65. W. J. Sturm
66. M. T. Robinson
67. A. F. Cohen
68. J. W. Cleland
69. J. C. Pigg
70. M. C. Wittels
71. G. T. Murray
72. R. A. Weeks
73. W. W. Parkinson
74. C. D. Bopp

[redacted]

[redacted]

[redacted]

75. C. D. Baumann
76. J. L. Trice
77. J. G. Morgan
78. G. E. Klein
79. R. G. Berggren
80. D. K. Holmes
81. D. K. Stevens
82. A. J. Miller (Y-12)
83. R. S. Livingston (Y-12)
84. R. J. Jones (Y-12)
85. D. E. Cowen
86. R. M. Reyling
87-91. Central Files (O.P.)

EXTERNAL DISTRIBUTION

92-99. Argonne National Laboratory
100-102. Atomic Energy Commission, Washington
103-106. Brookhaven National Laboratory
107-110. Carbide and Carbon Chemicals Company (Y-12 Plant)
111-113. Knolls Atomic Power Laboratory
114-115. General Electric Company, Richland
116. Hanford Operations Office
117-120. Los Alamos
121-122. New York Operations Office
123. Patent Branch, Washington
124-138. Technical Information Service, Oak Ridge
139-142. University of California Radiation Laboratory
143. Massachusetts Institute of Technology (Kaufmann)
144. Battelle Memorial Institute
145-147. North American Aviation, Inc.
148. Westinghouse Electric Corporation
149. Savannah River Operations Office, Wilmington

[redacted]

[redacted]

[redacted]

Physics of Solids Institute quarterly progress reports previously issued in this series are as follows:

ORNL-1025	Period Ending January 31, 1951
ORNL-1095	Period Ending April 30, 1951
ORNL-1128	Period Ending July 31, 1951

[redacted]

[redacted]

[redacted]

TABLE OF CONTENTS

	PAGE
INTRODUCTION AND SUMMARY	1
BUILDING STATUS	8
Hot Cells	8
Dynamic Modulus Apparatus	8
SOLID-STATE REACTIONS	9
Bombardment of P-Type Germanium	9
Bombardment of N-Type Germanium	9
Silicon Bombardment Experiments	11
Cryostat for Pile Irradiation	11
Lithium-Iron Cyclotron Bombardment	11
RADIATION METALLURGY	13
Effect of Irradiation on Subsequent Aging of a Copper-Titanium Alloy	13
Investigation of a Beta Copper-Beryllium Alloy	13
Effect of Irradiation and Aging on the Temperature Dependence of Resistivity of a Copper-Beryllium Alloy	13
Subsequent Aging and Retrogression Phenomena in a Copper-Beryllium Alloy	15
Effect of Precipitate Nuclei on Resistivity of a Copper-Beryllium Alloy	19
Effect of Irradiation on X-Ray Structure of Copper and Alpha Brass	27
Annealing of Radiation Hardening in Copper Solid Solutions	27
Creep Under Irradiation	28
Radiation Damage to Ferromagnetic Materials	30
ENGINEERING PROPERTIES	32
LITR Liquid-Metals Loop	32
X-10 Graphite Pile Liquid-Metals Loop	35
Studies of Miscellaneous Materials	38
Physical Properties of Irradiated Plastics and Elastomers	39
Pile-Induced Radiation in Materials of Construction	45
Nuclear Heating	47
Measurement of Neutron Spectra	51

[redacted]

[redacted]

[redacted]

	PAGE
LIQUID FUELS	52
Radiation Damage to Liquid Fuels	52
CRYSTAL PHYSICS	59
Thermal Conductivity of Structural Materials	59
Thermal Conductivity of High-Purity Bismuth	60
Y-12 Cyclotron Studies	60
X-Ray Work	67

[redacted]

[redacted]

[redacted]

LIST OF FIGURES

FIGURE	TITLE	PAGE
1	Effect of Neutron Irradiation on Subsequent Aging of Copper-Titanium Alloy at 450°C	13
2	Stereographic Projection of Traces Appearing in One Grain on Two Surfaces at Right Angles	14
3	Stereographic Projection of Traces Appearing in a Beta-Quenched Copper-Beryllium Alloy Showing How the (110) Poles of a (111) Standard Projection May Be Rotated to Account for the Traces	15
4	Temperature Dependence of Resistivity of Irradiated, Aged, and Solution-Quenched Copper Alloys (2% Beryllium by Weight)	15
5	Effect of Neutron Irradiation on Subsequent Aging of Copper-Beryllium Alloy at 125°C	16
6	Effect of Neutron Irradiation on Subsequent Aging of Copper-Beryllium Alloy at 175°C	16
7	Effect of Neutron Irradiation on Subsequent Aging of Copper-Beryllium Alloys at 223 and 300°C	16
8	Effect of Neutron Irradiation on Subsequent Aging of a Copper-Beryllium Single Crystal at 300°C	17
9	Effect of Neutron Irradiation on Subsequent Aging of Copper-Beryllium Alloy at 325°C (Hardness Measurements)	17
10	Effect of Neutron Irradiation on Subsequent Aging of Copper-Beryllium Alloy at 300°C (Hardness Measurements)	17
11	Section Through the Potential Well	19
12	Graphical Interpretation of $\sum_{j}^{I_i} J_j$	25

[redacted]

[redacted]

[redacted]

FIGURE	TITLE	PAGE
13	The Graphical Solution of ξ_i and ω_i for i Odd	26
14	The Graphical Solution of ξ_i and ω_i for i Even	26
15	Radiation Hardening in Copper Alloys	27
16	Recovery Curves for Copper and Copper Alloys with 2 atom % Zinc, Gallium, Germanium, or Arsenic	28
17	Recovery Curve for Copper and Copper Alloys with 2 and 4 atom % Zinc	28
18	LITR Dynamic Stress-Corrosion Loop	32
19	Calibration of Air Extensometer	33
20	Diagram of Mockup Pumping System for LITR Corrosion and Creep Experiment	34
21	Change in Rate of Flow During Each Stroke of Mockup Sodium Pump (Without Air Relay)	35
22	Change in Rate of Flow During Each Stroke of Mockup Sodium Pump (With Air Relay)	35
23	Sodium Loop Assembly, Hole 58N	37
24	Irradiation of Plastics and Elastomers in the X-10 Graphite Pile with the Gamma Flux Increased by Cadmium	41
25	Gamma Decay of Metals (Curves 1 to 20)	44
26	Gamma Decay of Metals (Curves 21 to 27)	45
27	Gamma Decay of Metals (Curves 28 to 33)	45
28	Nuclear Heat Production Rate for Lead Irradiated in LITR.	49
29	Dynamic Calorimeter for Measuring Rates of Nuclear Heating.	50

[redacted]

[redacted]

[redacted]

FIGURE	TITLE	PAGE
30	Calibration Curves for Dynamic Calorimeter	50
31	Effect of Power Level and Temperature on Pressure of a Natural Uranyl Fluoride Salt	52
32	Effect of Power Level and Temperature on Pressure of an Enriched Uranyl Fluoride Salt	53
33	Effect of LITR Power and Temperature on Pressure of an Enriched Uranyl Fluoride Salt	54
34	Lavite Charging Boat Showing Positions of Four Capsules and Heaters	56
35	Sectioning Procedure for Microcapsule	56
36	LITR Vertical Tube Facility	57
37	LITR C-44 Test-Hole Tube and Capsule, Detail of Experiment	58
38	Capsule Container for LITR Bench Test	58
39	LITR Bench Test	58
40	Target Mounted in Special Housing	61
41	Thermocouple Accuracy Determination	62

[redacted]

[redacted]

[redacted]

LIST OF TABLES

TABLE	TITLE	PAGE
1	Rate of Change of Carrier Concentration per Incident Neutron for P-Type Germanium at -78°C	10
2	Rate of Change of Hole Concentration per Incident Neutron for P-Type Germanium at Ambient Temperature	10
3	Rate of Change of Electron Concentration per Incident Neutron for N-Type Germanium at Ambient Temperature	11
4	Metallographic Examination of Loop Sections	38
5	Properties of Elastomers and Plastics Exposed to Gamma Radiation from Au^{198}	42
6.	Physical Properties of Irradiated Elastomers	43
7	Length of Exposure of Metals Measured for Gamma Decay	46
8	Rate of Production of Heat Energy by Nuclear Bombardment of Lead in LITR	47
9	Rate of Production of Heat Energy by Nuclear Bombardment of Lead in LITR Lattice	48
10	Microcapsule History and Analysis	55
11	History of Cyclotron-Bombarded Fuel Pins	65

[redacted]

[redacted]

PHYSICS OF SOLIDS INSTITUTE QUARTERLY PROGRESS REPORT

INTRODUCTION AND SUMMARY

This report covers work performed in the Physics of Solids Institute of the Metallurgy Division for the period August 1 through October 31, 1951.

BUILDING STATUS

Hot Cells. Hot cells are complete except for some of the remotely controlled equipment. Most of the equipment parts are being made by subcontractors and will be assembled by ORNL shops. Rectilinear cells and master slave cells are now in use in spite of the shortage of remotely controlled equipment. Available equipment has been put to good use, and in many cases makeshift facilities have been utilized for work that could be performed better by equipment not yet delivered.

Dynamic Modulus Apparatus. Electrical shielding on the dynamic modulus apparatus was improved to reduce the noise level. A positioner has been developed so that the sample may be placed accurately by remote control.

SOLID-STATE REACTIONS

Bombardment of P-Type Germanium. A metal Dewar flask capable of keeping nitrogen liquid for periods up to 2½ hr outside of the pile has been constructed so that studies of conductivity vs. bombardment of germanium may now be made satisfactorily at low temperatures.

Bombardments were made of P-type germanium samples at −78°C, and the resulting ξ_{limit} was determined to lie between 0.165 and 0.137 ev, as compared with previous limits of 0.168 and 0.105 ev.

Bombardment of N-Type Germanium. An attempt was made to determine whether the initial slope of the conductivity vs. bombardment curve for N-type germanium is dependent on temperature or carrier concentration. Measurements could not be made with sufficient precision (possibly owing to inaccuracies of thermal-flux estimation) to permit a conclusion at this time.

Silicon Bombardment Experiments. The rate of hole removal in P-type silicon at about 55°C in the fast-flux region of the X-10 graphite pile was determined to be 1.90 and 1.98 per incident neutron for two samples. These values agree within the limit of reproducibility with values previously determined for N-type silicon under the same conditions.

Cryostat for Pile Irradiation. The cryostat was installed in hole 52 of the X-10 graphite pile, but vacuum difficulties in the out-of-pile section of the helium jacket are holding up operation.

Lithium-Iron Cyclotron Bombardment. No grain growth was found in the later specimens bombarded at 625°C in the Berkeley 60-in. cyclotron. Grain growth reported in earlier specimens is now believed to have been caused by pressure stresses produced in heating, whereas pressures in the later specimens were adjusted to be nearly atmospheric at running temperature.

It has been established that Globe iron in thicknesses of less than 0.008 in. is porous to lithium at temperatures above 900°C.

RADIATION METALLURGY

Effect of Irradiation on Subsequent Aging of a Copper-Titanium Alloy. Irradiation has been found to decrease the subsequent precipitation rate in a copper-titanium alloy during the early stages of aging at 450°C. This phenomenon was previously reported for temperatures at 300 and 350°C and will be studied at lower temperatures at a later date.

Investigation of a Beta Copper-Beryllium Alloy. Studies have begun on an alloy of 5% beryllium in copper cast and solution-quenched from 810°C to retain the beta phase. The surface of the coarse-grained sample contained numerous striations that could not be removed by etching and polishing and therefore are not slip lines. A stereographic projection indicates that the traces must be caused by crystallographic planes of the family (110). Several Laue back-reflection x-ray photographs were made with the beam incident on individual grains, but no back-reflection pattern could be obtained.

Effect of Irradiation and Aging on the Temperature Dependence of Resistivity of a Copper-Beryllium Alloy. Temperature vs. resistivity curves were run on a copper-beryllium specimen that had been thermally aged and on one that had been irradiated. The measurements indicate that $d\rho/dT$ increases slightly, owing to irradiation and thermal aging, but the results are not conclusive.

Subsequent Aging and Retrogression Phenomena in a Copper-Beryllium Alloy. Solution-quenched polycrystalline copper alloy (2% beryllium by weight) specimens were exposed to neutron fluxes and subsequently aged at various temperatures. Observations were made of the changes in either resistance or hardness. A retrogression occurred in the resistance vs. time curves at 175°C and above. This same phenomenon occurred in the hardness vs. time curves at 325°C but was not present at 300°C.

The resistance maximum is known to be reached earlier than the hardness maximum in the copper-beryllium alloy during aging. Geisler, in discussing the difference between the two maxima, has explained that strain effects increase resistance and depletion of the solid solution decreases resistance, whereas the hardness maximum is dependent only on strain effects. Results of retrogression experiments with irradiated samples show that this explanation is not satisfactory, but rather that resistance increases associated with precipitate nuclei are primarily caused by scattering from the nuclei and not by scattering from the strained region.

Effect of Precipitate Nuclei on the Resistivity of a Copper-Beryllium Alloy. The theoretical investigation of the effect of precipitate particles on the resistivity of a copper-beryllium alloy has been extended. Quantum mechanical methods have been used to derive an approximate expression for the electron density in and around a precipitate platelet.

Effect of Irradiation on the X-Ray Line Structure of Copper and Alpha Brass. Irradiation of powder compacts of copper and alpha brass samples to 4.5×10^{18} nvt produced no significant changes in the shape of the (311) line.

Annealing of Radiation Hardening in Copper Solid Solution. Samples of copper containing 2 and 4 at. % zinc, gallium, germanium, and arsenic, respectively, were exposed to 2.4×10^{18} nvt. Hardness measurements were

compared before and after irradiation. These measurements confirm previous reports that the hardness increase in copper and its alloys is about 20 diamond point hardness (DPH) numbers for this exposure and is insensitive to alloying. The 4% alloys of germanium and arsenic increased in hardness only by about 15½ and 12 DPH numbers, respectively.

After hardness measurements were made the samples were isothermally annealed for 15 min at various temperatures and the hardness was again measured to produce recovery curves. The recovery curves are affected by alloying in the same manner as indicated by previous studies of isothermal annealing.

Creep Under Irradiation. Since a 250-hr exposure gave a radiation-induced increase of about 20% in the total creep strain of type-347 stainless steel cantilever specimens, the test period was extended to 500 hr. One 500-hr irradiation was made at the same conditions (1500°F and 1500 psi), and final measurements will be made when the radioactivity has dropped to a safe level. Metallographic and x-ray comparisons will be made of both the irradiated sample and an unirradiated sample subjected to the same conditions of temperature and stress. A second test is being run for 500 hr at 8000 psi. The operating temperature began at 1200°F and will be raised in steps for observation of the temperature dependence of strain rate under irradiation compared with a companion bench test.

In the future, cantilever tests are planned in which (1) the flux is varied in steps so as to establish the flux dependence of creep rate and (2) the creep sample is a pure metal to eliminate phase effects that might form in stainless steel.

Since creep properties of metals are strongly dependent on temperature, an effort is being made to check calibration changes in the thermocouples being used in the creep experiments. These tests are being conducted under varied oxidizing conditions. Inpile thermocouple calibration tests are also being made.

A satisfactory furnace for bench tests of liquid-metal-filled creep specimens in tension has been built and tested. The Experimental Review Committee has tentatively approved a design for operation in a completely water-filled hole in which the water provides cooling of gamma-produced heat as well as most of the neutron and gamma shielding. The apparatus, together with handling equipment, is in the shops. Safety alarms have been designed and components have been obtained.

Radiation Damage to Ferromagnetic Materials. Observations of inpile work with microformers have been made at ORNL and WAPD which indicate that microformer output is to some extent influenced by pile power. It is possible that neutron bombardment of the microformer core causes an output change much the same as would result from a temperature change.

Preparations are being made to irradiate a microformer with a fixed core of known composition and structure, which will be shielded against electric and magnetic fields.

Inpile measurements of permeability, remanence, and coercive force will be made on a variety of possible core materials in an effort to develop a theoretical picture of the phenomena.

ENGINEERING PROPERTIES

LITR Liquid-Metals Loop. Design is near completion for the stress-corrosion and creep testing of inconel

specimens in a circulating sodium loop to be installed in the LITR. An assembly drawing of the inpile portion of the apparatus is shown. Stress is applied to the specimen by means of a dead-weight load of about 30 lb. Strain is measured by the flow of helium gas through two orifices, one fixed and the other varied according to the specimen length. The pressure in the line between the orifices will be the gaging pressure.

A mockup of the pumping system has been built and operated satisfactorily with water instead of sodium. Variations in rate of flow during a pump stroke are given both with and without an air relay in the system.

X-10 Graphite Pile Liquid-Metals Loop. The neutron flux for hole 58N of the X-10 graphite pile has been determined by measuring the gammas from cobalt foil that had been exposed in the pile while embedded in lithium in a section of tube similar to the loop material (type-316 stainless steel). The energy released at equilibrium per cubic centimeter of natural lithium through beta decay of Li^8 was calculated to be 0.76×10^9 Mev/cm^3·sec. This value represents about one-third of the energy measured from Bremsstrahlung activity, possibly explained by the fact that the chamber used was calibrated against a gamma source with too high an energy. The chamber will be calibrated with low-energy photons for better correlation.

A metallographic examination of sections of type-316 stainless steel loop made by Gray and Roche indicates little or no change in the metal that can be attributed to radiation.

Construction, calibration, and preliminary tests have been completed for an inconel loop to circulate liquid sodium at 1000°F through hole 58N.

Only one ionization chamber is needed to measure the activity of the sodium loop since the half life of sodium is relatively long and therefore no evidence of activated corrosion particles can be picked up during normal pile operation.

Studies of Miscellaneous Materials. Materials investigated were thorium, EDF gamma-shielding glass, lithium fluoride single crystals, $ZrBe_{16}$, and graphite-uranium. Properties that were measured for each of the materials included dynamic modulus of elasticity, electrical resistivity, thermal conductivity, hardness, and light transmission; x-ray studies were also made.

After a 10^6-r exposure to a Co^{60} source, EDF gamma-shielding glass turned black. Although the coloration could not be annealed out by exposure to light alone, as in the case of high-density glass, a heat treatment at 200°C did remove the coloration.

Lithium fluoride single crystals also turned black after exposure to a flux of 2×10^{18} nvt. The coloration could be removed by a 24-hr treatment at 450°C. X-ray studies have not been conclusive.

The electrical resistivity of a $ZrBe_{16}$ sample increased 10%, and the hardness increased approximately 130 DPH numbers after an exposure of 2×10^{18} nvt.

Graphite-uranium rods containing various sizes of UO_2 nodules were supplied by Battelle Memorial Institute and are being prepared for irradiation. Fission-fragment damage will be studied as a function of uranium particle size. The studies are expected to provide information that will be of use in considerations of solid material, homogeneous reactors.

Physical Properties of Irradiated Plastics and Elastomers. In order to separate the effects of gamma radiation from the effects of fast-neutron radiation, samples were encased in cadmium and irradiated in the X-10 graphite pile. The cadmium converts slow neutrons to gamma photons but has no effect on fast neutrons. A relation is derived that equates the radiation dose with and without cadmium for equal damage to the energy absorbed with and without cadmium per unit exposure.

Materials that do not follow the general formula are those that contain chlorine or fluorine and those that have a large proportion of carbon atoms of the main polymer chain attached to two branching groups.

A second method of separating gamma radiation effects from fast-neutron effects was by use of an activated Au^{198} source to produce a neutron-free gamma radiation. Beta radiation was filtered out by steel sheet placed between the gold and the sample. A comparison of calculated and experimental values for X-10 graphite pile exposure necessary to produce the same changes in properties as that caused by gamma exposure indicates again that materials mentioned in the previous paragraph are not in agreement with the formula.

Radiation effects on the properties of gasket materials have been extended to 10^{19} nvt.

Preliminary studies of elastomers and plastics irradiated in an inert atmosphere show no changes over those irradiated in air.

Tests now in progress indicate that properties of elastomers do not change appreciably with time of storage after irradiation. There is, however, a marked change in the properties of some plastics.

Other tests include the measurement of gas given off by the plastics and elastomers owing to irradiation, as well as compression-set measurements on elastomer gasket materials.

Pile-Induced Radiation in Materials of Construction. Gamma decay curves are given for numerous metals that were exposed in the X-10 graphite pile for 4700 ± 400 hr. Metals include Armco iron, Carpenter-20 steel, Duriron, various types of stainless steels, carbon steels, aluminum alloys, Hastelloys, columbium, titanium, tungsten, zirconium, K Monel, and nickel.

Nuclear Heating. In order to provide cooling design data for experiments to be placed in the LITR and develop methods of nuclear heat measurement for use in the MTR, the single-specimen-type calorimeter described in the previous quarterly report has been placed in operation in the LITR.

Heat production rates for lead were obtained in the LITR at the bottom of the northwest downbeam hole and in vertical hole C-44 within the lattice. Vertical measurements indicate that maximum heating occurs about 3 or 4 in. below the reactor center line and decreases rapidly toward the reactor top.

Measurement of Neutron Spectra. Measurements are being made in strategic locations in the LITR to determine the characteristics of bombarding neutrons. Neutron spectra above approximately 2 Mev are being obtained by use of the reactions $P^{31}(n,p)S^{31}$, $S^{32}(n,p)P^{32}$, $Al^{27}(n,p)Mg^{27}$, $Mg^{24}(n,p)Na^{24}$, and $Al^{27}(n,\alpha)Na^{24}$.

LIQUID FUELS

Radiation Damage to Liquid Fuels. Uranium salts of interest to the ANP

program are being investigated in the X-10 graphite pile and the LITR. Pressure tests were run on natural and enriched uranium salts at 1500°F under irradiation to determine whether irradiation causes a buildup of pressure. No pressure increase was detected other than that caused by rising temperature.

Experiments were conducted using microcapsules irradiated in the X-10 graphite pile at a 1.04×10^{12} flux and a temperature of 1500°F for periods of 200 to 450 hr. The salt was analyzed for decomposition and corrosion products. No evidence was found to indicate that irradiation had increased the capsule components in the salts above that of salts subjected to the same temperature conditions without irradiation. Metallographic studies of the capsules likewise showed no more corrosion than had been found in the bench-test capsules. Before experimenting with LITR corrosion tests at higher fluxes, bench runs and calculations were made to determine the amount of air cooling necessary to maintain the exterior capsule temperature at the desired value.

A sample of enriched uranium metal was irradiated at the same flux (1.04×10^{12}) and for the same length of time as the enriched uranium salt for the purpose of determining whether xenon is evolved from the liquid salt under irradiation. There is at present no indication that xenon escapes from the melt, although results are not conclusive and further experiments are felt necessary.

CRYSTAL PHYSICS

Thermal Conductivity of Structural Materials. In order to verify the large decrease in conductivity in inconel observed after approximately three days irradiation in a fuel channel in the X-10 graphite pile at 825°C, another inconel specimen was made and carefully heat treated. No change in conductivity could be observed either with or without radiation for periods up to 670 hr at 575°C, or in 135 hr at 250°C. The temperature was then raised to approximately 825°C to duplicate the first experiment. The data are not yet complete for this temperature.

Preliminary investigations of relative changes in the thermal conductivity of nickel under irradiation in the X-10 graphite pile have been conducted concurrently with the inconel studies. No changes have been observed within accuracy of measurements for 350 hr at 100°C.

An independent, absolute method of measuring thermal conductivity has been designed and tested. The specimen is made in the form of a long cylinder with an interior heater to provide radial heat flow outward. Bench tests have been completed using type-316 stainless steel, and the apparatus is now in operation in the LITR.

Thermal Conductivity of High-Purity Bismuth. A solid, cylindrical specimen of high-purity bismuth was vacuum cast, fitted with thermocouples, and surrounded by a heater. It was irradiated at 100°C in doughnut hole 1768 of the X-10 graphite pile at a flux of 1.5×10^{12} neutrons/cm^2 · sec for 390 hr. No decrease in thermal conductivity could be detected. There appears to be a slight increase in the conductivity.

Y-12 Cyclotron Studies. Proton beams of 20 to 22 Mev produced by the 86-in. cyclotron were used to bombard various liquid fuels and coolants within inconel and type-316 stainless steel containers. Energy input to

the target was calculated from measurements of water flow rate and temperature change and was compared with that obtained from the target microammeter reading. Agreement over a wide range of proton beam currents was always within 6%.

Eleven inconel fuel pins containing eutectic mixtures of fluorides of uranium, sodium, and potassium were successfully bombarded without melting the cases. Bombardment was approximately equivalent to 45 min in the ARE or about 7 min in the final aircraft reactor. These samples were compared with samples bench tested under similar conditions but without bombardment.

Depth of intergranular corrosion was not changed within ±50% by bombardment. Grain growth appeared in localized spots on the bombarded samples and was found to be dependent upon the change in radius of the fuel pin caused by flattening of the originally circular cross section and the local overheating produced when the inhomogeneous cyclotron beam was used to bombard early targets.

No difference could be found in the amount of uranium in the eutectic when comparing bench-test pins to bombarded pins. Similarly, bombardment did not appear to affect fluoride decomposition nor solubility of iron, chromium, or nickel. Chromium did, however, exhibit some dissolution in both bench and bombardment tests, whereas nickel precipitated in both cases.

A determination of the effects of radiation upon inconel and type-316 stainless steel containing potassium hydroxide has been started. Methods will be quite similar to those already discussed. A group of KOH-stainless steel targets have been bombarded at 635°C for several hours. These samples, along with their controls, await analysis.

X-Ray Work. A Philips x-ray head and a copper-target diffraction tube have been mounted on a table and will be supplied with power from the Hilger unit. They will be used with the Philips spectrometer, Laue camera, and powder cameras.

The General Electric spectrometer is being bench tested and modified for use inside the hot cell.

The x-ray program has included routine work in addition to various experimental studies of materials before and after irradiation. Studies have also been made of single crystals of irradiated copper to determine at what stress cold-work effects appear and whether lattice parameters are changed by irradiation.

BUILDING STATUS

HOT CELLS

S. E. Dismuke

Construction of rectilinear cells and master slave cells has been completed except for the installation of some of the remotely controlled equipment. Several old machines have been modified so that they can be remotely controlled fairly satisfactorily, and some of the necessary work can be performed. A lathe has been mounted in cell 4 and a milling machine in cell 5b.

Most of the parts for remotely controlled equipment have been made by subcontracting shops and shipped to ORNL for assembly. Most of the parts for the permanent lathe and milling machine, both of which are to be housed in cell 1, have been received and final installation is expected soon.

The metallographic equipment is to include a remotely operated cut-off saw, a specimen-mounting press, a polishing machine, and a metallograph. The mounting press is being made by the research shops. The polishing machine is being tested by R. J. Gray of the Metallurgy Division. Until this equipment is available for remote use, all metallographic examinations of irradiated metals will be taken to WAPD, Pittsburgh, for remote preparation and examination.

DYNAMIC MODULUS APPARATUS

R. H. Kernohan

The apparatus designed to measure Young's modulus in the hot cells was improved during the last quarter. The refinements added include better shielding to reduce the noise level, and a positioner for remotely mounting and positioning the sample to be measured.

The modulus apparatus in effect measures the resonance of fluxual vibration. The dynamic modulus of elasticity may be calculated from the resonance frequency. The rod or bar of material to be measured is vibrated at one end by means of a wire attached to an ordinary loud-speaker voice coil driven by an audio-oscillator. A string attached to a phonograph pickup detects vibrations at the other end of the rod. The leads from the pickup go to the vertical plates of a cathode-ray oscilloscope. Tests on standard material have shown good accuracy with slight dependence on methods of attachment and resonant frequency.

SOLID-STATE REACTIONS

BOMBARDMENT OF P-TYPE GERMANIUM

J. W. Cleland
J. H. Crawford, Jr.
J. C. Pigg
K. Lark-Horovitz[1]

The work reported in previous quarterly reports[2,3] on the effect of carrier concentration on the rate of change of carrier concentration per incident neutron for P-type germanium has been continued. The program has included the investigation of the slopes of conductivity vs. bombardment curves for P-type germanium single crystals, with a wide range of carrier concentrations at two temperatures (−78°C and pile ambient, which measures approximately 50°C). Experiments at the low temperature have been hampered by the lack of a suitable Dewar flask to hold solid CO_2 for periods sufficiently long to permit accurate initial slope determinations. A solution to this problem has been found by use of a metal Dewar designed and constructed by R. J. Fox of the research shops. This container will hold liquid nitrogen outside of the pile for periods up to 2½ hr. Unfortunately, because of the mass of metal involved in its construction, some of which is brass and stainless steel, it is necessary to allow a long cooling-off period between pile exposures for decay of the activity of the Dewar to a safe level.

Two judiciously chosen P-type germanium samples were exposed in the new Dewar at −78°C. These samples, whose initial hole concentrations were 3.74×10^{15} and 3.83×10^{15} cm^{-3}, showed hole concentration decreases of 0.173 and 0.238 holes per incident neutron, respectively. Previous data[2,3] showed that samples whose hole concentrations were less than 7.2×10^{14} cm^{-3} showed a decrease in conductivity on bombardment at −78°C. Thus the limiting value of hole concentration, $(n_h)_{limit}$, above which a decrease in hole concentration with bombardment is expected, lies between 7.2×10^{14} and 3.74×10^{15} cm^{-3}. The relation between $(n_h)_{limit}$ and ζ_{limit} may be written as

$$\zeta_{limit} = kT \ln \frac{2(2\pi mkT)^{3/2}}{h^3 (n_h)_{limit}}, \qquad (1)$$

from which it can be shown that ζ_{limit} lies between 0.165 and 0.137 ev. This compares favorably with the results obtained at room temperature,[3] which indicate that 0.168 ev $> \zeta_{limit} >$ 0.105 ev.

A summary of all P-type slopes is shown in Tables 1 and 2. Table 1 lists carrier concentration and initial rate of change of carrier concentration per incident neutron at −78°C, and Table 2 lists the values for bombardment at ambient temperature.

BOMBARDMENT OF N-TYPE GERMANIUM

J. W. Cleland
J. H. Crawford, Jr.
J. C. Pigg
K. Lark-Horovitz

A number of N-type germanium samples have been bombarded at pile

---

[1] Consultant from Purdue University.

[2] J. W. Cleland, K. Lark-Horovitz, J. H. Crawford, Jr., and J. C. Pigg, "Silicon Bombardment Experiments," *Physics of Solids Institute Quarterly Progress Report for Period Ending April 30, 1951*, ORNL-1095, p. 35.

[3] J. W. Cleland, J. H. Crawford, Jr., K. Lark-Horovitz, J. C. Pigg, and F. W. Young, Jr., "Bombardment of P-Type Germanium," *Physics of Solids Institute Quarterly Progress Report for Period Ending July 31, 1951*, ORNL-1128, p. 11.

TABLE 1

Rate of Change of Carrier Concentration per Incident Neutron for P-Type Germanium at -78°C

SAMPLE	n_h^0 (cm^{-3})	$\left[\frac{dn_h}{d(nvt)_{fast}}\right]_I$
1	4.9×10^{13}	0.485
2	1.9×10^{14}	0.382
3	3.9×10^{14}	0.240
4	4.60×10^{14}	0.200
5	5.40×10^{14}	0.224
6	6.52×10^{14}	0.226
7	7.20×10^{14}	+ (uncertain magnitude)
8	3.74×10^{15}	-0.173
9	3.83×10^{15}	-0.238
10	4.01×10^{16}	-0.99
11	4.69×10^{16}	-1.12
12	4.86×10^{16}	-1.03
13	7.23×10^{16}	-1.10

TABLE 2

Rate of Change of Hole Concentration per Incident Neutron for P-Type Germanium at Ambient Temperature

SAMPLE	n_h^0 (cm^{-3})	T_{exp} (°C)	$\left[\frac{dn_h}{d(nvt)_{fast}}\right]_I$
1	2.5×10^{14}	0	0.61
2	4.2×10^{14}	20	0.70
3	1.7×10^{15}	30	0.77
4	4.01×10^{16}	55	0.20
5	4.69×10^{16}	55	0.39
6	7.00×10^{17}	32	-5.0
7	1.01×10^{19}	37	-5.0
8	1.30×10^{19}	48	-2.2
9	1.50×10^{19}	48	-2.9

ambient temperature to check carefully any temperature or carrier concentration dependence of the initial slope of the conductivity vs. bombardment curve. The results of these experiments are listed in Table 3.

It is obvious from these results that the precision of measurement is not sufficiently great to permit any statement as to carrier concentration or temperature dependence of the initial rate of change of carrier concentration of N-type germanium. The lack of precision may be caused by inaccuracies in estimation of the thermal flux.

TABLE 3

Rate of Change of Electron Concentration per Incident Neutron for N-Type Germanium at Ambient Temperature

SAMPLE	n_e^0 (cm^{-3})	T_{exp} (°C)	$\left[\frac{dn_e}{d(nvt)_{fast}}\right]_I$
1	1.01×10^{16}	40	-2.24
2	1.12×10^{16}	40	-2.05
3	1.20×10^{16}	36	-2.23
4	1.22×10^{16}	40	-1.93
5	-1.24×10^{16}	63	-2.31
6	-1.58×10^{16}	40	-2.94
7	-2.02×10^{16}	36	-2.94

SILICON BOMBARDMENT EXPERIMENTS

J. W. Cleland
J. H. Crawford, Jr.
J. C. Pigg
K. Lark-Horovitz

In the last report[3] the rate of carrier removal during fast-neutron bombardment for N-type silicon was listed as 1.60 and 1.72 per incident neutron for exposure at room temperature. Two P-type silicon samples were exposed in a high fast-flux region in the X-10 graphite pile. The initial slope of the conductivity vs. bombardment curves indicates that for these samples exposed at approximately 55°C the rate of hole removal is 1.90 and 1.98 per incident neutron. The values for N- and P-type silicon are thus the same within 20%, which is about the limit of reproducibility of the experiments. These values are smaller than reported previously, but it is felt that they are more reliable than the earlier results.

CRYOSTAT FOR PILE IRRADIATION

R. P. Metcalf J. T. Howe

The cryostat has been modified to eliminate silver-to-aluminum joints on the outside helium lines of the cryostat after experiencing failure of one of the four joints. After checking for vacuum tightness the cryostat was inserted directly into the jacket already in hole 52 of the X-10 graphite pile. Outside shielding was built up and outside helium lines and vacuum jackets were installed. The cryostat has not yet gone into operation because of leaks discovered in the outer vacuum system. A satisfactory vacuum has been obtained on all inpile portions, however, so the problem resolves into one of standard vacuum technique. Operation can begin shortly after the vacuum troubles are cleared up.

LITHIUM-IRON CYCLOTRON BOMBARDMENT

North American Aviation, Inc.,
W. W. Parkinson

Postirradiation study of samples irradiated as reported in the previous

quarterly[4] has been completed. Contrary to the earlier findings, there was no grain growth in the later specimens bombarded at 625°C. It is believed that in the case of the earlier specimen the low pressure within the capsule subjected the specimen plate to stress (during heating) that caused the grain growth. For the later specimens the internal pressures were adjusted to be almost equal to atmospheric when at temperature. As in the earlier tests no other changes in the specimens that could be ascribed to the influence of irradiation were noted.

[4] North American Aviation, Inc. and W. W. Parkinson, "Lithium-Iron Cyclotron Bombardment," *op. cit.*, ORNL-1128, p. 14.

Experience with lithium leaks at temperatures above 900°C has indicated that transverse sections of less than 0.008 in. thickness from billets of Globe iron are not impervious to molten lithium. All three capsules bombarded or heated above 900°C showed evidence of lithium exuding through the specimen plate, although no visible hole could be found. Examination of the later specimens completed the study of the lithium-iron system under bombardment, and the experiments have been described in a report issued by North American Aviation, Inc.[5]

[5] W. W. Parkinson, *Stability of Iron Toward Lithium at Elevated Temperatures Under Cyclotron Irradiation* (Work done at North American Aviation, Inc. by A. Andrew, A. A. Epp, Jr., K. Imlake, R. D. Moeller, W. W. Parkinson, L. Silverman, W. J. Taylor, and K. K. Trego), NAA-SR-73 (to be published).

RADIATION METALLURGY

EFFECT OF IRRADIATION ON SUBSEQUENT AGING OF A COPPER-TITANIUM ALLOY

W. E. Taylor G. T. Murray

The investigation of the effect of irradiation on the subsequent aging of a copper alloy (2.5% titanium by weight) has been continued. It was previously reported[1] that the rate of precipitation was decreased during the early stages of aging (300 and 350°C) as a result of irradiation. This same phenomenon was experienced on aging at higher temperatures; the aging curves at 450°C are shown in Fig. 1. Experiments are now being conducted to determine the effect of irradiation on subsequent aging at lower temperatures.

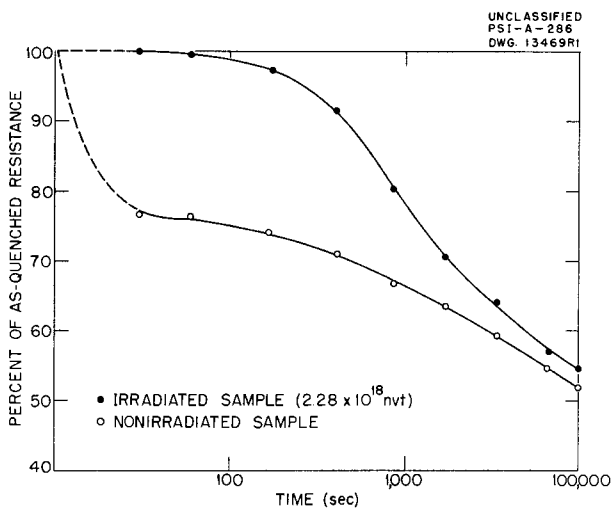

Fig. 1. Effect of Neutron Irradiation on Subsequent Aging of Copper-Titanium Alloy at 450°C.

INVESTIGATION OF A BETA COPPER-BERYLLIUM ALLOY

W. E. Taylor G. T. Murray

A copper alloy (5% beryllium by weight) was cast and solution-quenched from 810°C to retain the beta phase (body-centered cubic). Specimens for resistance and hardness measurements were prepared in the form of square bars approximately 1/8 by 1/8 by 2½ in. The following properties were observed:

$$\rho_{23°C} = 12.95\ \mu\text{ohm-cm}\ ,$$

$$\text{Hardness} = 516\ \text{DPH numbers}\ .$$

Numerous striations appeared on the surface of the specimens that were coarse grained (approximately 2½ mm). These traces could not be removed by polishing and etching and so could not be slip lines. A stereographic projection was made of the traces appearing in one grain on two surfaces at right angles. These two faces are shown in Fig. 2. The stereographic projection (Fig. 3) shows that the traces must be caused by crystallographic planes of the family (110). Since this is a possible slip plane, but an unlikely twinning plane, a Laue back-reflection x-ray photograph was made with the x-ray beam incident on this grain. The resulting film showed no spots or other evidence of a diffraction pattern using different grains. In all cases the films showed either no spots or a few badly smeared spots with pronounced streaking. Additional work is planned to determine the nature of the material.

EFFECT OF IRRADIATION AND AGING ON THE TEMPERATURE DEPENDENCE OF RESISTIVITY OF A COPPER-BERYLLIUM ALLOY

W. E. Taylor G. T. Murray
F. M. Blacksher

Earlier measurements of the effect of irradiation (nvt = 10^{18}) on $d\rho/dT$ by Kernohan[2] and May[3] have indicated that there is no change in this

(1) W. E. Taylor, G. T. Murray, and F. M. Blacksher, "Neutron Irradiation of Age Hardening Alloys," *Physics of Solids Institute Quarterly Progress Report for Period Ending July 31, 1951*, ORNL-1128, p. 20.

(2) Unpublished work done at ORNL.

(3) B. May, Masters Thesis, Purdue University (August 1950).

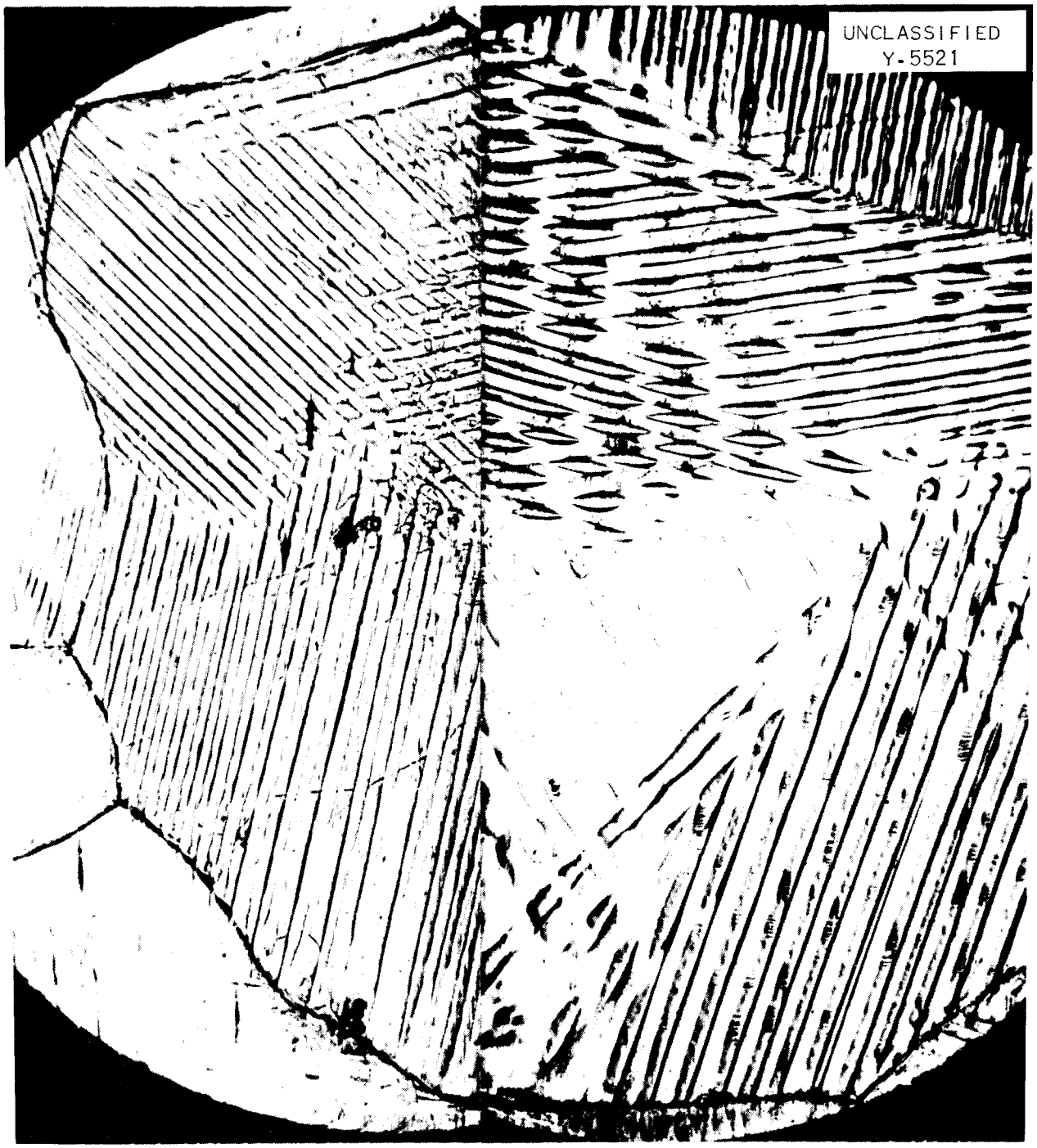

Fig. 2. Stereographic Projection of Traces Appearing in One Grain on Two Surfaces at Right Angles.

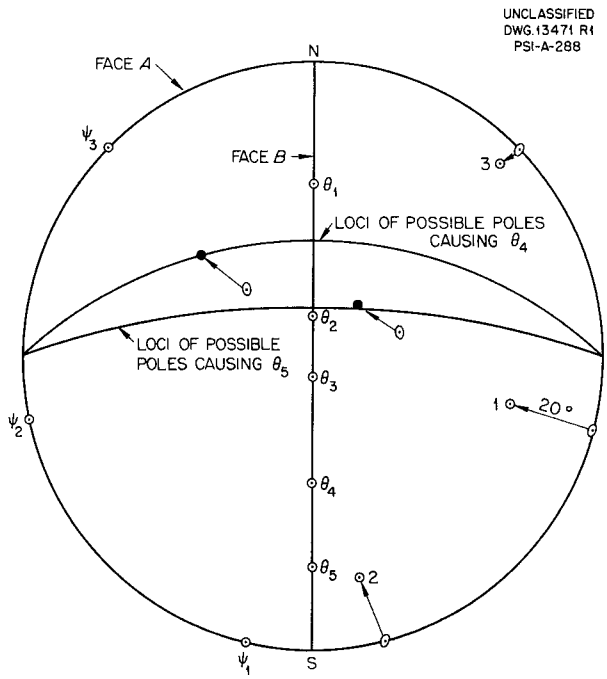

Fig. 3. Stereographic Projection of Traces Appearing in a Beta-Quenched Copper-Beryllium Alloy Showing how the (110) Poles of a (111) Standard Projection may be Rotated to Account for the Traces.

quantity as a result of irradiation. Similar measurements were made on a copper-beryllium sample (2% beryllium by weight) exposed to a much greater neutron flux (1.7×10^{19} nvt) and on a sample aged at 75°C to a condition giving nearly the same resistivity increase as the irradiated sample. The temperature-resistivity curves are shown in Fig. 4. Observed values were:

Sample XA, solution-quenched, irradiated (nvt = 1.7×10^{19}), $d\rho/dt$ = 0.01127,

Sample B3, solution-quenched, aged 4594 hr at 75°C, $d\rho/dt$ = 0.01126,

Sample H, solution-quenched, $d\rho/dt$ = 0.01080.

The samples were obtained from the same lot of material but were not

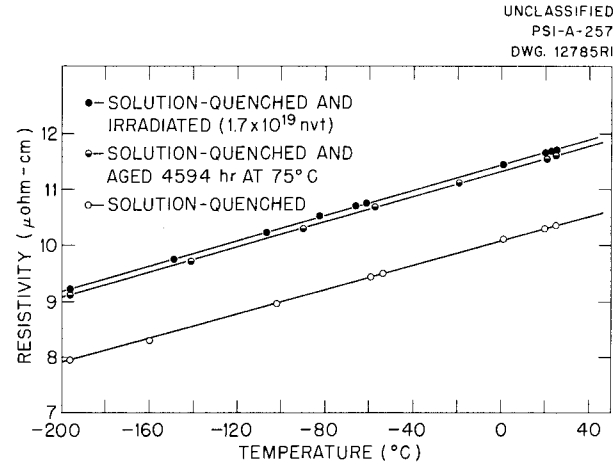

Fig. 4. Temperature Dependence of Resistivity of Irradiated, Aged, and Solution-Quenched Copper Alloys (2% Beryllium by Weight).

solution-quenched together, therefore the difference between $d\rho/dt$ for sample H and $d\rho/dt$ for samples XA and B3 may be the result of variations in the solution-quenching treatments.

The resistivity increase of sample XA as a function of prolonged irradiation is continuing. No evidence of saturation has been observed with a total fast-neutron exposure of 1.7×10^{19} nvt.

SUBSEQUENT AGING AND RETROGRESSION PHENOMENA IN A COPPER-BERYLLIUM ALLOY

W. E. Taylor G. T. Murray
F. M. Blacksher

Studies of the effect of prior neutron irradiation on the subsequent precipitation in a copper-beryllium alloy (2% beryllium by weight), as followed by electrical resistance measurements, have been reported previously.[1] Similar experiments have been completed in which hardness measurements were used to follow precipitation in polycrystalline samples, and resistance measurements were used to follow precipitation in polycrystalline and single-crystal samples.

Solution-quenched polycrystalline resistance specimens were exposed to an integrated fast-neutron flux of 1.7×10^{18} nvt. These samples were then aged with standard samples at temperatures of 125, 175, 223, and 300°C. The aging curves are shown in Figs. 5, 6, and 7. The retrogression phenomenon that was observed at 325°C in irradiated samples is also present at 300 and 223°C, and to a lesser extent at 175°C. At 125°C it does not appear to be present. The retrogression phenomenon may be accounted for by the redissolving of radiation-induced precipitate nuclei. The

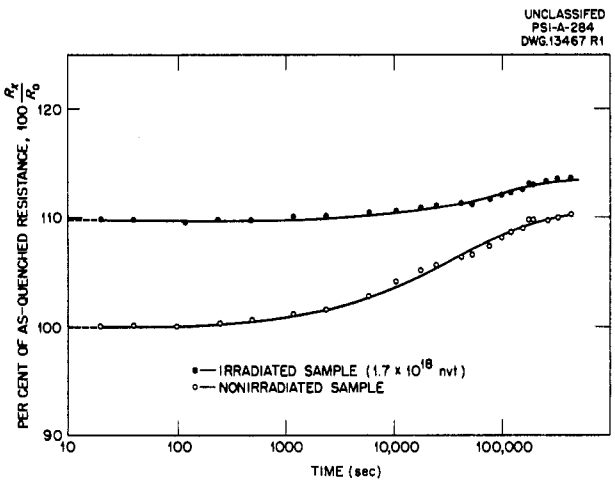

Fig. 5. Effect of Neutron Irradiation on Subsequent Aging of Copper-Beryllium Alloy at 125°C.

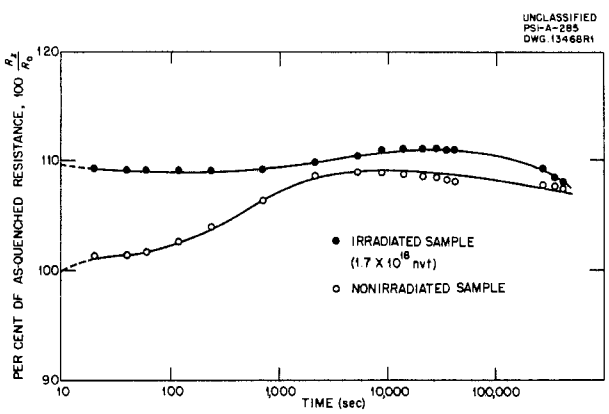

Fig. 6. Effect of Neutron Irradiation on Subsequent Aging of Copper-Beryllium Alloy at 175°C.

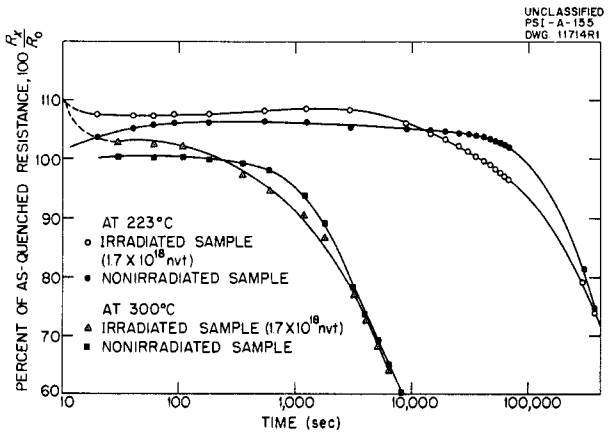

Fig. 7. Effect of Neutron Irradiation on Subsequent Aging of Copper-Beryllium Alloys at 223 and 300°C.

apparent extent of the retrogression is caused by two factors:

1. The maximum size of redissolved nuclei will increase with increasing temperature; if a range of sizes is present the retrogression will be greater as the temperature increases.

2. Nucleation and growth phenomena will occur concurrently with the retrogression and will tend to reduce the magnitude of the observed effect.

The retrogression effects observed might also be caused by the growth of the radiation-induced nuclei.

A solution-quenched single-crystal specimen of the copper-beryllium alloy was exposed to 2.5×10^{18} nvt and was subsequently aged at 300°C. The aging curves of the irradiated specimen and an unirradiated standard are shown in Fig. 8. The recovery and accelerated aging of the irradiated sample are similar to the behavior of the polycrystalline samples.

Solution-quenched polycrystalline hardness specimens were exposed to an integrated fast-neutron flux of

1.92×10^{18} nvt and were subsequently aged with unirradiated standard samples at temperatures of 300 and 325°C. The aging curves as determined by hardness measurements are shown in Figs. 9 and 10.

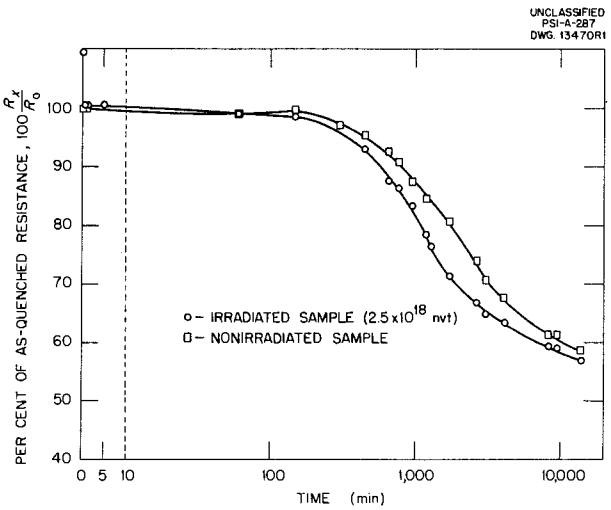

Fig. 8. Effect of Neutron Irradiation on Subsequent Aging of a Copper-Beryllium Single Crystal at 300°C.

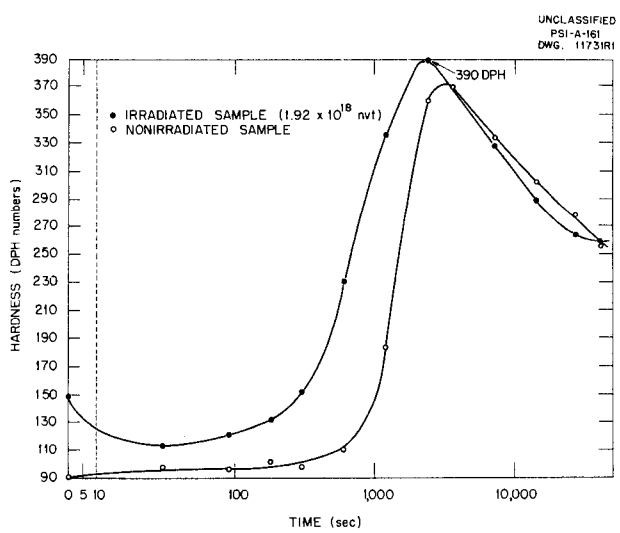

Fig. 9. Effect of Neutron Irradiation on Subsequent Aging of Copper-Beryllium Alloy at 325°C (Hardness Measurements).

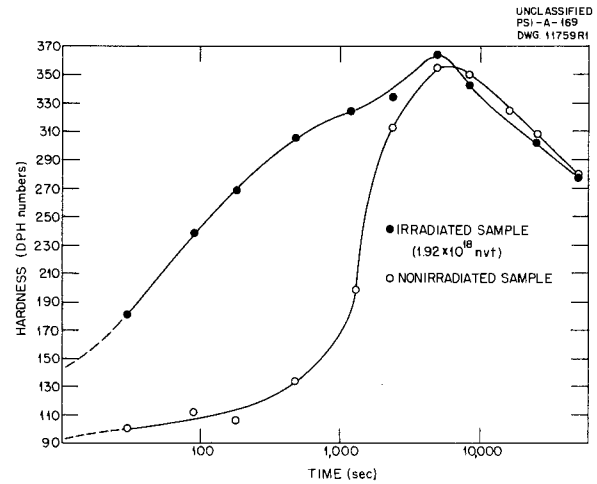

Fig. 10. Effect of Neutron Irradiation on Subsequent Aging of Copper-Beryllium Alloy at 300°C (Hardness Measurements).

At 325°C the aging curves (hardness) are similar to those obtained at slightly lower temperatures by using electrical resistance measurements. These data show that there is a rapid recovery of the radiation-induced effects (in this case a decrease of the radiation hardening effect), and that the recovery period is followed by an accelerated rate of change of hardness; at 300°C the recovery period is absent.

The recovery period may also be ascribed to the retrogression phenomenon, i.e., the redissolving of precipitate nuclei. In the case of hardness, the situation is not so well-defined as it is in the case of resistance observations. The radiation-induced hardness increase consists of two components: a hardness increase caused by the mechanism of lattice vacancies and interstitials similar to that experienced in pure copper and simple copper-base solid solutions and a hardness increase caused by the radiation-induced precipitate nuclei.

For the exposures involved the total hardness increase as a result of irradiation will be approximately equally divided between the two mechanisms. Studies[1] of annealing of radiation hardening indicate that the hardness caused by the first component may be removed quite rapidly at temperatures as high as 300°C. Therefore it could be predicted that a recovery effect of about 25 DPH numbers could occur with no retrogression phenomenon present.

When the data of Fig. 8 are examined with these considerations in mind, it may be stated that retrogression as measured by hardness appears to be completely absent at 300°C and recovery of vacancies and interstitials is more than counterbalanced by hardness increases resulting from the growth of radiation-induced nuclei. On the other hand, considerably more than half of the radiation-induced hardness was recovered at 325°C, so that retrogression had almost certainly occurred at this temperature. The appearance of retrogression between the two temperatures will occur if there is a minimum-size nucleus that is associated with hardening. Since the size of nuclei that will be redissolved increases with increasing temperature, retrogression will occur at some minimum temperature that will cause the dissolution of the limiting nuclei size. However, the hardness retrogression at 325°C cannot be attributed to growth of nuclei, since the increase in hardness at 300°C must be related to the growth of nuclei.

Observations of retrogression in irradiated specimens by measurement of electrical resistance indicate that the nuclei associated with the resistance increase are largely redissolved at 300°C, and partial recovery occurs as low as 175°C. It is well known that the resistance maximum in a copper-beryllium alloy is reached earlier during aging than the hardness maximum.[4] Geisler[5] has explained the time difference of the two maxima to be a result of a balance between strain effects (increasing resistance) and depletion of the solid solution (decreasing resistance). This depletion of the solid solution causes the resistance maximum to be reached in a shorter time than the hardness maximum, which is only related to strain effects. If the interpretation of the radiation effects (owing to precipitate nuclei) is correct, then the observed retrogression effects in irradiated samples imply that resistance increases associated with precipitate nuclei are primarily caused by scattering from the nuclei, and are not a result of scattering from the strained region. If the increases were caused by scattering from the strained region then the resistance increase should be associated with the same nuclei that cause the hardness increase, and very little or no retrogression in electrical properties should be observed at temperatures below 300°C. Therefore, in contradiction with Geisler's explanation, the resistance increase must be largely a result of scattering from the nuclei, and strong scattering must be limited to nuclei smaller than some maximum size. Additional experiments are contemplated to check the reproducibility of the retrogression phenomenon and to obtain a more complete pattern of the retrogression behavior in order to verify the above hypothesis.

---

(4) A. G. Guy, C. S. Barrett, and R. F. Mehl, "Mechanism of Precipitation in Alloys of Beryllium in Copper," *Trans. Am. Inst. Mining Met. Engrs.* **175**, 216 (1948).

(5) A. H. Geisler, "Property Changes During Aging," *Trans. Am. Inst. Mining Met. Engrs.* **180**, 230 (1949); also published in *Metals Technol.* **15**, TP-2436 (August 1948).

EFFECT OF PRECIPITATE NUCLEI ON RESISTIVITY OF A COPPER-BERYLLIUM ALLOY

W. E. Taylor D. K. Holmes

Charge Distribution of Electrons Trapped in the Potential Well. In a previous report[6] the depth of a potential well associated with a coherent platelet of copper-beryllium in a solid solution matrix has been calculated. The potential well may be considered to result from the presence of excess ionic charge and was found to have a depth of 2.39 ev (3.82×10^{-12} ergs). The excess positive ionic charge in the platelet is 0.4 positive charge per atom over the range of the platelet. In this report an expression is derived for the distribution of negative charge caused by the trapped electrons.

The electron density at any position (x, y, z) as a result of one energy level is given by two times the absolute square of the wave function associated with that level. For all levels in the potential well the electron density is given by

$$\rho(x,y,z) = 2 \sum_{ijk} |\psi_{ijk}|^2 \quad , \qquad (1)$$

where ψ is the wave function for the energy level having the quantum numbers i, j, and k and the factor 2 accounts for two electrons of opposite spin. The summation is to be carried out over all energy levels in the potential well.

Solution of the Wave Equation. The penetration of electrons into nonclassical regions of y and z (the thick dimensions of the platelet) will have a negligible effect on the electron density within the platelet except near the edges. The electron distribution in the x direction (thin dimension of platelet) will be considered in this report. If regions near the edge of the platelet are not considered, penetration into nonclassical regions of y and z may be neglected. This approximation may be achieved by assuming that the potential becomes infinite at and beyond the y and z edges of the platelet. Within the platelet there will be a finite potential that will be taken as zero. In regions of x that are outside the platelet (but within classical regions of y and z) there will be a potential V_0 (3.82×10^{-12} ergs) that allows penetration of electrons into nonclassical regions of x. Such a potential (see Fig. 11) will be given by

$$V = V(x) + V(y) + V(z) \quad , \qquad (2)$$

$$V\begin{bmatrix} y \\ z \end{bmatrix} = \infty$$

$$\text{for } \left(-\infty < \begin{matrix} y \\ z \end{matrix} < -Ra\right)\left(Ra < \begin{matrix} y \\ z \end{matrix} < \infty\right) ,$$

$$V\begin{bmatrix} y \\ z \end{bmatrix} = 0$$

$$\text{for } \left(-Ra < \begin{matrix} y \\ z \end{matrix} < Ra\right) ,$$

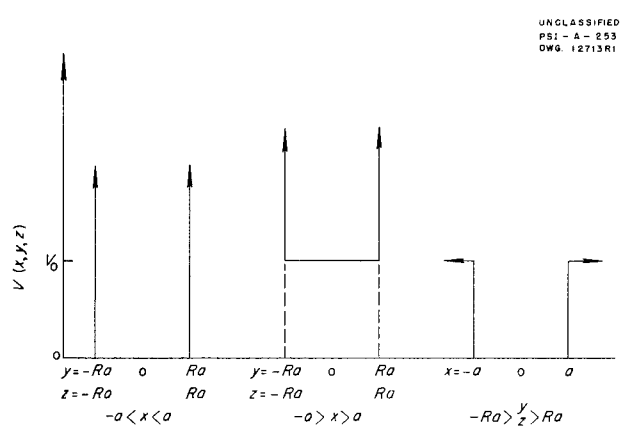

Fig. 11. Section Through the Potential Well.

[6] W. E. Taylor and J. S. Koehler, "Effect of Precipitate Particles on Resistivity of Cu-Be Alloys," *op. cit.*, ORNL-1128, p. 24.

$$V(x) = 0$$

$$\text{for } (-\infty < x < -a)(a < x < \infty) ,$$

$$V(x) = 3.82 \times 10^{-12} \text{ ergs} = V_0$$

$$\text{for } (-a > x > a) ,$$

where a is the half-thickness of the platelet and R is the ratio of width to thickness.

The wave functions ψ will consist of a set of functions that are solutions of

$$-\frac{h^2}{8\pi^2 m} \nabla^2\psi + V\psi = E\psi , \qquad (3)$$

where

h = Planck's constant,

m = mass of the electron,

E = energy, and

$$\nabla^2 = \frac{\partial^2}{\partial x^2} + \frac{\partial^2}{\partial y^2} + \frac{\partial^2}{\partial z^2} .$$

Solutions that represent bound electron states, i.e., $E < V_0$, are of interest.

Equation 3 may be separated by the substitution

$$\psi_{ijk} = X_i(x)\, Y_j(y)\, Z_k(z) , \qquad (4)$$

where $X_i(x)$ is a function of x alone, $Y_j(y)$ is a function of y alone, and $Z_k(z)$ is a function of z alone. Such a substitution results in three ordinary differential equations,

$$\frac{h^2}{8\pi^2 m} \frac{d^2Q}{dq^2} = (V_q - \eta_q^2)Q , \qquad (5)$$

where $q = x$, y, or z and Q = the corresponding function $X(x)$, $Y(y)$, or $Z(z)$ with the condition that

$$\eta_x^2 + \eta_y^2 + \eta_z^2 = E . \qquad (6)$$

Solutions for $Q = Y(y)$ or $Z(z)$ will be considered first. For these functions the quantity $(V - \eta_q)$ is

negative finite if $(-Ra < \frac{y}{z} < Ra)$,

positive infinite if $(-\infty < \frac{y}{z} < -Ra)$,

$(Ra < \frac{y}{z} < \infty)$.

The physically acceptable solutions of Eq. 5 under these conditions are

$$\left.\begin{aligned} &Q = 0 \\ &\qquad \text{for } (-\infty < \tfrac{y}{z} < -Ra) , \\ &\qquad (Ra < \tfrac{y}{z} < \infty) , \\ &Q_{j_k} = A_{j_k} \sin(\alpha_{j_k} q) - B_{j_k} \cos(\alpha_{j_k} q) \\ &\qquad \text{for } (-Ra > \tfrac{y}{k} > Ra) , \end{aligned}\right\} \qquad (7)$$

where

$$\alpha_{j_k}^{\,2} = \frac{8\pi^2 m}{h^2} (\eta_q)_{j_k}^{\,2} .$$

This solution is similar to the solution of the wave equation for a one-dimensional, square potential well. It may be shown[7] that the

[7] L. I. Schiff, *Quantum Mechanics*, McGraw-Hill, New York, 1949.

functions defined by Eq. 7 may be divided into two classes:

(*a*) one for which

$$A_{\substack{j\\k}} = 0 \text{ and } \cos\left(\alpha_{\substack{j\\k}} Ra\right) = 0,$$

(*b*) one for which

$$B_{\substack{j\\k}} = 0 \text{ and } \sin\left(\alpha_{\substack{j\\k}} Ra\right) = 0 .$$

These conditions require that

$$\alpha_j Ra = \frac{j\pi}{2} \text{ and } \alpha_k Ra = \frac{k\pi}{2} ,$$

where $\begin{bmatrix} j \\ k \end{bmatrix}$ is an odd integer for class (*a*) and an even integer for class (*b*).

Therefore

$$\left.\begin{aligned} Q_{\substack{j\\k}} &= B_{\substack{j\\k}} \cos \frac{\begin{bmatrix} j \\ k \end{bmatrix} \pi q}{2\ Ra} \\ &\text{for } \begin{bmatrix} j \\ k \end{bmatrix} \text{ odd ,} \\ Q_{\substack{j\\k}} &= A_{\substack{j\\k}} \sin \frac{\begin{bmatrix} j \\ k \end{bmatrix} \pi q}{2\ Ra} \\ &\text{for } \begin{bmatrix} j \\ k \end{bmatrix} \text{ even,} \end{aligned}\right\} \quad (8)$$

and

$$\left(\eta_q\right)_{\substack{j\\k}} = \frac{1}{2m} \frac{\begin{bmatrix} j \\ k \end{bmatrix} h^2}{4Ra} . \quad (9)$$

The constants A and B can be evaluated from the requirement that the wave function be normalized:

$$\int_{-\infty}^{\infty} Q^2 dq = 1 . \quad (10)$$

Normalizing Eq. 8 gives[8]

$$\int_0^{Ra} B_j^{\ 2} \cos^2 \left[\frac{j\pi y}{2\ Ra}\right] dy = \frac{1}{2}$$

and

$$\int_0^{Ra} A_j^{\ 2} \sin^2 \left[\frac{j\pi y}{2\ Ra}\right] dy = \frac{1}{2} .$$

Upon integrating and simplifying, it is found that

$$A_j^{\ 2} = B_j^{\ 2} = \frac{1}{Ra} . \quad (11)$$

Similarly

$$A_k^{\ 2} = B_k^{\ 2} = \frac{1}{Ra} .$$

The wave equation in $X(x)$ is

$$\frac{h^2}{8\pi^2 m} \frac{d^2X}{dx^2} = (V_x - \eta_x^{\ 2})X ,$$

where $(V_x - \eta_x^{\ 2})$ is finite negative if $(-a < x < a)$ and $(V_x - \eta_x^{\ 2})$ is finite positive (for the bound states) if $(-\infty < x < -a)$ and $(a < x < \infty)$. Again there is a one-dimensional, potential well problem. Designating solutions in the classical region (Fig. 11),

[8] Solutions for negative values of y are symmetric with those for positive values of y, so only the positive octant need be considered.

$-a < x < a$, by the subscript I and those in the nonclassical regions, $-\infty < x < -a$ and $a < x < \infty$, by the subscript II, the solutions may be written as

$$X_{Ii} = A_i \sin(\alpha_i x) + B_i \cos(\alpha_i x) \quad (12)$$

$$\text{for } (-a < x < a) ,$$

where

$$\alpha_i^2 = \frac{8\pi^2 m}{h^2} (\eta_x)_i^2 = \left[\frac{\xi_i}{a}\right]^2 , \quad (13)$$

and

$$X_{IIi} = C_i \exp(\beta_i x) + D_i \exp(-\beta_i x) \quad (14)$$

$$\text{for } (-\infty < x < -a)$$

$$(a < x < +\infty) ,$$

where

$$\beta_i^2 = \frac{8\pi^2 m}{h^2} (V_0 - \eta_x^2) = \left[\frac{\omega}{a}\right]^2 , \quad (15)$$

with the conditions that

$$X_{Ii}(\pm a) = X_{IIi}(\pm a) , \quad (16)$$

$$\left[\frac{dX_I}{dx}\right]_{\pm a} = \left[\frac{dX_{II}}{dx}\right]_{\pm a} , \quad (17)$$

$$\left.\begin{aligned} C_i &= 0 \quad \text{for} \quad (-a < x < \infty) , \\ D_i &= 0 \quad \text{for} \quad (-\infty < x < a) . \end{aligned}\right\} (18)$$

Again the solutions may be divided into two classes:

$$\left.\begin{aligned} &(a) \text{ one for which} \\ &\quad A_i = 0,\ C_i = D_i, \\ &\quad \text{and } \alpha_i \tan(\alpha_i a) = \beta_i \\ &\quad \text{for } i \text{ even;} \\ &(b) \text{ one for which} \\ &\quad B_i = 0,\ C_i = -D_i, \\ &\quad \text{and } \alpha_i \cot(\alpha_i a) = -\beta_i \\ &\quad \text{for } i \text{ odd.} \end{aligned}\right\} (19)$$

To normalize the wave function write

$$A_i^2 \int_0^a \sin^2(\alpha_i x)\, dx + D_{ai}^2 \int_a^\infty \exp(-2\beta_i x)\, dx = \frac{1}{2}$$

and

$$B_i^2 \int_0^a \cos^2(\alpha_i x)\, dx + D_{bi}^2 \int_a^\infty \exp(-2\beta_i x)\, dx = \frac{1}{2}$$

for the functions in class (a) and (b), respectively. Integration and simplification gives

$$K'\beta_i \left[\alpha_i a \pm \sin(\alpha_i a) \cos(\alpha_i a)\right] + K''\alpha_i \exp(-2\beta_i a) = \alpha_i \beta_i , \quad (20)$$

where

$$K' = A_i^2 \text{ or } B_i^2$$

and

$$K'' = D_{ai}^2 \text{ or } D_{bi}^2 \quad .$$

Condition 13 requires that

$$\left.\begin{aligned} A_i \sin(\alpha_i a) &= D_{ai} \exp(-\beta_i a) \\ &= D_{ai} \exp(-\beta_i a) \ , \\ B_i \cos(\alpha_i a) &= D_{bi} \exp(-\beta_i a). \end{aligned}\right\} \quad (21)$$

Condition 17 is satisfied by Eq. 21,[1] together with the relation between α_i and β_i given in Eq. 19.

Making the substitutions $\xi_i = \alpha_i a$ and $\omega_i = \beta_i a$ and using the relations between ξ and ω from Eq. 19, Eqs. 20 and 21 can be solved simultaneously for A, B, and D in terms of the parameters ξ and ω with the following result:

$$A_i^2 = \frac{1}{a}\left[\frac{\omega_i}{\omega_i + 1}\right]$$

for i even, (22a)

$$B_i^2 = \frac{1}{a}\left[\frac{\omega_i}{\omega_i + 1}\right]$$

for i odd, (22b)

$$D_{ai}^2 = A_i^2 \sin^2 \xi_i \exp(2\omega_i)$$

for i even, (22c)

$$D_{bi}^2 = B_i^2 \cos^2 \xi_i \exp(2\omega_i)$$

for i odd. (22d)

General Expression for Electron Density in the x Direction. The summation of Eq. 1, which will be written in the following form, can now be considered:

$$\rho(x,y,z) = 2 \sum_{ijk} X_i^2 Y_j^2 Z_k^2 \ .$$

Within the classical region of q the planes $q = 0$ are nodal planes for the functions Q_i, i.e.,

$$Q_{ia}^2 = 0$$

and

$$Q_{ib}^2 = B_{iq}^2 \quad ,$$

since at this plane $\sin(\alpha_{iq})$ and $\cos(\alpha_{iq})$ are 0 and 1, respectively. Moreover the electron density will be very nearly independent of y and z if regions near the y and z edges of the well are not considered. It will therefore be written as an approximation that

$$\rho(x,y,z) \cong \rho(x,0,0)$$

for $(0 < x < \infty)$

$(0 < \frac{y}{z} < Ra)$

and hence

$$\rho(x,y,z) \cong 2 \sum_{i}^{\nu} X_i^2 \sum_{j}^{I_i} B_j^2 \sum_{k}^{J_j} B_k^2 \quad (23)$$

for j and k odd

$(-Ra < \frac{y}{z} < Ra)$,

where

$$B_j^2 = B_k^2 = \frac{1}{Ra}$$

for all j and k .

It may therefore be written that

$$\rho(x,y,z) = \frac{1}{(Ra)^2} \sum_i^{\nu} X_i \sum_j^{I_i} 1 \sum_k^{J_j} 1 \qquad (24)$$

for j odd, $k = 1, 2, 3, \ldots$.

But

$$\sum_k^{J_j} 1 = J_j ,$$

hence

$$\rho(x,y,z) \cong \frac{1}{(Ra)^2} \sum_i^{\nu} X_i^2 \sum_j^{I_i} J_j \qquad (25)$$

for j odd .

Now J_j is the largest value that k can have for any given i or j. Upon substituting Eq. 9 in Eq. 6 and solving for k_{max} it is found that

$$J_j = \left[2m \left(\frac{4\ Ra}{h}\right)^2 (V_0 - \eta_x^2) - j^2 \right]^{1/2} ,$$

so that Eq. 25 becomes

$$\rho(x,y,z) = \frac{1}{(Ra)^2} \sum_i^{\nu} X_i^2 \sum_j^{I_i} \left[2m \left(\frac{4Ra}{h}\right)^2 (V_0 - \eta_x^2) - j^2 \right]^{1/2} \quad \text{for } j \text{ odd.} \qquad (26)$$

The summation over j may be written as

$$\sigma = \sum_j^{I_i} (c^2 - j^2)^{1/2} , \qquad (27)$$

where

$$c^2 = 2m \left(\frac{4\ Ra}{h}\right)^2 (V_0 - \eta_x^2) .$$

From Eq. 27 it is apparent that σ is the sum of a sequence of lines extending from $\sigma = 0$ to points along the circle

$$\sigma^2 = c^2 - j^2 ,$$

as shown in Fig. 12. Thus

$$\sigma = a + b + c + \ldots + m$$

with the limiting terms $m = 0$ when $j = I_i \cong c$. If the lines are so spaced along the j axis as to be unit distances apart, then σ is approximately equal to the area under the circle between $j = 0$ and $j = c$. Since the lines are spaced at two unit distances, the approximation is nearly achieved by dividing the total area by two.

Therefore

$$\sigma = \frac{1}{2} \int_0^c (c^2 - j^2)^{1/2}\, dj ,$$

$$\sigma = \frac{\pi}{8} c^2 = \frac{\pi}{8} 2m \left(\frac{4\ Ra}{h}\right)^2 (V - \eta_x^2) ,$$

or

$$\sigma = \pi m \left[\frac{2Ra}{h}\right]^2 (V_0 - \eta_x{}^2) ,$$

and Eq. 1 becomes

$$\rho(x,y,z) \cong \frac{4\pi m}{h^2} \sum_i^{\nu} (V_0 - \eta_x{}^2) X_i{}^2$$

$$\text{for } (-Ra < \begin{matrix} y \\ z \end{matrix} < Ra) ,$$

where η_x is dependent on the i's. Substituting from Eq. 15 and simplifying,

UNCLASSIFIED
PSI-A-254
DWG. 12714R1

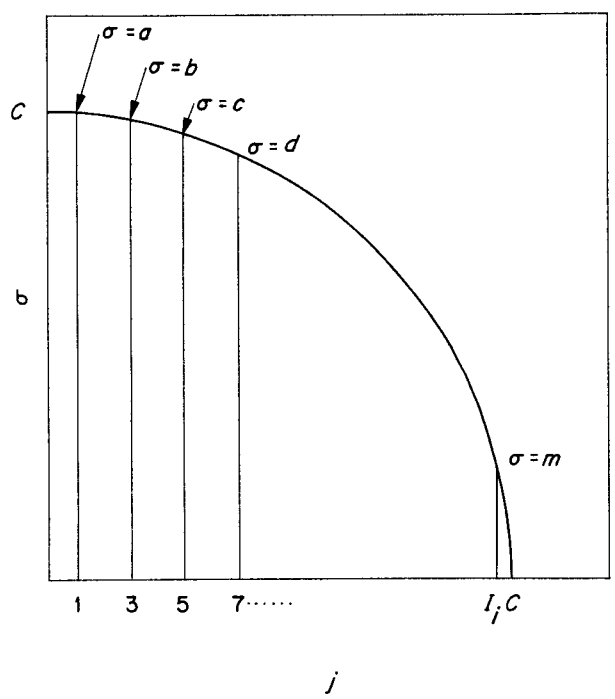

Fig. 12. Graphical Interpretation $\sum_j^{I_i} J_j$.

$$\rho(x,y,z) \cong \frac{1}{2\pi a^2} \sum_i^{\nu} \omega_i{}^2 X_i{}^2 \qquad (28)$$

$$\text{for } (-Ra < \begin{matrix} y \\ z \end{matrix} < Ra) .$$

The ξ's and ω's may be determined from Eqs. 13, 15, and 19. Combining Eqs. 13 and 15 it is found that

$$\alpha_i{}^2 + \beta_i{}^2 = \frac{8\pi^2 m}{h^2} V_0 ,$$

which, on making the substitutions

$$\left.\begin{aligned} \xi_i &= \alpha_i a \\ \text{and} \quad \omega_i &= \beta_i a , \end{aligned}\right\} \qquad (29)$$

becomes

$$\xi_i{}^2 + \omega_i{}^2 = \frac{8\pi^2 m}{h^2} V_0 a^2 . \qquad (30)$$

The same substitution in Eq. 19 leads to

$$\xi_i \tan \xi_i = \omega_i \qquad \text{for } i \text{ even,} \qquad (31a)$$

and

$$\xi_i \cot \xi_i = -\omega_i \qquad \text{for } i \text{ odd.} \qquad (31b)$$

Simultaneous solution of Eqs. 30 and 31a gives the desired values of ξ_i and ω_i for X functions of class a. Similarly the solutions of Eqs. 30 and 31b lead to values of ξ_i and ω_i for X functions of class b. Graphical solutions are shown in Figs. 13 and 14.

Substitution of Eqs. 12 and 13 for X_i in Eq. 28 leads to

$$\left.\begin{aligned} \rho_i &\cong \frac{1}{2\pi a^2}\left[\frac{\omega^3}{\omega_i + 1}\right] \cos^2\left[\xi_i \frac{x}{a}\right] \quad \text{for } i \text{ odd} \\ &\text{and} \\ \rho_i &\cong \frac{1}{2\pi a^2}\left[\frac{\omega_i^{\,3}}{\omega_i + 1}\right] \sin^2\left[\xi_i \frac{x}{a}\right] \quad \text{for } i \text{ even} \end{aligned}\right\} \quad (32)$$

for the classical region $(-a < x < a)$, and

$$\left.\begin{aligned} \rho_i &\cong \frac{1}{2\pi a^2}\left[\frac{\omega_i^{\,3}}{\omega_i + 1}\right] \cos^2 \xi_i \exp 2\omega_i \left[1 - \frac{x}{a}\right] \quad \text{for } i \text{ odd} \\ &\text{and} \\ \rho_i &\cong \frac{1}{2\pi a^2}\left[\frac{\omega_i^{\,3}}{\omega_i + 1}\right] \sin^2 \xi \exp 2\omega_i \left[1 - \frac{x}{a}\right] \quad \text{for } i \text{ even} \end{aligned}\right\} \quad (33)$$

for the nonclassical region

$$-\infty < x < -a$$

and

$$a < x < \infty .$$

Equations 32 and 33 have validity only in the region

$$-Ra < \begin{matrix} y \\ z \end{matrix} < Ra .$$

Finally,

$$\rho(x,y,z) \cong \sum_i^{\nu} \rho_i . \quad (34)$$

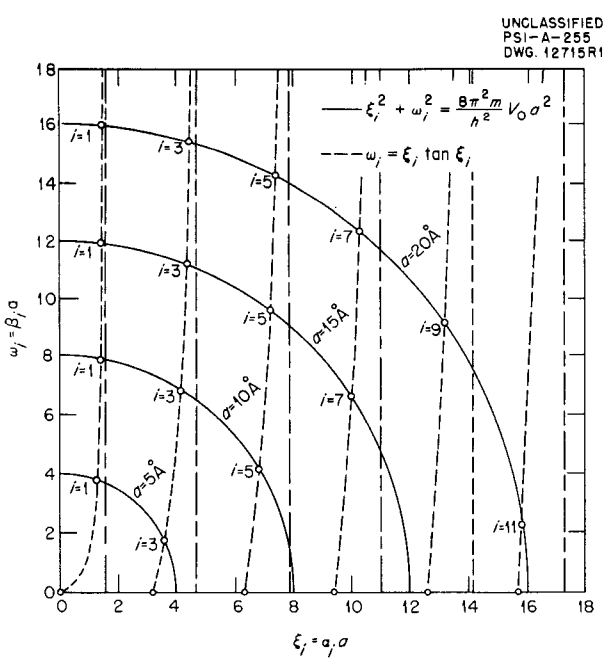

Fig. 13. The Graphical Solution of ξ_i and ω_i for i Odd.

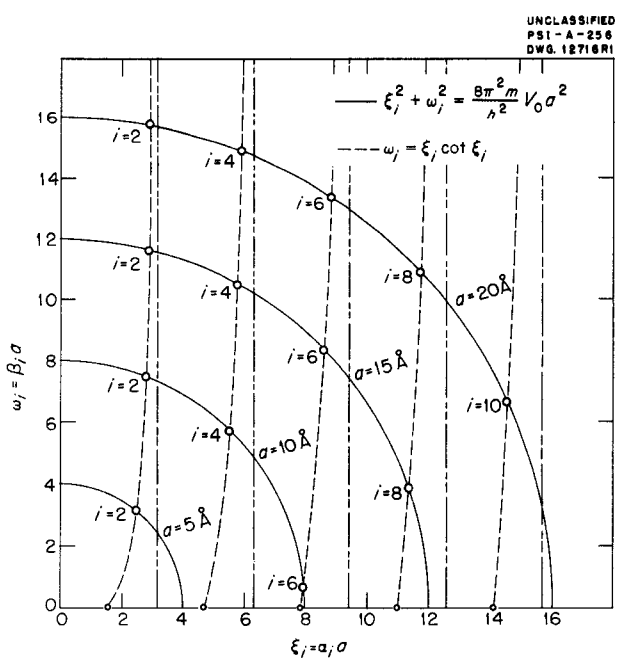

Fig. 14. The Graphical Solution of ξ_i and ω_i for i Even.

Equations 32, 33, and 34 are being evaluated in order to estimate the scattering potential due to the platelet.

EFFECT OF IRRADIATION ON X-RAY STRUCTURE OF COPPER AND ALPHA BRASS

W. E. Taylor G. T. Murray
F. M. Blacksher

Annealed powder compacts of copper and alpha brass (11.35% zinc) and a cold-worked powder compact of alpha brass were exposed to an integrated fast-neutron flux of 4.5×10^{18} neutrons per square centimeter. The shape of the (311) line was studied with the Philips high-angle spectrometer before and after irradiation. No significant differences were found.

ANNEALING OF RADIATION HARDENING IN COPPER SOLID SOLUTIONS

W. E. Taylor G. T. Murray
F. M. Blacksher

Previous observations[9] of isothermal annealing of radiation hardening in alloys of copper containing 2 and 4 at.% of zinc, gallium, germanium, or arsenic indicated that the alloys recovered more easily than pure copper. The rate of recovery increased with increasing alloy content and with increasing atomic number of the alloying element. This work has been extended by annealing irradiated samples at various temperatures for a fixed time duration (15 min) in order to obtain a recovery curve.

Samples were exposed to 1.5×10^{18} nvt. Hardness measurements before and after irradiation are compared in Fig. 15. The hardness increases observed confirm previous observations[4] that for exposures to 1.5×10^{18} nvt the hardness increase in copper and its alloys is about 20 DPH numbers and is insensitive to alloying with the exception of some anomalies in the case of 4% germanium and arsenic alloys.

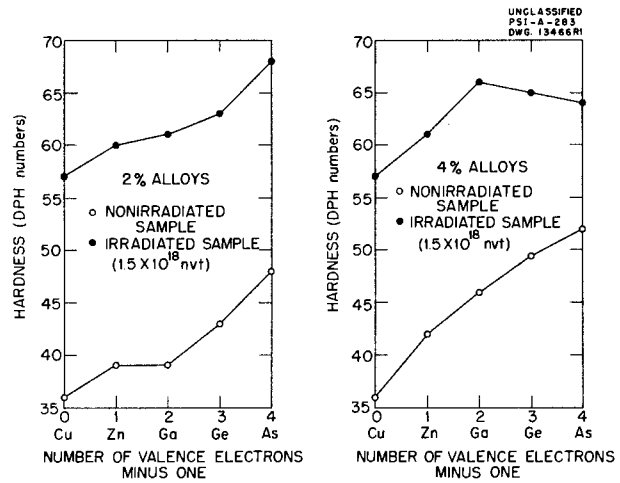

Fig. 15. Radiation Hardening in Copper Alloys.

These samples were then annealed at 150, 175, 200, 250, 300, and 350°C for 15 min, with a different sample being used at each temperature. Hardness measurements after annealing yielded the recovery curves shown in Fig. 16. The effect of alloying on the recovery curves is in agreement with the previous results of isothermal annealing. Similar curves were obtained for 4% alloys with the recovery temperature displaced to lower values. Figure 17 compares the recovery curves of copper with 2 and 4 at.% zinc alloys. Similar curves were obtained from gallium, but the anomalies in the radiation hardening of germanium and arsenic alloys render such a comparison meaningless.

[9] W. E. Taylor, G. T. Murray, and F. M. Blacksher, "Recovery of Radiation Hardening in Copper-Base Solid-Solution Alloys," *op. cit.*, ORNL-1128, p. 28.

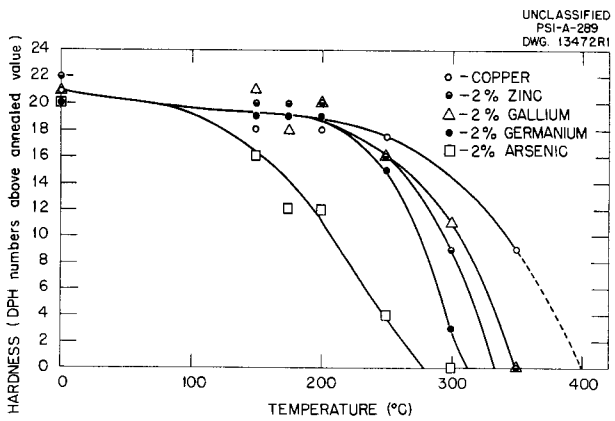

Fig. 16. Recovery Curves for Copper and Copper Alloys with 2 atom % Zinc, Gallium, Germanium, or Arsenic.

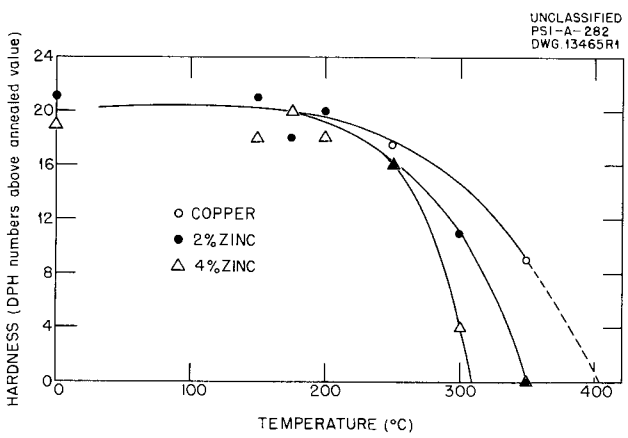

Fig. 17. Recovery Curve for Copper and Copper Alloys with 2 and 4 atom % Zinc.

CREEP UNDER IRRADIATION

J. C. Wilson J. C. Zukas
W. W. Davis

Only two inpile cantilever creep tests were completed this quarter, owing to a series of furnace burnouts, the extended duration of the tests, and sharing of the hole facility with other experimenters. The cause of the burnouts has not yet been determined, but subsequent tests have been run in which no such difficulties occurred.

Work during the last quarter[10] showed that pile radiation caused an increase in total creep strain of about 20% in type-347 stainless steel after about 250 hr of exposure, which was the duration of the tests. Furthermore, extrapolation of the bench and inpile curves to longer times indicated that the difference between them increased with time. The first of the current tests should confirm the above observations. The time has been extended to 500 hr under the same conditions (1500°F and 1500 psi), but because the expected beam deflection would exceed the range of the microformer, the transducer has been omitted and fiducial marks on the loading beam and base plate will permit measurement of the total extension after the experiment has been withdrawn from the reactor. The deflection will then be compared with that observed in a bench test at the same temperature and stress levels. The irradiation has been completed and the activity of the apparatus will be permitted to drop to a safe level for handling. Metallographic and x-ray comparison of bench and irradiated samples will be made.

The second test is still in the pile. It was stressed to 8000 psi and for its first 500 hr has been operating at 1200°F. The temperature of this test will be subsequently raised in steps to observe the temperature dependence of strain rate under irradiation for comparison with a companion bench test.

The next scheduled test will be moved into the pile in steps during the time of the test to try to establish the flux dependence of the creep rate. Movement of the apparatus during a test has been found to result in only very small perturbations in

[10] Figure 3.11, *op. cit.*, ORNL-1128, p. 30.

the creep curve. Subsequent tests at 1600°F will be made as soon as a sufficiently reliable furnace for this temperature can be built. Some creep tests under irradiation are also planned in which a pure metal sample will be used to eliminate effects of the several phases that might form in type-347 stainless steel. Consequently some pure nickel creep specimens have been machined, but the grain structure has not proved stable over a 500-hr period at 1500 or 1600°F, therefore further annealing tests are being run at lower temperatures. A facility for operating four cantilever bench tests is complete except for some electrical wiring.

Phase stability tests on type-347 stainless steel from the creep specimen material are still awaiting metallography. A set of inconel specimens has been run for periods up to 500 hr at 1400, 1500, and 1600°F to assess the structural stability of this metal.

The great temperature sensitivity of creep properties of metals of interest to the ANP program at the anticipated operating temperatures (1500°F and higher) and the relatively small effects of neutron bombardment so far observed emphasize the need for precise knowledge of test temperatures. Changes of calibration of 22-gage chromel-alumel couples after 500 hr at 1500°F have been reported.[11] The same paper shows that the smaller the thermocouple wire size, the greater the expected change in calibration. Since space and induced-activity considerations limit the size of wire for inpile work, No. 30 wire, which is used in these experiments, should show even greater departures than No. 22. Accordingly a set of four chromel-alumel couples was welded to a piece of stainless steel and exposed for a three-week period in the calibrating furnace in the Instrument Department. A National Bureau of Standards calibrated platinum, platinum-rhodium thermocouple was used as a standard. The results have not been completely analyzed but there is no monotonic change in calibration as had been expected, and the errors are apparently less than the accuracy of measurement (about ±2°F). Two other sets of couples have been prepared for exposure under two different degrees of oxidizing conditions for tests of 1000 hr or longer.

To confirm earlier inpile thermocouple calibration carried out by checking the melting point of aluminum,[12] a more refined apparatus was built and is now being bench tested. Improved instrumentation will permit recording of the cooling curves on suppressed zero recorders. A duplicate unit will then be irradiated. A companion unit for use with silver or copper has been designed for thermocouple calibration at their respective melting points.

A satisfactory furnace for bench tests of hollow creep specimens in tension has been built and tested at temperatures up to 1700°F. A set of six specimens has been filled with sodium, and after radiography to check the fill, they will be leak tested at 1500°F. A sulfur cast method for determining the internal diameter of the tubular specimens has been devised. Results are reproducible to ±0.0002 inch. Microformers (Schaevitz type-0100) have been received for the extensometer. A pair of microformers

(11) A. I. Dahl, *Stability of Base-Metal Thermocouples in Air from 800 to 2200°F*, National Bureau of Standards Research Paper RP1278 (1940).

(12) J. C. Wilson, M. J. Feldman, J. C. Zukas, and W. W. Davis, "Creep Under Irradiation," *Physics of Solids Institute Quarterly Progress Report for Period Ending January 31, 1951*, ORNL-1025, p. 44.

with outputs in series will be attached to the gage length through push rods, and a similar pair with primaries and secondaries in parallel will be attached to the supermicrometer used as a measuring instrument. With this scheme of interconnections 0.0001 in. on the micrometer will correspond to a specimen extension of 25 microinches (0.000025 in.). It has been found possible to incorporate a heater inside the tensile specimens so that the effects of gamma heating in the pile can be simulated and the performance of several proportioning controllers can be evaluated for use in the LITR and MTR. A number of low spring-rate stainless steel bellows has been ordered to serve as end seals on the inpile rigs if dead-weight loading is used, or alternatively, internal gas pressure in the apparatus acting on the bellows may provide sufficient force for stressing.

The Experimental Review Committee has tentatively approved a design for a completely water-filled hole facility in which the water cools the experiment as well as provides the bulk of the neutron and gamma shielding. The inpile end of the facility, experimental cans, a handling tool for insertion and withdrawal, and withdrawal shields for the experimental apparatus are in the shop. Instrumentation for safety devices such as low-flow alarm and experimental-can leakage alarm has been designed and the components have been procured.

Testing of several types of extensometers still awaits return of the Templin calibrator from the National Bureau of Standards. An orifice-type gas flow extensometer has been tested at 1200°F, and calculations indicate that 1500°F operation will reduce the usable range only slightly. A small microformer (Schaevitz type-0100) has been stripped of all unnecessary insulation and protection for heat dissipation and cooling studies to determine whether it may be possible to use the commercial unit in the MTR. A light-weight cobalt core microformer for high temperature use was built and tested. The sensitivity (15 μin./μv) is inadequate at 60 cycles, but operation at higher frequencies may improve this figure.

RADIATION DAMAGE TO FERROMAGNETIC MATERIALS

R. A. Weeks

In a previous report[13] Wilson *et al.* reported some observations of the output of a microformer used in creep tests in the X-10 graphite pile. It was noted that the output of the microformer was dependent upon pile power and that change in pile power was reflected by a small change in microformer output. A similar observation of the behavior of a microformer in a pile is reported in WAPD-MR-21.[14] In this report, change in microformer output with temperature is compared with change in output when the microformer was in the pile. The observed change in temperature of the microformer in the pile is not sufficient to account for the change in output observed. It would seem that the effect is a result of neutron bombardment of the microformer. In view of this observation it was thought that a more accurate measurement of the relationship of pile power to microformer output would be of interest. It is probable that the neutron bombardment of the core of the microformer is the cause of the change in output.

---

[13] J. C. Wilson, J. C. Zukas, and W. W. Davis, "Creep Under Irradiation," *Physics of Solids Institute Quarterly Progress Report for Period Ending April 30, 1951*, ORNL-1095, p. 46.

[14] Westinghouse Atomic Power Division, *Monthly Technical Progress Report; Naval Reactor Program; for the Month of September 1951*, WAPD-MR-21 (Modified).

This change then reflects the effect of neutron bombardment on the magnetic properties of the core material. If this is the case then it is probable that the effect of the neutrons on the core is analogous to that of temperature.

Preparations are now under way to place a microformer in the pile with a fixed core of known composition and structure. The microformer will be carefully shielded against stray electric and magnetic fields. The output of the inpile microformer will be balanced out in amplitude and phase when the pile is off. Then any change in microformer output as a function of pile power will be measured from a null position. By placing cores of different materials in the inpile rig a comparative measurement of the magnitude of the effect of neutron bombardment on the cores can be made. After these measurements, samples of a variety of materials will be procured and studied under inpile conditions. Measurements of permeability, remanence, and coercive force will be made. From these measurements it should be possible to develop a theoretical picture of the phenomena.

ENGINEERING PROPERTIES

LITR LIQUID-METALS LOOP

A. S. Olson W. W. Parkinson
W. E. Brundage O. Sisman

Design of the equipment for stress-corrosion and creep testing of inconel in a sodium-circulating loop at 1500°F in the LITR is nearing completion. Complete assembly drawings have been made and the detailed drawings are about half finished. Fabrication in the research shops has been started and instrument design for this equipment is in progress. Two creep specimens have been machined from solid bars of inconel in the research shops. They each have a length of 5 7/16 in., an internal diameter of 0.241 in., and a wall thickness of 0.025 inch.

Figure 18 shows part of the equipment - namely, the sodium loop including a creep specimen, the sodium pump, and the extensometer. Sodium at 1500°F is pumped at about 10 ft/sec from the two tanks through the check valves and then through the inconel tubing and creep specimen. The flow is only in one direction through the tubing and specimen.

The inconel loop is heated by means of an enclosing heater unit with a maximum power rating of 5 kw. Another heating unit, located in the center of the sodium tank assembly, provides an additional 2 kw (maximum). All equipment containing sodium and both heating units are enclosed in a stainless steel shell and operate in an atmosphere of helium. The shell, in turn, is enclosed in a vacuum envelope that aids in reducing heat losses and provides a means of detecting possible sodium leaks. An aluminum jacket also surrounds the equipment and water provides the necessary cooling so that the outside temperature of the water jacket will not exceed 180°F.

A gas-operated extensometer, mounted parallel to the creep specimen,

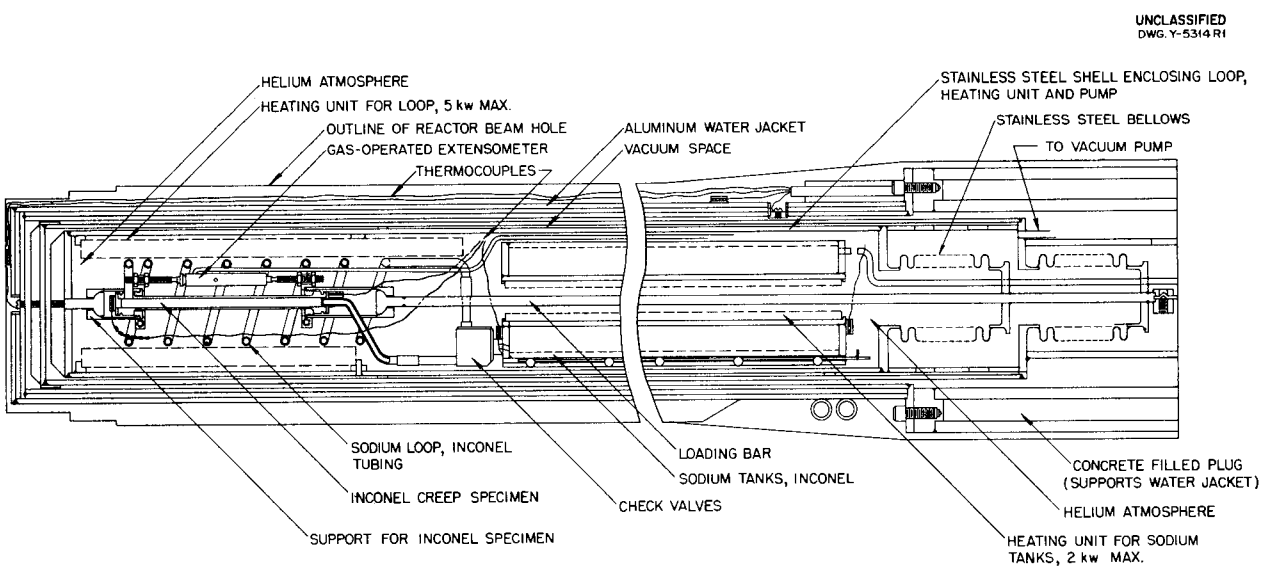

Fig. 18. LITR Dynamic Stress-Corrosion Loop.

measures the extension of the specimen under a stress of approximately 1500 psi. The load is applied by a bar that extends through the center of the sodium tanks. A stainless steel cable attached to one end of the loading bar passes through the internal shielding plug to the outside of the reactor. A 30-lb load applied to the outside end of the cable provides the necessary stress in the creep specimen.

Measurement of extension of the test specimen requires an instrument with a sensitivity of 0.0001 in. through a range of 0.010 inch. The extensometer must operate satisfactorily at temperatures up to 1500°F. Since there is a minimum of space available for the extensometer, there must be a minimum amount of connecting network. These requirements indicate that a pneumatic type of gage would be the best to use. The helium gas from the extensometer can be exhausted directly into the region around the test specimen to provide the necessary inert atmosphere. The pressure in this region is maintained slightly positive by a regulator on the exhaust tube from the equipment.

Several types of pneumatic gages were tried. The one that seemed best suited for this application has a needle-type variable orifice. The inlet gas is regulated to about 15 psi and fed through a nonvariable orifice. The variable orifice is fixed on the specimen and is in series with the nonvariable orifice. The pressure in the line between the orifices is the gaging pressure. The size of the first orifice largely determines the characteristics of the extension-pressure relationship. Figure 19 shows the effect of two different first orifices with other conditions remaining the same. It can be seen from Fig. 19 that a smaller orifice for the first part of the run permits a shorter range, higher sensitivity instrument to be used than is possible with a larger orifice. Since the first orifice is outside the equipment, it is easy to change the smaller orifice when its usable range has been exceeded.

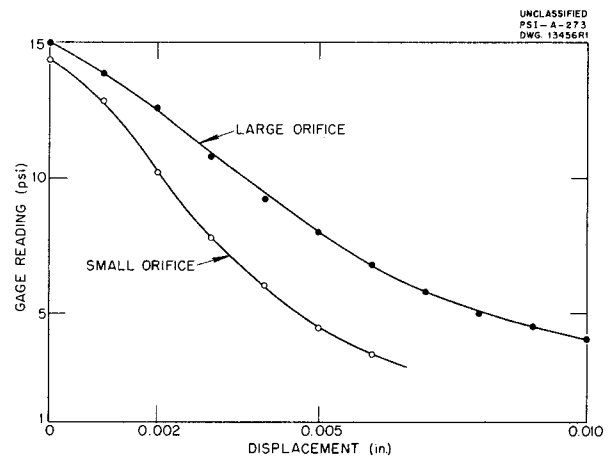

Fig. 19. Calibration of Air Extensometer.

An inconel extensometer for high temperature tests and calibration in the sodium loop is now being constructed. Calibrations will be made under operating conditions at the required back pressure at various temperatures, since it is not possible to predict accurately the temperature of the extensometer owing to the cooling effect of the gas flow through it.

A mockup of the sodium pump, using water in place of molten sodium, has been constructed to test its operating characteristics. The system, shown in Fig. 20, simulates the operation of the pump to be used for moving sodium at 1500°F through an inconel loop. This pump provides a pulsating flow that is unidirectional through the loop (represented in the mockup system by the flowmeter, *K*, and connecting rubber tubing). The pumping action is obtained by the use of four glass

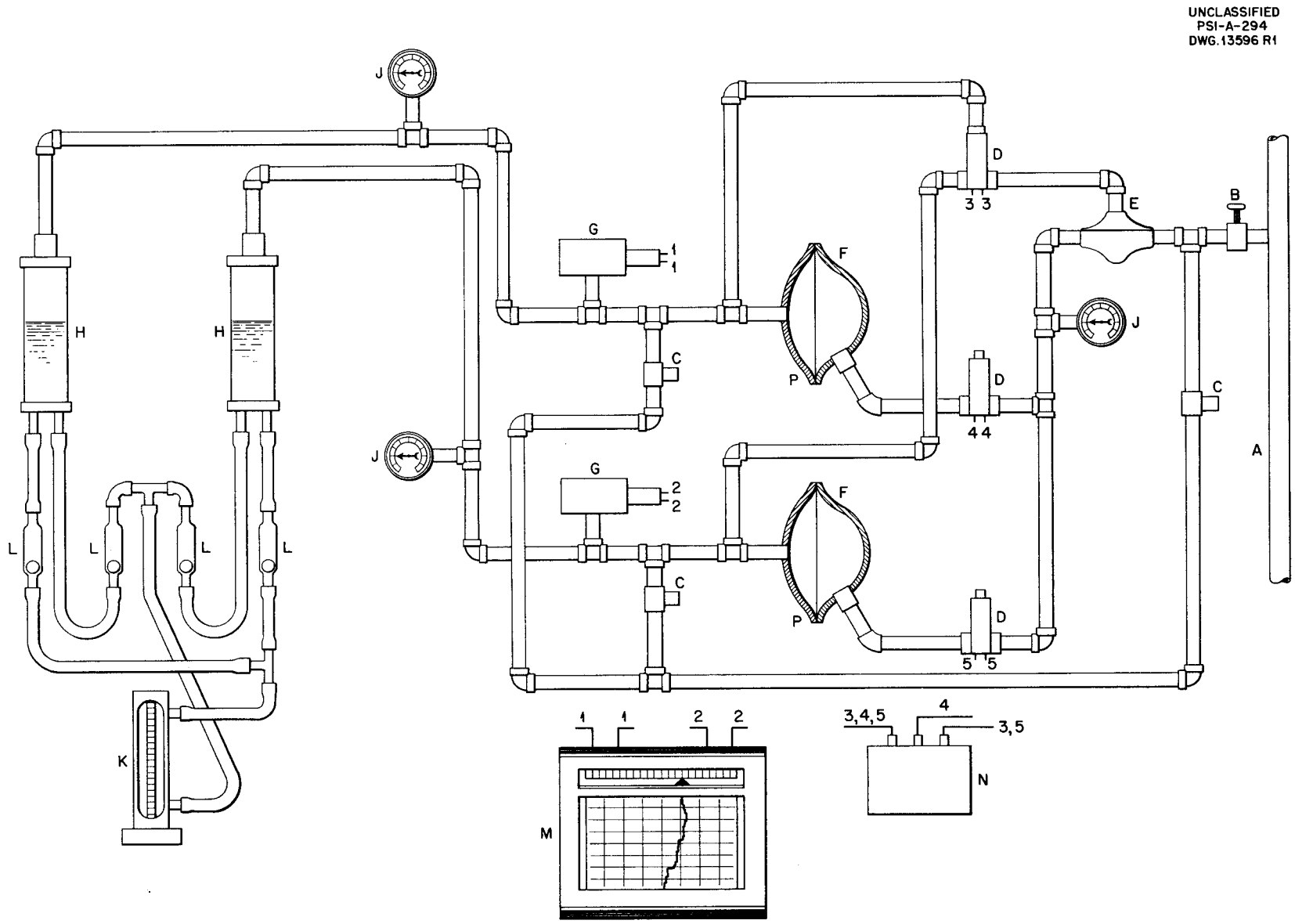

Fig. 20. Diagram of Mockup Pumping System for LITR Corrosion and Creep Experiment.

check valves, *L*, and two pressure-driven diaphragms, *F*. These solenoid valves, connected to the diaphragm housings, alternately provide air pressure to the right sides of the rubber diaphragms. As a result water is pumped from the left tank, *H*, to the right tank. The operation is then reversed in the second half of the pumping cycle. By means of an air relay, *E*, with a magnification of 1 to 6 (signal pressure to outlet pressure ratio), and a solenoid valve, *D*, an almost constant pressure difference can be maintained between the two tanks for about two-thirds of the pumping cycle. A relay system, *N*, includes a motor-driven switch that operates the solenoid valves to give a 15-sec pump stroke.

Figures 21 and 22 show the variation in the rate of flow during each pump stroke. Figure 22 indicates the performance of the pump diagrammed, and Fig. 21 shows the performance of a similar pumping system without the use of a Moore air relay (Fig. 20, *E*) as a variable pressure regulator. The maximum rates of flow shown on the graphs correspond to a velocity through the connecting tubing and flowmeter of approximately 10 ft/sec.

The flow rate in this system can be measured by determining the pressure differential between the two tanks. The Brown recorder, *M*, shown in Fig. 20, monitors the flow by measuring the pressure difference as indicated by the two pressure cells, *G*. This flowmeter is being calibrated with a rotometer, *K*.

A stainless steel mockup of the sodium pump system of the LITR liquid-metal loop has been fabricated for testing various components of the final pumping system. It will be operated with the control system that has been developed for the water

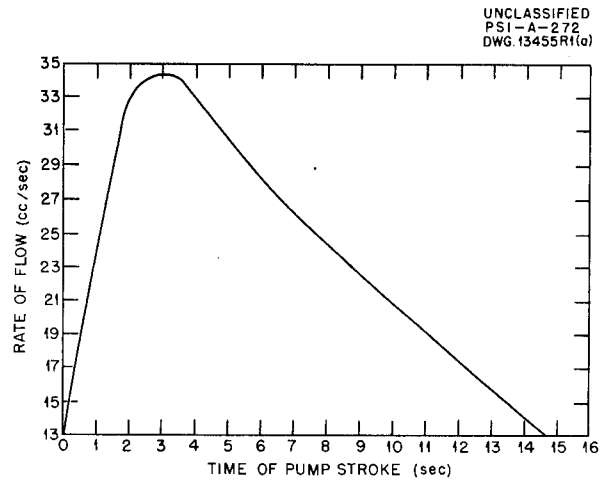

Fig. 21. Change in Rate of Flow During Each Stroke of Mockup Sodium Pump (Without Air Relay).

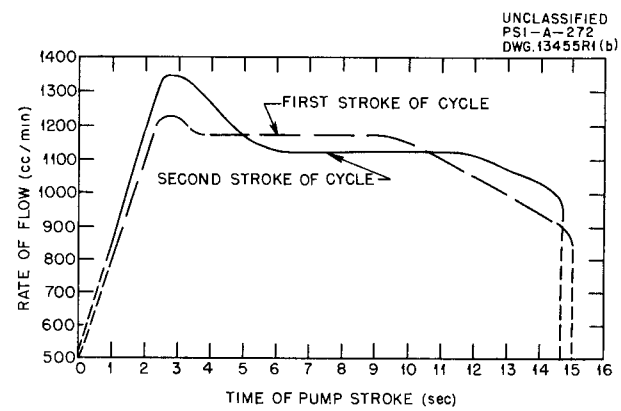

Fig. 22. Change in Rate of Flow During Each Stroke of Mockup Sodium Pump (With Air Relay).

mockup. An electromagnetic flowmeter will be used on this system to calibrate the differential pressure flowmeter that will be used on the inpile loop.

X-10 GRAPHITE PILE LIQUID-METALS LOOP

C. D. Baumann O. Sisman
R. M. Carroll W. W. Parkinson
C. Ellis

The general results of circulating lithium at 1000°F through hole 58N of

the X-10 graphite pile were reported in the last quarterly.[1] Since then the neutron flux of hole 58N has been determined by measuring the gammas from a cobalt foil that had been placed in the hole for one week. The cobalt was embedded in lithium in a section of tubing similar to the type-316 stainless steel loop material. The energy released at equilibrium can then be calculated from the relation:

$$E = \phi N_0 \sigma E_\beta ,$$

where E is the energy (Mev) per cubic centimeter of natural lithium per second from beta decay of Li^8, φ is the measured neutron flux (1.33×10^{11} neutrons/cm^2·sec), N_0 is the number of Li^7 atoms per cubic centimeter of natural lithium (3.88×10^{22}), σ is the cross section of Li^7 (0.033 barn), and E_β is the average energy of the Li^8 beta [(~13.4/3) Mev]. From these, $E = 0.76 \times 10^9$ Mev/cm^3·sec. This figure is about one-third the value of the energy measured from Bremsstrahlung activity.[2] This is not unreasonable, however, since the chamber used in measuring the Bremsstrahlung activity was calibrated with a 1.2-Mev gamma source and can be expected to have a much higher response from the 0.06-Mev Bremsstrahlung photon. The chamber is being calibrated for the low-energy photons, and a better correlation will be made at a later date.

Gray and Roche[3] made a metallographic examination of sections removed from the loop. Their findings are summarized in Table 4. The change in grain size and hardness is attributed to temperature rather than radiation.

An improved electromagnetic pump cell for operation at temperatures of about 1000°F was designed and built. A sodium test loop made of inconel tubing was bench tested using this pump. An electromagnetic flowmeter was calibrated during the same run.

An inpile sodium loop (Fig. 23) has been built and is now ready for loading and bench testing prior to insertion in the X-10 graphite pile. The loop, made of 0.225-in.-OD inconel tubing (with 0.025-in. walls) will extend approximately 18½ ft into the pile and about 2 ft outside the pile. An electromagnetic pump will circulate the liquid sodium through the tubing in the pile, and the flow will be measured with an electromagnetic flowmeter.

It is planned to operate the inpile section of the loop as near 1500°F as possible. To accomplish this, the tube is heated by three 4000-w, 230-v Calrod heaters in series. One end of the series of heaters extends through the front flange and the other end is grounded to the tubes, thus no lead wires are needed inside the jacket surrounding the inpile loop. The heaters are fed from either a 500- or 750-v supply. It is hoped that the series connections of the heaters will stand up better than the parallel lead wire connections in the earlier loop containing lithium. A second set of heaters has been provided in case of failure of the first set.

The same type of ionization chamber will be used to measure the activity of the sodium as was used for the lithium loop. Only one chamber is required, since the half life of sodium is relatively long and no evidence of activated corrosion particles can be picked up during

---

[1] C. D. Baumann, R. M. Carroll, O. Sisman, W. W. Parkinson, and C. Ellis, "Liquid-Metals Loop," *Physics of Solids Institute Quarterly Progress Report for Period Ending July 31, 1951*, ORNL-1128, p. 35.

[2] Figure 4.2, *op. cit.*, ORNL-1128, p. 36.

[3] R. J. Gray and T. K. Roche, *Metallographic Examination of 316 Stainless Steel Tubing*, ORNL Metallurgy Division Memo. 16 (Oct. 29, 1951).

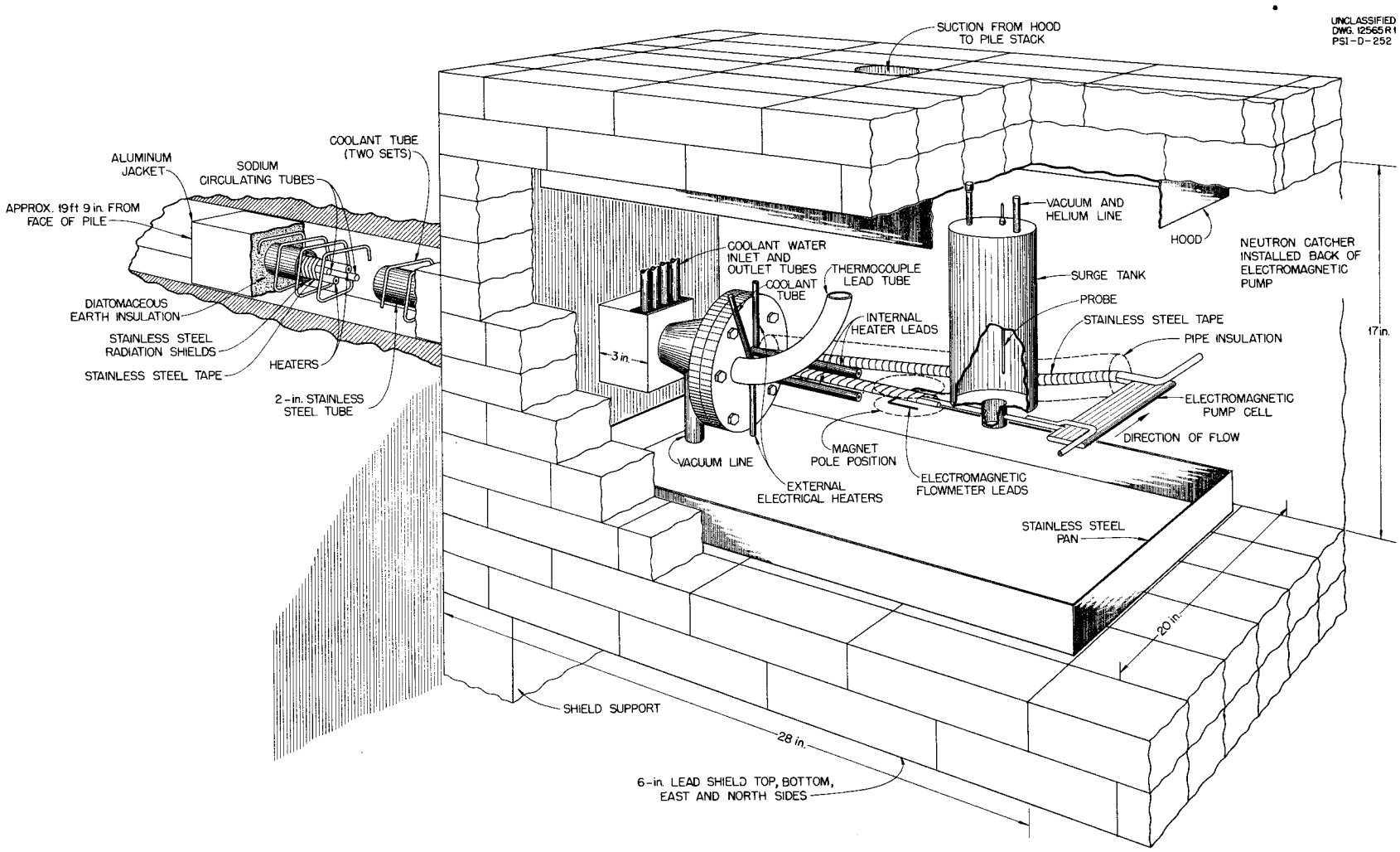

Fig. 23. Sodium Loop Assembly, Hole 58N.

TABLE 4

Metallographic Examination of Loop Sections

FLUX AND TEMPERATURE EXPOSURE OF SECTIONS REMOVED	INTERGRANULAR PENETRATION	ROUGHENING OF TUBE SURFACE	GRAIN SIZE	AVERAGE VICKERS HARDNESS
Sample 1 Exposed 1 wk to avg. flux of 1.33×10^{11} neutrons/cm^2·sec at 1000°F	No appreciable amount	Slight	Much larger than blank	136.6
Sample 2 Exposed 1 wk to negligible flux at 1000°F	No appreciable amount	Slight, mostly concentrated around grain boundaries	Much larger than blank	131.8
Sample 3 Blank of same material, no flux or temperature exposure		Dispersed, not necessarily concentrated at grain boundaries		169.8

normal pile operation. If the pile is down for an appreciable length of time and if corrosion particles are abundant in the sodium stream, it may be possible to observe some of the longer half-life corrosion products. Similarly, at the end of the experiment, after the sodium has stopped circulating through the pile, it may be possible to observe and identify some of the longer lived corrosion particles after the sodium activity has died.

STUDIES OF MISCELLANEOUS MATERIALS

R. H. Kernohan

Two thorium bars (1/4 in. dia. by 4 in.) were tested for R. E. Adams of the Metallurgy Division, with the following results:

Dynamic modulus of elasticity, 9.17×10^6 psi,

Electrical resistivity, 20.12 μohm-cm at 25°C,

Thermal conductivity, 19 Btu/hr/ft^2/°F/ft at 340°F (0.08 cal/sec/cm^2/°C/cm at 170°C).

Two samples of EDF glass furnished by F. Ring of the Engineering Department were tested for resistance to gamma radiation. The manufacturers of the glass, Chance Brothers Limited of Birmingham, England, state (see their report No. 64/51) that this clear glass turns slightly yellowish when exposed to gamma radiation and that the coloration can be largely removed by heating to 200°C for several hours.

The two samples had an optical transmission of 85 to 90% over the visible wavelength region. After an exposure of 10^6 r to a Co^{60} source both samples were black and opaque. An attempt was made to anneal out the coloration by ordinary illumination in a manner similar to that used with high-density glass.[4] After two weeks of illumination the EDF glass samples had recovered less than half their original transmission. Heating at 200°C did remove the coloration as reported by the manufacturers.

Two single-crystal wafers of lithium fluoride were irradiated in a doughnut hole in the X-10 graphite pile for a period of four weeks, which corresponded to a fast flux approaching 2×10^{18} nvt. Both crystals turned black. One of the crystals lost most of its coloration after 24 hr in a furnace held at 450°C. X-ray studies of the crystals before and after irradiation have thus far proved inconclusive.

An intermetallic compound made by the GE-ANP group and believed to be $ZrBe_{16}$ was tested and irradiated in a doughnut hole in the X-10 graphite pile for four weeks (2×10^{18} nvt). The electrical resistivity of the specimen increased 10%, and the hardness increased approximately 130 DPH numbers.

The study of fission-fragment damage to graphite as a function of uranium particle size has continued. The knowledge gained will be useful in consideration of homogeneous reactors constructed of solid materials.

Test results of a series of pure graphite bars were given in the last quarterly report.[5] Eight additional series composed of bars with the same UO_2 nodule size have been received from Battelle Memorial Institute. Nodule sizes are 586, 334, 94, and less than 44 microns. Four of the series contain UO_2 nodules made of natural uranium, and the other four series are duplicates containing 93% enriched uranium. All bars are molded of resin-bonded graphite and baked at 2500°F (not graphitized). They are of uniform size, about 0.230 by 0.300 by 2.86 inches. Each bar weighs about 5.5 g and contains 0.27 g of uranium.

Three containers for irradiating samples have been fabricated by the research shop. They have been assembled and are ready for loading. Three thermocouples are located inside each of the steel containers to measure temperatures at several points. After eight graphite-uranium bars are fitted into each container, it is evacuated and filled with dry helium gas.

PHYSICAL PROPERTIES OF IRRADIATED PLASTICS AND ELASTOMERS

C. D. Bopp R. L. Towns
O. Sisman W. K. Kirkland

To supplement the information already available for pile-induced changes in plastics and elastomers it was desired to separate the effects of gamma radiation and fast-neutron radiation. This was accomplished by two methods:

1. The sample was encased in cadmium and exposed in the X-10 graphite pile. The cadmium served to capture thermal neutrons and give off gamma photons. Thus the sample was exposed to an increase of gamma

[4] R. H. Kernohan and G. M. McCammon, *Fading Characteristics of Gamma Induced Coloration in High Density Glass*, ORNL-975 (Mar. 20, 1951).

[5] R. H. Kernohan, "Irradiation of Graphite-Uranium Rods," *op. cit.*, ORNL-1128, p. 47.

radiation while the fast neutrons were unaffected and the thermal neutrons were essentially eliminated. This method gave an intensity of about 9.0×10^6 r/hr from gamma radiation plus the equivalent of 2.5×10^6 r/hr from fast-neutron radiation.

2. Gold was activated in the X-10 graphite pile and the samples were later exposed to the resulting neutron-free source of gamma radiation. The average intensity of radiation produced as measured with an ionization chamber was 1.5×10^4 r/hr.

For the first method, assuming that all of the damage by pile radiation results from fast neutrons and gamma radiation and that damage by each is proportional to the energy absorbed by the plastic or elastomer, then the equivalent damage (or energy absorbed) to the sample is:

$$(N + G)a = (N + G_2)b$$

and the ratio of the dose (nvt) without cadmium to the dose within a cadmium enclosure that produces the same change in property is

$$\frac{a}{b} = \frac{N + CG}{N + G},$$

where

N = energy absorbed from fast neutrons per unit time with or without cadmium,

G = energy absorbed from gammas per unit time without cadmium,

G_2 = energy absorbed from gammas per unit time with cadmium ($G_2 = CG$),

a = exposure (nvt) for a given damage without cadmium,

b = exposure (nvt) for the same damage with cadmium, and

$C = G_2/G$.

Now letting

$$y = \frac{a}{b} = \frac{nvt_0}{nvt_{Cd}}$$

and

$$x = \frac{N}{G},$$

then

$$y = \frac{x + C}{x + 1}.$$

Figure 24 shows y plotted against x for several plastics and elastomers. The values of x were calculated from data given in ORNL-129[6] in which the energy absorbed from fast neutrons and gammas was determined calorimetrically for individual elements in the X-10 graphite pile. A sample calculation for polyethylene is given in ORNL-928.[7] Since the proportions of filler material were not known for Silastic and paper-base phenolic, x was calculated for the unfilled polymers.

Complete curves of radiation exposure vs. change in property have been determined for pile irradiations without cadmium. For each exposure (in nvt) with cadmium, the nvt that gave an equivalent change in physical property was taken off the curves and y was then plotted as the ratio of these nvt's.

[6] D. M. Richardson, *Calorimetric Measurement of Radiation Energy Dissipated by Various Materials Placed in the Oak Ridge Pile*, ORNL-129 (Dec. 23, 1948).

[7] O. Sisman and C. D. Bopp, *Physical Properties of Irradiated Plastics*, ORNL-928 (June 29, 1951).

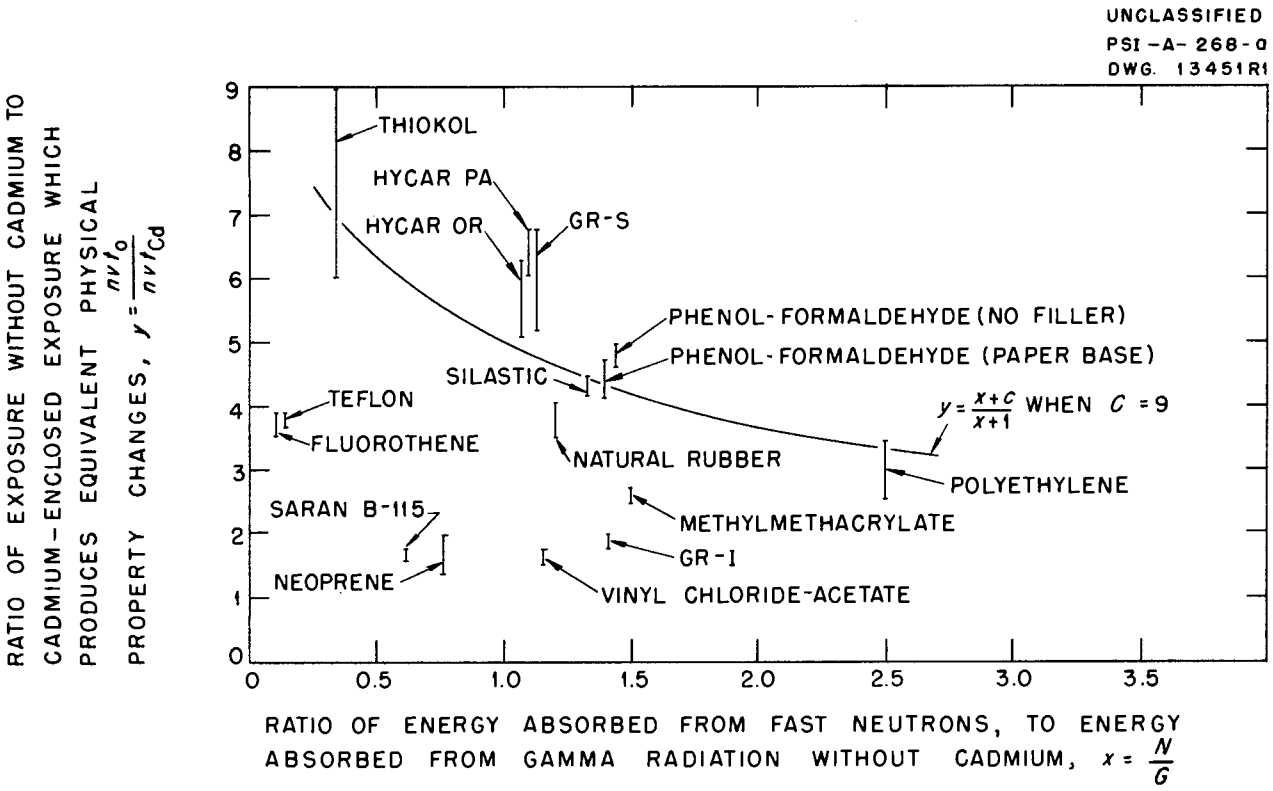

Fig. 24. Irradiation of Plastics and Elastomers in the X-10 Graphite Pile with the Gamma Flux Increased by Cadmium.

When C is taken as 9, the curve of Fig. 24 is obtained. This curve gives the best fit for experimental values obtained. It follows then that the energy absorbed from gamma radiation, and therefore the gamma intensity, has been increased nine-fold by the cadmium.

The sensitivity of determining the y values of Fig. 24 depends on the rate of change of the property chosen for study. The length of the lines plotted in Fig. 24 is an indication of this sensitivity. There is good agreement when more than one property is studied, indicating that the damage produced with cadmium is similar in nature to that produced without cadmium. This means that the damage produced by gamma radiation is similar to that produced by fast neutrons.

The points plotted in Fig. 24 that do not fall near the curve represent materials in one of two categories: (1) those containing chlorine or fluorine (fluorothene, Teflon, Saran, neoprene, and vinyl chloride-acetate); and (2) those having a large proportion of carbon atoms of the main polymer chain attached to two branching groups (methylmethacrylate and GR-I).

For materials in the first category the cross section for slow-neutron reactions (which have been neglected) is appreciable and it is assumed that damage to these materials comes from the beta radiation plus the recoil atoms released by decaying Cl^{38} and F^{20}. For materials in the second category it is assumed that the rate of damage is a function either of the energy spectrum of gamma radiation or of the intensity of the radiation. Materials falling in either category have been shown to have little resistance to pile radiation.

Preliminary results on the irradiation of elastomers by gamma rays from Au^{198} are shown in Table 5. Beta radiation was filtered out by a steel sheet placed between the gold and the materials irradiated. Listed in the column labeled "Experimental" are the values of nvt for X-10 graphite pile exposures that produce similar changes in properties to the changes listed for the gamma irradiations. Listed in the column labeled "Calculated" are the values of nvt that are equivalent in energy absorption, both from fast-neutron radiation and gamma radiation, in the X-10 graphite pile to the energy absorbed in the Au^{198} irradiation. This value depends upon the composition of the materials as described previously. The calculated values for some of the materials come out lower than the experimental values, though there is agreement within a factor of 3. Here again it is assumed that the difference is accounted for in that the rate of damage is a function of the energy spectrum of the gamma radiation or the intensity of the radiation.

Properties of elastomers compounded as gasketing materials and irradiated in the X-10 graphite pile for an exposure of 10^{19} nvt are listed in Table 6 along with the properties at 5×10^{18} nvt, the longest exposure reported previously. After the 10^{19}-nvt exposure neoprene was hygroscopic, probably from the presence of HCl formed as a decomposition product. Hycar PA-21, which contains only a small amount of chlorine, was also hygroscopic, though to a lesser extent than neoprene.

TABLE 5

Properties of Elastomers and Plastics Exposed to Gamma Radiation from Au^{198}

(Log mean intensity of 1.5×10^4 r/hr)

ELASTOMER OR PLASTIC	CATEGORY (see text)	GAMMA EXPOSURE (r)	TENSILE STRENGTH (lb/in.^{2})	SHORE DUROMETER HARDNESS	REQUIRED EXPOSURE IN X-10 GRAPHITE PILE FOR SIMILAR PROPERTY CHANGES (10^{18} nvt)	
					EXPERIMENTAL	CALCULATED
GR-S 50		0	1800	67		
		2.6×10^7	1800	76	0.04	0.04
Silastic 7-170		0	550	60		
		2.6×10^7	550	78	0.06 to 0.07	0.04
Neoprene W	1	0	2800	85		
		1.2×10^7	2400	78	0.04	0.02
GR-I 50	2	0	1050	67		
		1.2×10^7	550	65	0.04 to 0.06	0.02
Methylmethacrylate	2	0	8700			
		2.6×10^7	2100		0.07	0.04
Teflon	1	0	2500			
		2.6×10^7	350		0.2 to 0.3	0.08

TABLE 6

Physical Properties of Irradiated Elastomers

	ELASTOMERS					
	NATURAL RUBBER	HYCAR OR-15	HYCAR PA-21	GR-S 50	NEOPRENE W	SILASTIC 7-170
Tensile Strength (lb/in.^{2})						
(a)	2600	1900	2000	1700	2900	520
(b)	6500	7500	1500	5000	2500	400
(c)	5500	7000	3000	4000	2500	800
Rockwell Hardness[d]						
α scale						
(b)	87	119	-155	114	114	71
(c)	104	118	5	115	115	93
R scale						
(b)	110	126	66	124	123	124
(c)	112	117	70	117	116	116
Specific Gravity (25°/4°)						
(a)	1.186	1.229	1.269	1.210	1.418	1.382
(b)	1.247	1.304	1.289	1.287	1.459	1.493
(c)	1.257	1.317	1.302	1.298	1.468	1.539
Weight Change (%)						
(b)	0.06	0.14	-6.4	0.20	0.23	2.5
(c)	0.24	0.26	-11.5	0.40	-0.58	4.8
Volume Resistivity (ohm-cm)						
(a)	10^{10}	10^{9}	10^{10}	10^{14}	10^{11}	10^{14}
(b)	10^{10}	10^{12}	10^{6}	10^{11}	10^{5}	10^{13}
(c)		10^{12}	10^{4}	10^{11}	10^{5}	10^{13}
Dielectric Strength (v/mil)						
(a)	170	200	115	170	300	>380
(b)	120	300	115	160	120	>380
(c)	120	200	115	160	120	>380

[a] No exposure.
[b] Exposure, 5×10^{18} nvt.
[c] Exposure, 10^{19} nvt.
[d] The durometer hardness of the elastomers with no irradiation was from 60 to 80, which is too soft to read on the Rockwell α or R scale.

To study the effect of the presence of oxygen during irradiation, the elastomers were placed in glass capsules, which were then evacuated and filled with helium. The change in properties was the same as that reported in the last quarterly for irradiation in the presence of air. A similar procedure is being followed for plastics, and even though results are not complete, preliminary data on a few materials show no difference between the rate of change in properties in air or helium.

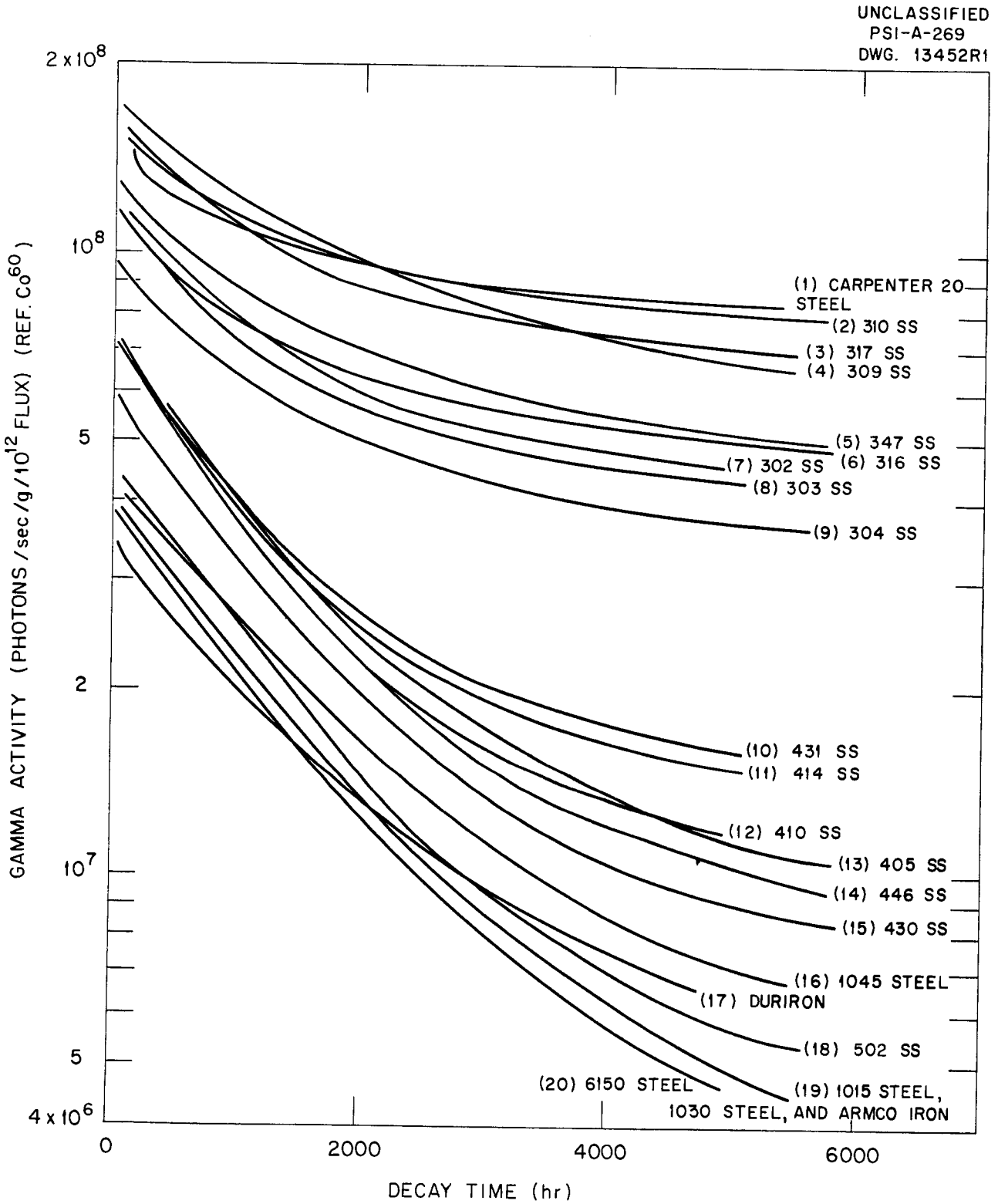

Fig. 25. Gamma Decay of Metals (Curves 1 to 20).

Tests are in progress to determine the change in properties with time of storage after irradiation. Preliminary results indicate that this change is not appreciable for elastomers but that there is a marked difference for some plastics where the properties continue to change in the same way (though at a slower rate) as they change during irradiation.

The amount of gas given off during the irradiation of elastomers and plastics is now being measured. The materials are sealed in glass capsules and are irradiated, after which they are broken open and the amount of gas is measured.

A compression-set test during irradiation is under way on elastomers compounded as gasketing materials. The elastomers are placed in a constant-strain compression jig, irradiated, removed from the jig, and the change in thickness is measured.

PILE-INDUCED RADIATION IN MATERIALS OF CONSTRUCTION

C. D. Bopp R. L. Towns
O. Sisman W. K. Kirkland

Decay of the gamma radiation induced in metals by exposure in the X-10 graphite pile is given in Figs. 25 through 27 (see Table 7). Activity was measured in the 100% geometry ionization chamber described in ORNL MonC-399.[8] The chamber was calibrated in terms of photons with average energy of 1.2 Mev (those given off by Co^{60}). The curves start at about 100 hr. (The decay period from 3 to 100 hr was covered in earlier reports.)

The exposure time for all the metals is in the range of 4700 ± 400 hr. Exact exposure times are given in Table 7.

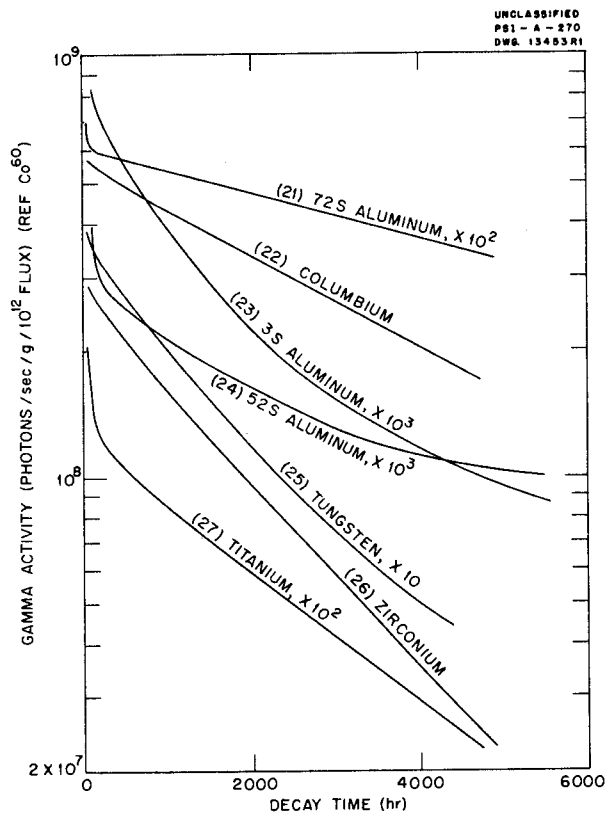

Fig. 26. Gamma Decay of Metals (Curves 21 to 27).

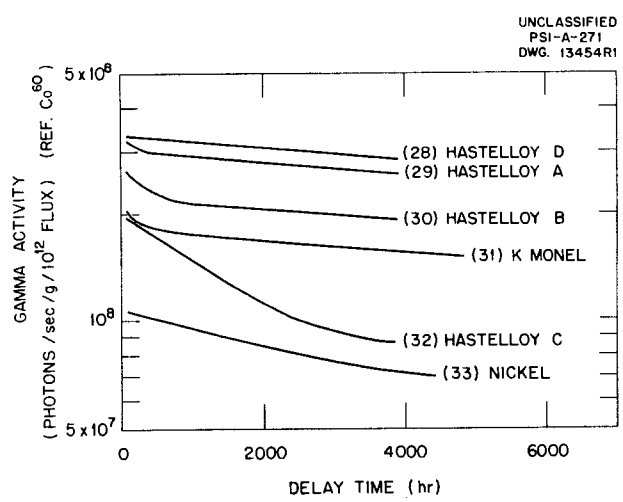

Fig. 27. Gamma Decay of Metals (Curves 28 to 33).

[8] J. W. Jones and R. T. Overman, *The Use and Calibration of a 100% Geometry Ion Chamber*, ORNL MonC-399 (Mar. 20, 1948).

TABLE 7

Length of Exposure of Metals Measured for Gamma Decay

METAL	EXPOSURE TIME (hr)	CURVE NUMBER
		(see Fig. 25)
Armco iron	5050	19
Carpenter 20 steel	4280	1
Duriron	4870	17
302 stainless steel	4700	7
303 stainless steel	4340	8
304 stainless steel	4280	9
309 stainless steel	4540	4
310 stainless steel	4500	2
316 stainless steel	4500	6
317 stainless steel	4700	3
347 stainless steel	4500	5
405 stainless steel	4500	13
410 stainless steel	4870	12
414 stainless steel	4540	11
430 stainless steel	4280	15
431 stainless steel	4540	10
446 stainless steel	4280	14
502 stainless steel	4510	18
1015 steel	4700	19
1030 steel	4700	19
1045 steel	4700	16
6150 steel	4700	20
		(see Fig. 26)
3S Aluminum	4510	23
52S Aluminum	4510	24
72S Aluminum	4870	21
Columbium	5050	22
Titanium	4870	27
Tungsten	5050	25
Zirconium	4700	26
		(see Fig. 27)
Hastelloy A	4680	29
Hastelloy B	4680	30
Hastelloy C	4680	32
Hastelloy D	4680	28
K Monel	4700	31
Nickel	5050	33

TABLE 8

Rate of Production of Heat Energy by Nuclear Bombardment of Lead in LITR

(Northwest downbeam hole)

TIME	SPECIMEN TEMPERATURE, T_1 (°C)	WALL TEMPERATURE, T_2 (°C)	TEMPERATURE DROP, $T_1 - T_2$ (°C)	HEAT CAPACITY, C_p (cal/g)	$\frac{dT_1}{dt}$	NUCLEAR HEATING RATE (cal/g·sec)	POWER LEVEL OF LITR*
SEPTEMBER 19, 1951							
AM	39.30	36.6	2.6	0.0311	0.015	0.0005	
1600	40.50	38.35	2.15	0.031	0.04	0.0012	1.00
1700	43.01	42.67	0.34	0.031			Low
1800	35.69	35.21	0.48	0.030			Low
1900	39.05	36.64	2.41	0.031	0.03	0.0009	Low
2000	44.50	41.19	3.31	0.032	0.04	0.0013	
2030	58.01	45.44	2.57	0.034	0.04	0.0014	
2131	58.02	51.36	3.03	0.0034	0.04	0.0014	
2310	54.07	50.81	3.26	0.033	0.04	0.0014	
SEPTEMBER 20, 1951							
1230	51.16	52.68	3.48	0.0314	0.035	0.0011	1.00
1530	57.32	55.70	2.30	0.0314	0.022	0.0007	1.00
1730	58.47	55.00	3.47	0.0314	0.035	0.0011	1.00
1830	58.47	55.0	3.47	0.0314	0.035	0.0011	1.00
2316	58.00	54.53	3.47	0.0314	0.035	0.0011	1.00
SEPTEMBER 21, 1951							
0030	58.00	54.35	3.65	0.0314	0.037	0.0012	1.00
AM	57.6	53.9	3.7	0.0311	0.04	0.0012	1.00

*Power level of 1.00 refers to 770 kw reactor power.

NUCLEAR HEATING

J. B. Trice

Investigation of heating rates caused by nuclear bombardment of various materials was continued. A preliminary apparatus was developed to obtain such information rapidly and to provide nuclear heat production data for materials placed in an MTR-type reactor. The objective is to provide cooling design data for experiments in the LITR and the MTR.

Heat production rates in lead have been obtained for two locations in the LITR. The apparatus used was the single-specimen calorimeter described in the last quarterly report.[9] Table 8 shows nuclear heating values

[9] J. B. Trice, "Nuclear Heating," *op. cit.*, ORNL-1128, p. 37.

TABLE 9

Rate of Production of Heat Energy by Nuclear Bombardment of Lead in LITR Lattice

(Hole C-44, September 24, 1951)

TIME	SPECIMEN TEMPERATURE, T_1 (°C)	WALL TEMPERATURE, T_2 (°C)	TEMPERATURE DROP, $T_1 - T_2$ (°C)	HEAT CAPACITY, C_p (cal/g)	$\frac{dT_1}{dt}$	NUCLEAR HEATING RATE (cal/g·sec)	DISTANCE ABOVE LATTICE CENTER LINE (in.)	POWER LEVEL OF LITR*
1330	71.0	63.3	7.7	0.0315	0.08	0.0025	12.4	1.0
1400	72.5	67.6	4.9	0.032	0.045	0.0014	12.4	1.0
1430	128.31	104.32	24.0	0.034	0.036	0.0013	8.4	1.0
1530	128.3	104.3	24.0	0.034	0.36	0.012	5.2	1.0
1229	115.3	145.0	29.7	0.032	0.38	0.12	5.2	1.0
1300	199.8	156.0	43.8	0.033	0.80	0.026	2.4	1.0
1500	176.1	141.6	35.1	0.033	0.59	0.020	2.4	1.0
1530	202.5	151.0	51.5	0.034	0.95	0.032	-0.5	1.0

*Power level of 1.0 refers to 770 kw reactor power.

for lead exposed in the LITR at the bottom of the northwest downbeam hole. This hole extends into the river sand and is adjacent to the reactor cooling water. The average heating per gram, measured September 19 to 21, 1951, was 0.0012 cal/g·sec.[10] Comparison of successive sets of data indicates that the heating at full reactor power is fairly constant and that the measurements are reproducible. The low values for heating found on September 19 coincide in each case with a period during or immediately following a shutdown period. In Table 8, values observed during September 19 appear to increase slightly over a period of about 5 hr from start-up time. This increase might be attributed to a build-up of fission products and induced radioactivity except for its failure to reappear following a shutdown period on September 20. Values of nuclear heating given in Table 8 are probably lower than those in the horizontal beam holes, which extend closer to the reactor fuel elements.

The values given in Table 9 were observed in hole C-44 within the active lattice. Entry to the reactor was made from the top by means of an aluminum tube extending down through the cooling water and completely through the active lattice. Nuclear heating as a function of distance above the reactor lattice center line is shown in Fig. 28.

The nuclear heating does not appear to be symmetrical with respect to the

[10] This is based on a reactor power level of 1.0 (770 kw) or approximately $10^{13}(nv)_{th}$ at the center of the reactor.

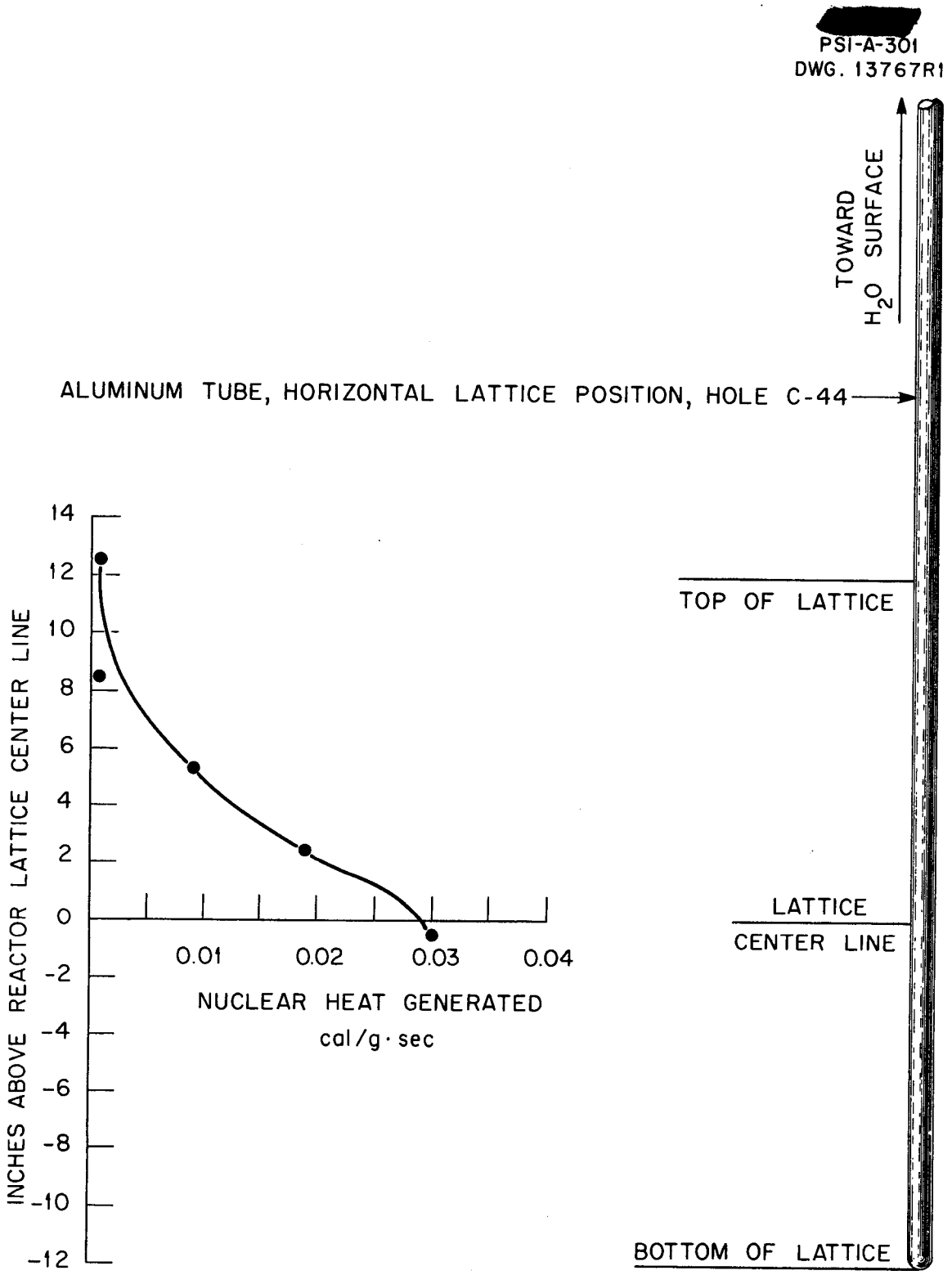

Fig. 28. Nuclear Heat Production Rate for Lead Irradiated in LITR.

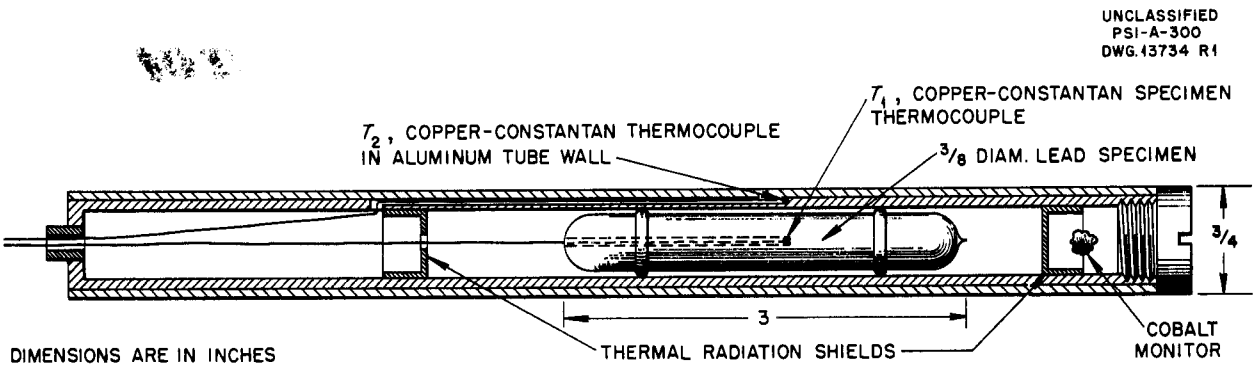

Fig. 29. Dynamic Calorimeter for Measuring Rates of Nuclear Heating.

reactor center line. The maximum occurs about 3 or 4 in. below the center line. This heating up was especially noticeable during experimental operation when the temperature of the specimen began to approach unsafe values (>250°C) as it was lowered below the center line. To prevent overheating, it was necessary to raise the apparatus only 3 or 4 in.; hence the highest values observed were probably not far below the true maximum heating rate.

Heat production rates decreased rapidly toward the reactor lattice top. Also, measurements taken from the top of the reactor upward through the cooling water indicated that nuclear heating decreases rapidly with distance above the reactor. This decrease in heating was demonstrated by the closeness of the two temperatures in the apparatus, which were almost equal to each other when the calorimeter was elevated a few inches above the reactor lattice.

A sketch of the apparatus is shown in Fig. 29. Gammas and neutrons are absorbed or scattered by the specimen during irradiation. The thermal energy imparted causes the temperature (T_1) of the specimen to rise until thermal equilibrium is reached. The rate of heat loss from the specimen is then equal to the rate of nuclear heat produced and is a function of T_2, the calorimeter wall temperature, and the temperature difference ($T_1 - T_2$) between the specimen and the calorimeter wall. Heat generation per gram is given by the following equation:

$$\left[\frac{dH}{dt}\right] = C_p \left[\frac{dT_1}{dt}\right] \text{ cal/g·sec.}$$

The quantity (dT_1/dt) is a function of ΔT and T_2 and is obtained from calibration cooling curves for lead. A composite picture of these is shown in Fig. 30, which gives (dT_1/dt) vs. ($T_1 - T_2$) for several values of T_2.

Major errors are principally caused by failure of the thermocouples to respond rapidly to changes in temperatures during calibration runs. This

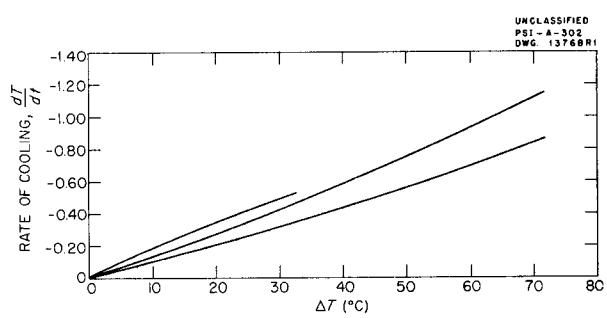

Fig. 30. Calibration Curves for Dynamic Calorimeter.

lagging effect resulted in differences between true temperatures and those recorded at the thermocouple positions. Other important errors are caused by lack of reproducible positioning of the specimen with respect to the calorimeter walls. It was estimated that the largest error probably did not exceed 20% except for very small values of the nuclear heating.

It is planned to improve the calorimeter design and the experimental procedure as follows:

1. The calorimeter will consist essentially of two concentric aluminum thin-walled cylinders with thermocouples imbedded in each. This will eliminate the specimen thermocouple and thus permit rapid specimen changes.

2. The calibration will be made with an electrical heater operating at known power levels. This will eliminate the necessity for running extensive calibration cooling curves and one calibration will suffice for many different specimens. Better accuracy of measurement should be possible since all measurements will be made during equilibrium temperature conditions.

MEASUREMENT OF NEUTRON SPECTRA

J. B. Trice

A project has been started to obtain as much information as possible about the neutron spectra in various strategic locations in the LITR. The objective is to determine the characteristics of the bombarding neutrons that produce radiation damage in materials. For the initial phase of the project five threshold reactions are being used to obtain the neutron spectrum. These reactions are: $P^{31}(n,p)Si^{31}$, $S^{32}(n,p)P^{32}$, $Al^{27}(n,p)Mg^{27}$, $Mg^{24}(n,p)Na^{24}$, and $Al^{27}(n,\alpha)Na^{24}$. They occur at energies above 2, 3, 5, 6, and 8 Mev, respectively. The initial method to be used is essentially the one described in ORNL-525.[11]

[11] C. D. Bopp and O. Sisman, *The Neutron Flux Spectrum and Fast and Epithermal Flux in Hole 19 of the ORNL Reactor*, ORNL-525 (July 28, 1950).

LIQUID FUELS

RADIATION DAMAGE TO LIQUID FUELS

G. W. Keilholtz
J. G. Morgan
H. E. Robertson
C. C. Webster
P. R. Klein
B. Kinyon

The purpose of testing materials at the lower fluxes of the X-10 graphite pile before testing them in the higher flux of the LITR is twofold: first, the screening engineering tests eliminate materials that prove to be unsatisfactory at the lower fluxes and provide more time and facilities for those of greater interest, and second, as a safety measure, materials are first tested at lower fluxes to anticipate any experimental hazards at higher fluxes. When it is decided which materials are of greatest interest, the tests can be modified for more precise investigations.

Measurements were made with an accuracy of ±0.5 psi to be certain that irradiation of the liquid fuels would not cause a pressure build-up sufficient to rupture the capsule. A natural uranium salt was first pressure tested at 1500°F in hole 12 of the pile under a flux of 8.5×10^{11}. The results, using the same apparatus previously reported,[1] are shown in Fig. 31. The composition of the uranium salt and subsequent test salts are as follows:

Salt	Mole %
NaF	46.5
KF	26.0
UF_4	27.5

A pressure test was conducted using a 10-g sample of enriched uranium salt in an inconel capsule; the results are shown in Fig. 32. From this graph it can be seen that under a flux of 8.5×10^{11} there was no sudden surge of pressure other than that from the thermal expansion of the helium, and there was no slow increase of pressure over the period of the irradiation.

A final pressure test was made in the LITR by using a 0.5-g sample of enriched uranium salt in an inconel capsule. The results are shown in Fig. 33. During the 115-hr test

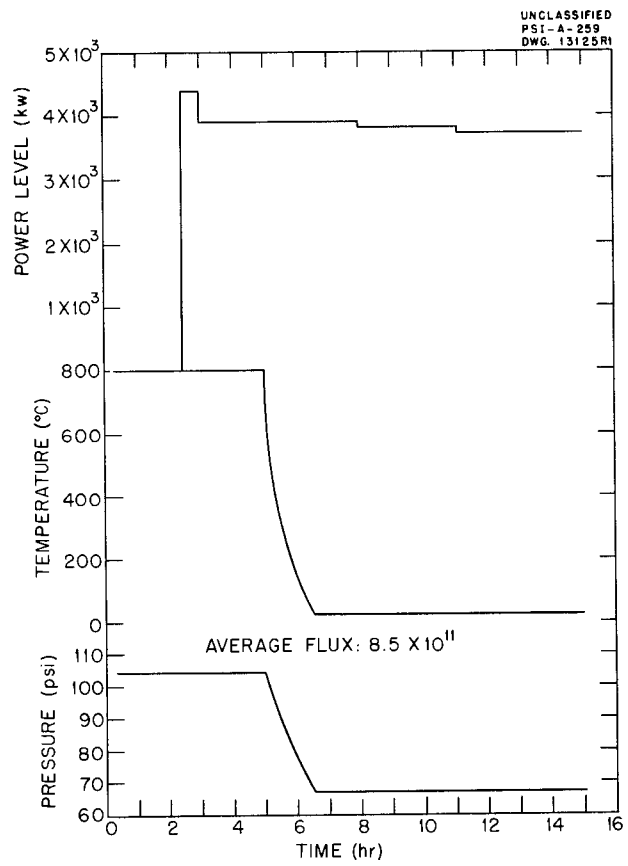

Fig. 31. Effect of Power Level and Temperature on Pressure of a Natural Uranyl Fluoride Salt.

[1] G. W. Keilholtz, J. G. Morgan, C. C. Webster, and H. E. Robertson, "Radiation Damage to Liquid Fuels," *Physics of Solids Institute Quarterly Progress Report for Period Ending July 31, 1951*, ORNL-1128, p. 50.

period the flux of the LITR was 1.6×10^{13}. No abnormal pressures were observed other than the thermal expansion of the helium.

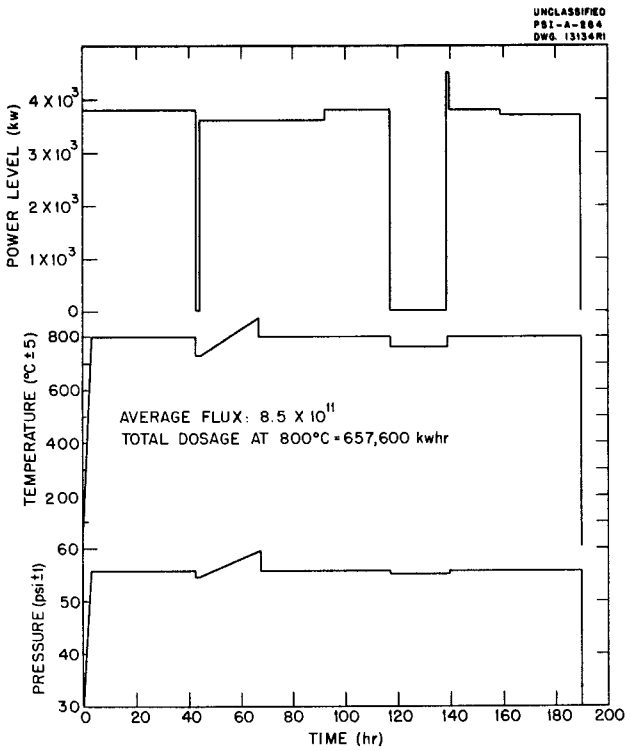

Fig. 32. Effect of Power Level and Temperature on Pressure of an Enriched Uranyl Fluoride Salt.

A series of microcapsules were irradiated at 1500°F in hole 54 of the X-10 graphite pile. The hole was equipped with an aluminum liner extending to the center line of the pile. This liner provided cooling to prevent an excessive temperature rise within the reactor. The temperature of each capsule was controlled by a chromel-alumel thermocouple spot welded to the outside metal surface. The capsule material was inconel and its contents consisted of enriched uranium fluoride. For charging, four capsules were placed in a lavite boat as shown in Fig. 34. The flux was 1.04×10^{12} and the runs varied from 200 to 450 hr.

Bench tests were conducted using identical capsules and heaters to duplicate the history of the inpile runs. A capsule with no treatment was examined as a further check on salt composition.

After the microcapsules were irradiated they were transported to the hot cells. The ends were cut off (Fig. 35) by using a remotely controlled lathe and grinder. Care was taken to prevent the salt from becoming contaminated with inconel chips. After this operation the salt was melted out and analyzed by the Analytical Chemistry Division for decomposition and corrosion products. The capsules were split longitudinally (Fig. 35) and again sectioned. This section (*X*) was metallographically examined at WAPD in Pittsburgh, Pa.[2] In all salt tests a small piece of inconel was placed in the melt to check weight loss. Up to the present time no method has been found to dissolve all the salt off the slug after irradiation without also attacking the inconel.

The first 12 samples are omitted from this report because the analysis indicated that oxidation of the uranium salt had occurred prior to irradiation. The remaining 11 samples are tabulated in Table 10. It should be emphasized that extreme precautions are necessary in the preparation and handling of liquid salts at high temperatures. The Materials Chemistry Division at Y-12 now has this problem well under control.

The samples tabulated in this report have received identical treatment throughout unless otherwise specified. It may be noted that the iron impurities increase during the welding operation and the long heat

[2] Acknowledgment is made of the cooperation and assistance of W. E. Johnson and R. Fillnow of WAPD.

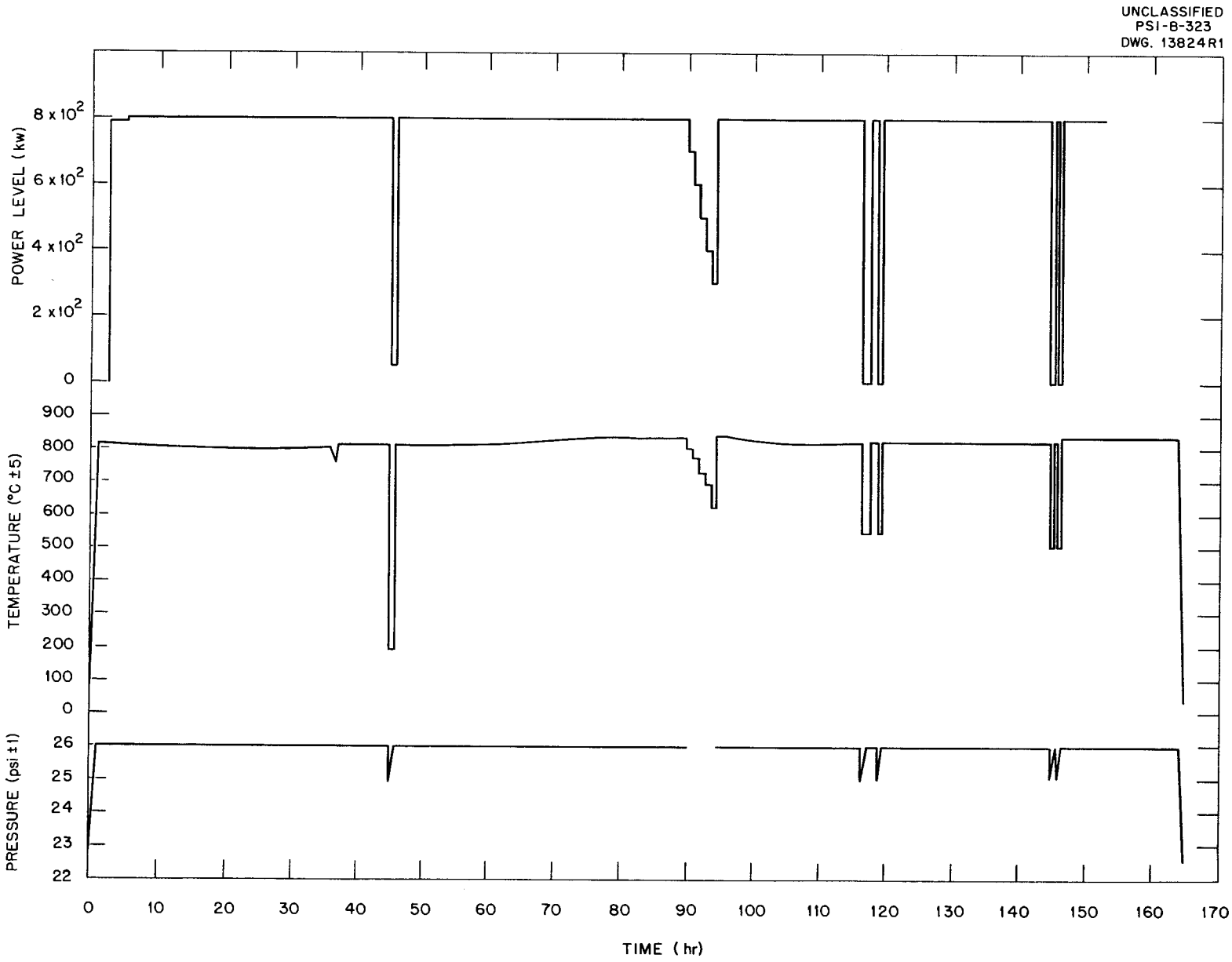

Fig. 33. Effect of LITR Power and Temperature on Pressure of an Enriched Uranyl Fluoride Salt.

TABLE 10

Microcapsule History and Analysis

SAMPLE NUMBER		DATE INSERTED	TOTAL TIME AT 1500°F (hr)	TOTAL INPILE TIME AT POWER LEVEL (hr)	AVERAGE PILE POWER (kw)	TOTAL TIME AT 1500°F AT PILE POWER (hr)	TOTAL DOSAGE AT 1500°F (neutrons/cm^2)	TOTAL DOSAGE AT PILE POWER (neutrons/cm^2)	DATE WITHDRAWN	CHEMICAL ANALYSIS					REMARKS
MICRO-CAPSULE NO.	OFFICIAL NO.									U (%)	F (%)	Fe (ppm)	Ni (ppm)	Cr (ppm)	
001	10	8/27/51													Never processed, opened and checked after welding cap
002	11	8/27/51	478	457	3750	443	1,674,293	1,718,668	9/17/51			1030	194	194	In pile at 1500°F
003	12	8/27/51	462	457	3750	427	1,605,400	1,718,668	9/17/51	51.5		1634	262	120	In pile at 1500°F
004	13	8/27/51	462	457	3750	427	1,606,400	1,718,668	9/17/51	50.3		1130	120	188	In pile at 1500°F
005	14	8/28/51	472						9/17/51	53.4		2635	160	125	Bench test
0001	15	9/24/51	334	298	3750	298	1,111,154	1,111,154	10/8/51	52.1		1534	93	232	In pile at 1500°F
0002	16	9/24/51	334	298	3750	298	1,111,154	1,111,154	10/8/51	51.5		2348	148	532	In pile at 1500°F
0003	17	9/24/51		298	3750			1,111,154	10/8/51	53.4		622	183	146	In pile at 590°F
0004	18	9/24/51	334						10/8/51	52.2		548	98	186	Bench test
Batch No. 1900-4 (master sample X-10 analysis)										55.3	27.9	311	123	207	No treatment
Batch No. 1900-4 (master sample Y-12 analysis)										54.4	28.2	425	85	280	No treatment

treatment. The chemical analyses must be compared on an inpile and out-of-pile basis. When this is done, there is no evidence that exposure to radiation has increased the inconel components (iron, chromium, and nickel) in the fused salts.

The metallographic studies show a small amount of intergranular corrosion. The corrosion is on the average of 1 mil (0.001 in.) or less. These results are comparable with the corrosion found by similar heat treatment out of the pile.

Exposure to radiation fluxes of 1.0×10^{12} for 400 hr has not appreciably increased the corrosion rate. These results should not be extrapolated to higher fluxes for interpretation.

Hole C-44 in the LITR was borrowed from the HRE group to continue screening tests at higher fluxes. Work was started to provide a top LITR facility,

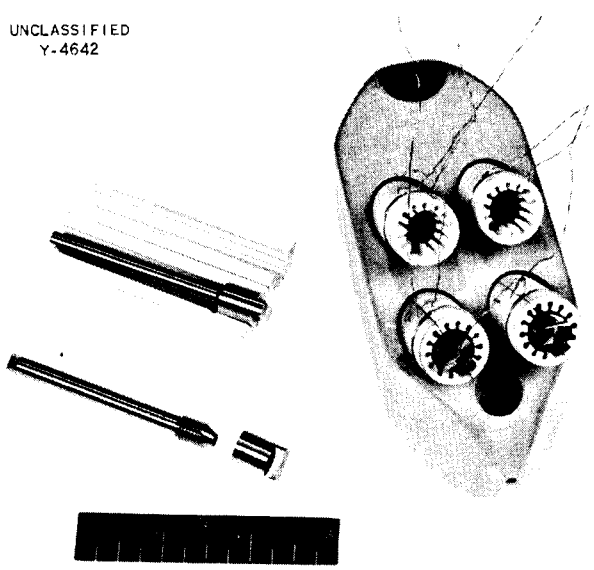

Fig. 34. Lavite Charging Boat Showing Positions of Four Capsules and Heaters.

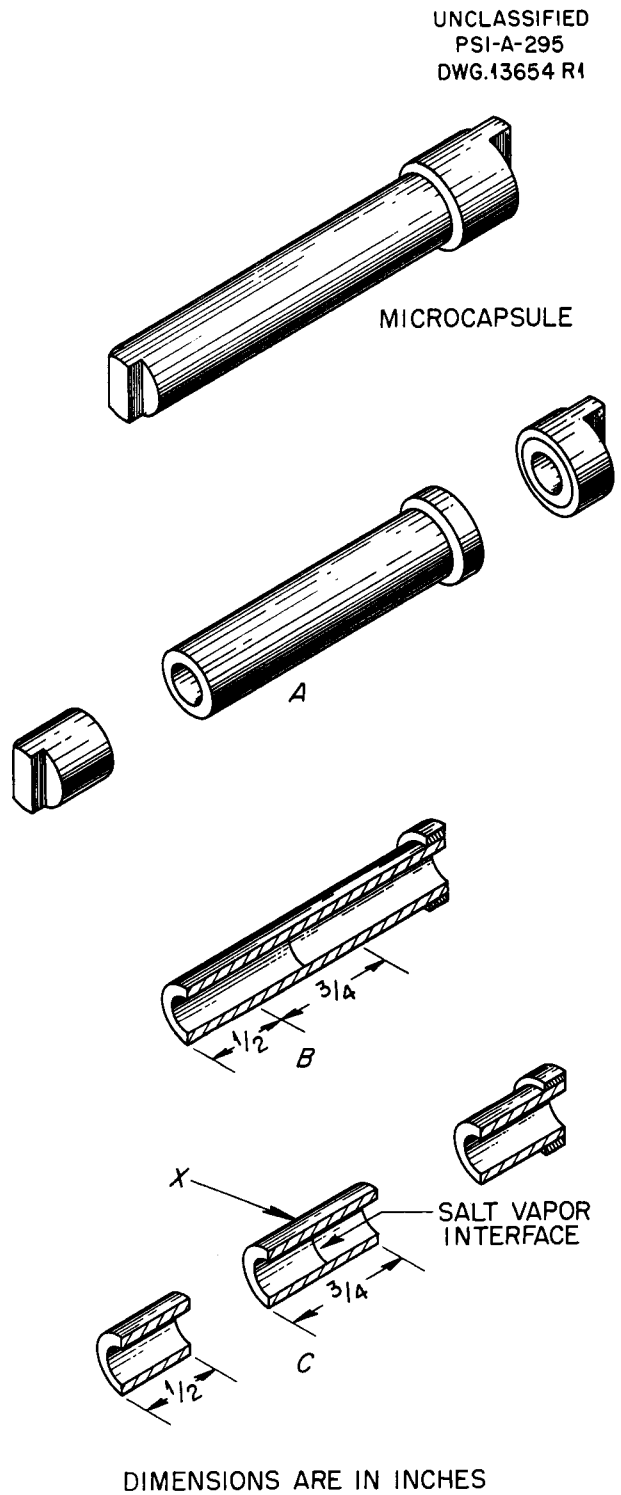

Fig. 35. Sectioning Procedure for Microcapsule.

hole C-48 (Figs. 36 and 37), for the use of this department. A beryllium block of the type used in the lattice was obtained and is being modified to provide a testing facility which is similar to hole C-44.

The northwest horizontal beam hole has also been investigated for operation of corrosion tests at high-flux levels. Owing to the hole geometry, preliminary preparation is more involved than in the case of the vertical holes. To determine heat dissipation and cooling needed in the northwest horizontal beam hole, a mockup using the same geometry as the final test was constructed (Fig. 38). A small platinum heater was placed inside the capsule to simulate fission and gamma heating. Temperature measurements were made of the outside capsule surface as well as the exit air. Exhaust was provided by positive displacement blowers in parallel. The air flow measurements were obtained by using a calibrated orifice and manometer. By use of the conduction formula for a cylindrical cross section, the exterior capsule temperature was estimated for an inside temperature of 1500°F and a given amount of fission heating. From the curves of Fig. 39, the air flow required to hold the capsule temperature at any desired steady-state value was obtained. These curves are a plot of air flow vs. wattage produced by the inside heater for various capsule surface temperatures.

In connection with the northwest side hole experiment, a secondary system is being constructed and tested to alleviate any emergency conditions that might arise during actual testing. The designs for the component test parts were completed and are being fabricated.

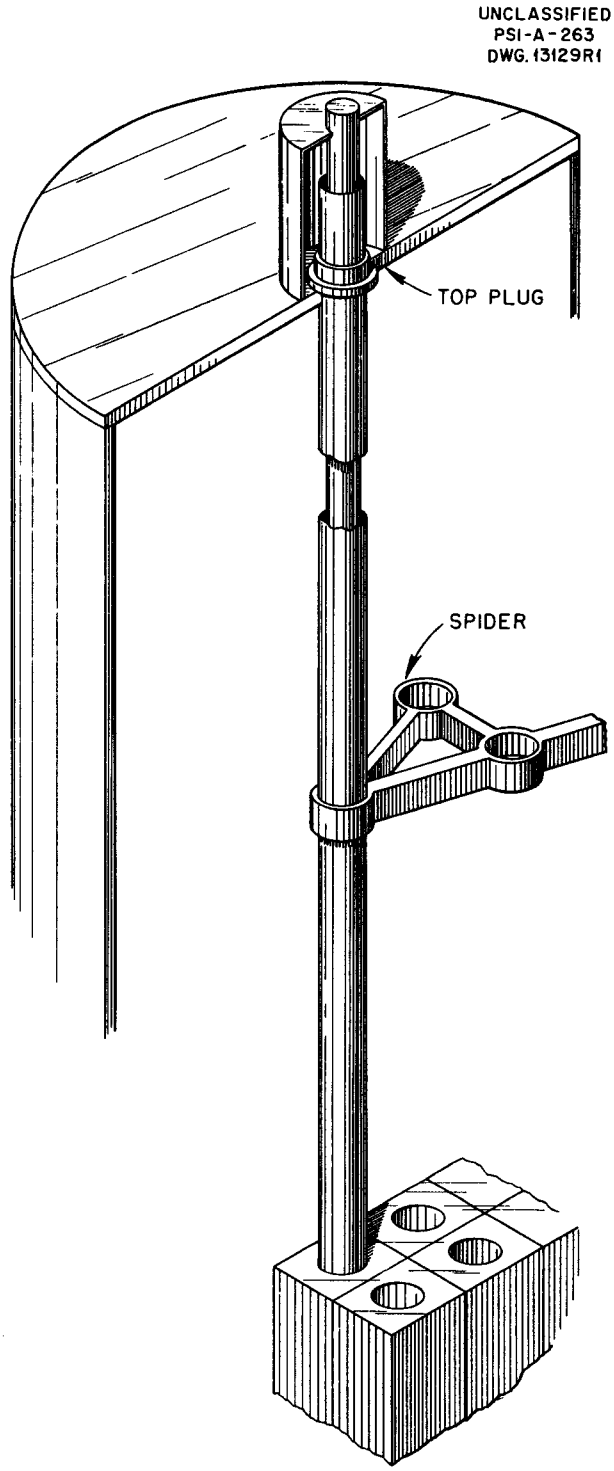

Fig. 36. LITR Vertical Tube Facility.

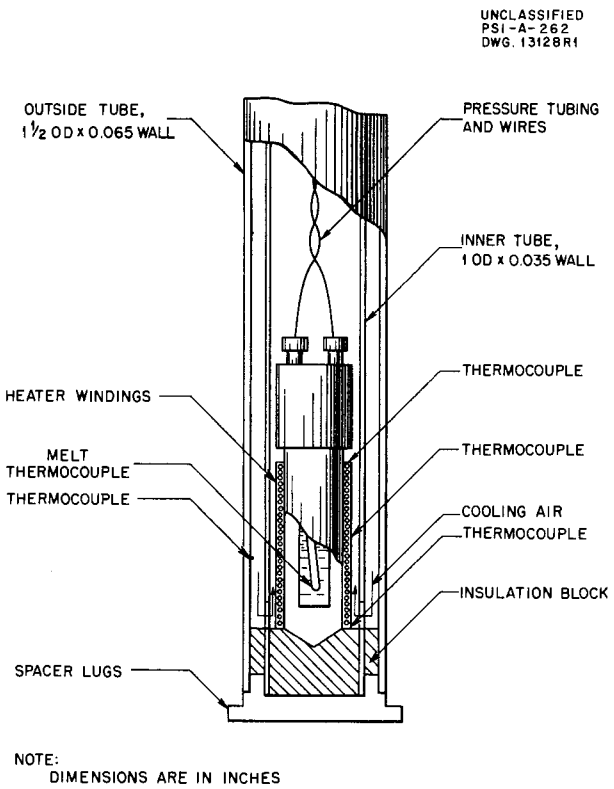

Fig. 37. LITR C-44 Test-Hole Tube and Capsule, Detail of Experiment.

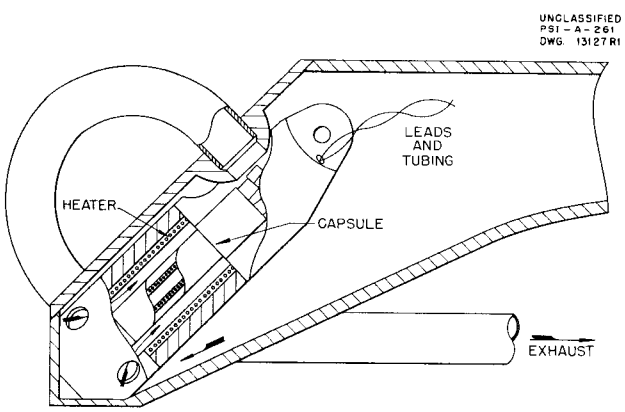

Fig. 38. Capsule Container for LITR Bench Test.

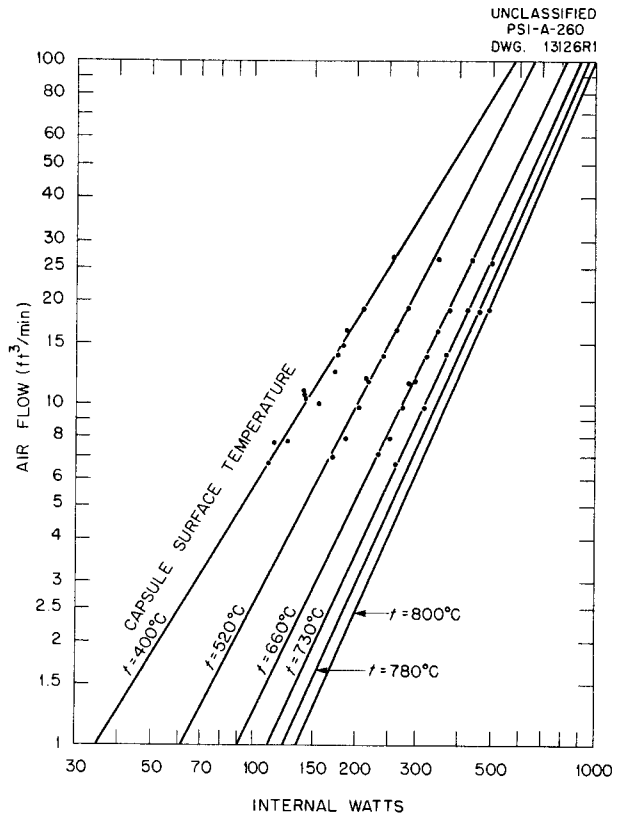

Fig. 39. LITR Bench Test.

To determine whether xenon is evolved from the melted salt under irradiation the following test was conducted. A sample of enriched uranium metal was placed in the same flux as a hole 54 microcapsule. After being irradiated for the same length of time as the melted salt, both were removed and counted. No significant difference in count was noted, which seems to indicate that the xenon formed did not escape from the melt. This test is not considered conclusive, and a new experiment is in progress in which helium gas will be circulated over the melted salt under radiation, so that fission gases will be removed as they are formed. This will prevent the possibility of the xenon or its decay products forming an equilibrium in the melt.

CRYSTAL PHYSICS

THERMAL CONDUCTIVITY OF STRUCTURAL MATERIALS

A. F. Cohen

In a preliminary thermal-conductivity experiment on inconel reported last quarter[1] a large decrease in the conductivity was observed after approximately three days irradiation in a fuel channel in the X-10 graphite pile. The inconel specimen in the experiment was maintained at about 825°C. It is necessary to check this result and in addition to investigate the effect of the fast-neutron flux on thermal conductivity as well as on temperature. With a carefully heat-treated inconel specimen, a sample that was a duplicate of that mentioned above was constructed and bench tested first at lower temperatures and then at 575°C for 75 hr. The specimen was subsequently introduced into fuel channel 1868 of the X-10 graphite pile at a position of 5% of maximum flux (estimated 3.9×10^{11} neutrons/cm^2· sec) of the hole. It was kept at 575°C for several hours at zero pile-power level. The pile power was then raised to normal operating level. No change in the thermal conductivity was observed over a 70-hr irradiation period. The sample was then pushed further into the fuel channel so that it was subjected to 30% of maximum flux, with the specimen temperature maintained constant. No change in thermal conductivity was observed during an 80-hr irradiation period. The specimen was then moved to the maximum flux position while the temperature was still maintained at 575°C. Measurements of temperature differentials that are proportional to the conductivity were obtained when pile power was zero and as a function of time when the pile was at the normal operating power level. No change in thermal conductivity was observed over a period of 670 hr at maximum flux.

The specimen was kept at the maximum flux position and the temperature decreased to 250°C, since any damage causing a change in the thermal conductivity was being annealed out at 575°C and it might show up at the lower temperature. However, no change in conductivity was observed at 250°C over a period of 135 hr. The temperature of the sample was then raised to approximately 825°C, which duplicated the first preliminary inconel experiment. Data are at present being obtained at this temperature level.

A preliminary experiment to detect relative changes in the thermal conductivity of nickel in the X-10 graphite pile has been running concurrently with that of inconel. Pure nickel (cobalt-free) was machined and vacuum annealed before being assembled. The specimen was placed in fuel channel 1964, and the temperature was maintained at 100°C for more than 350 hr. No thermal conductivity change within the fluctuation of the experimental conditions was observed. The temperature of the specimen will later be raised. The experiment was run first at the lower temperature to effect maximum damage. Also, the lower temperature was used because at higher temperatures the presence of air in the can might cause appreciable surface oxidation as a function of time.

In addition to the above experiment, an independent absolute method of measuring thermal conductivity has been designed and tested. The method employs a long cylindrical specimen

[1] A. F. Cohen, "In-Pile Thermal Conductivity of Structural Materials at High Temperatures," *Physics of Solids Institute Quarterly Progress Report for Period Ending July 31, 1951*, ORNL-1128, p. 55.

with the heater inside along its axis. Heat flow is radially outward over the specimen section of interest.

Designs for two experiments in horizontal beam hole 3 were completed and approved by the LITR Experimental Review Committee. Plugs, cooling provisions, withdrawal apparatus, etc. were completed and bench tested. The first of the two experiments using a type-316 stainless steel specimen is to be run at 100 or 200°C. The specimen will be cylindrical and heat will flow radially. Measurements of the absolute value of the thermal conductivity will be made as a function of irradiation time. The second experiment will use inconel as the material under test and may be run at 100 to 800°C. The experiment using type-316 stainless steel has been bench tested and is in the LITR at present. Experimental results will be discussed in the next report.

THERMAL CONDUCTIVITY OF HIGH-PURITY BISMUTH

A. F. Cohen L. C. Templeton

Bismuth (99.999% pure) was vacuum cast in the solid cylindrical shape standardized for thermal conductivity samples. Small holes were drilled along the length of the specimen and chromel-alumel couples are imbedded in these holes. A cylindrical heater surrounding the specimen provides the temperature level desired. In every other way, the experimental method is the same as that used for relative thermal conductivity changes on structural alloys.[2] The specimen was irradiated in doughnut hole 1768 of the X-10 graphite pile at a fast flux of 1.5×10^{12} neutrons/cm^2 · sec for a period of 390 hr at approximately 100°C throughout the irradiation period. Certainly no decrease in the thermal conductivity was evidenced. If anything, there appeared to be a slight increase in the conductivity.

[2] A. F. Cohen, "In-Pile Relative Thermal-Conductivity Measurements on Structural Materials at High Temperatures," *Physics of Solids Institute Quarterly Progress Report for Period Ending April 30, 1951*, ORNL-1095, p. 9.

Y-12 CYCLOTRON STUDIES

W. J. Sturm M. J. Feldman
R. J. Jones

A series of radiation damage experiments on proposed ANP reactor elements has occupied the full attention of this group during the last quarter. Three reactor programs were actively pursued as follows:

1. An investigation of proton radiation effects upon an inconel-encased eutectic mixture of the fluorides of uranium, sodium, and potassium, which includes the radiation effects at the eutectic-inconel interface as well as upon the inconel metal.
2. A similar examination of the effects of radiation upon potassium hydroxide in an inconel container.
3. A study of the effects of radiation upon potassium hydroxide in type-316 stainless steel.

Of the three investigations, only the first has been carried as far as possible with present techniques.

A facsimile reactor fuel element of inconel containing the fluoride eutectic was bombarded with a proton energy of 20 to 22 Mev in the 86-in. cyclotron at a specified temperature and with a known proton flux, duplicating as nearly as possible the temperature and specific energy dissipation of the proposed aircraft reactor. A metallurgical examination was made of the inconel metal and

a chemical analysis was run on the uranium-containing fuel mixture. Corrosion and grain studies comprised the major part of the metallographic analysis; quantitative determination of dissolved inconel metal components and a fluoride stability test, which was an assay of uranium to fluorine ratio, made up the chemical analysis.

The most common method of cylotron beam-current measurement involves the insertion of a microammeter between the target and ground potentials and consequently direct determination of the proton beam current. For routine low-flux bombardments this method is not satisfactory since the target is customarily connected to ground through a thermocouple circuit, and heavy secondary and thermal electron emission from the target tend to nullify the electrical effects of the proton current. Additionally, the effect of "walking electrons " (the electrons produced at the source or negative accelerating slit and conscribed by the electric and magnetic field to oscillate in the direction of the magnetic field between the source and target until they impinge or are removed by collision) further reduces the proton signal. As a consequence no current is detectable on the target microammeter for low values of the proton beam.

To compare the power as measured by water temperature methods with that measured by the more direct electrical method, a special target housing was devised. This housing (Fig. 40) consists of an outer graphite box that is at ground potential. A diagonal slot parallel to the target at front and rear of the graphite box permits passage of the proton beam to the target. Two inner graphite sheets are mounted at right angles to the axis of the target and are

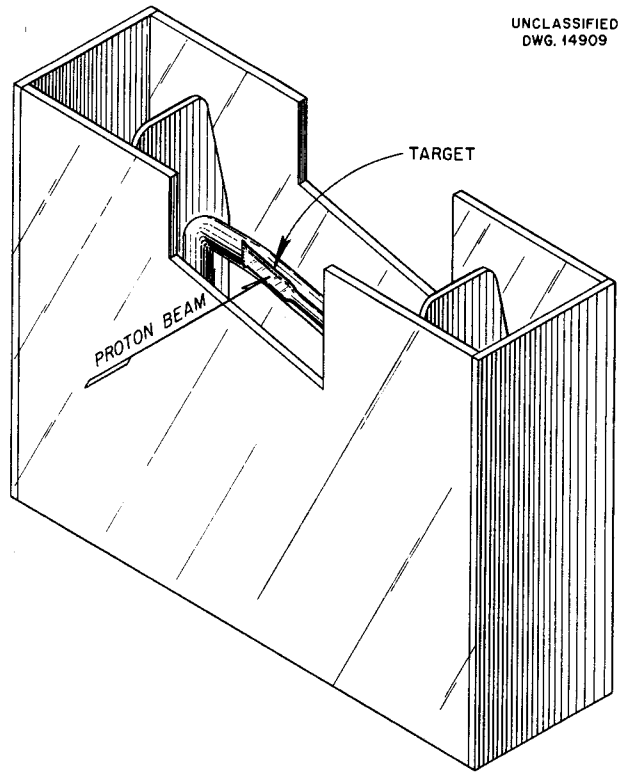

Fig. 40. Target Mounted in Special Housing.

connected electrically to the target and insulated from ground.

During proton bombardment the outer housing shields the components at target potential from the effects of the "walking electrons." The inner graphite members serve to collect the secondary and thermal electrons emitted at the target, which also follow the magnetic field direction. Thus the net electrical effect of the proton bombardment is read on the target microammeter.

A stainless steel plate mounted in this housing and on the water-cooled backing was then bombarded with 22-Mev protons. Energy input to the target was calculated from measurements of water flow rate and temperature change and compared with the energy derived from the target

microammeter readings. Agreement over a wide range of proton beam currents was always within 6% and was considered adequate for these experiments.

Thermocouple reliability is not considered established for use in measuring target temperature during bombardment in the magnetic field of about 9000 gauss with the superimposed oscillating (13.4 megacycle) 340-kv electric field. These electric and magnetic field effects, combined with secondary electron emission effects at the target, and the fact that the thermocouples themselves are continuously bombarded with 20-Mev protons all contributed to this uncertainty. Thus an experiment was designed to check the thermocouples dynamically inside the cyclotron and in the proton beam.

To check the accuracy of the couples used in these experiments, a modification of the usual methods of melting point measurements was applied. A sheet of the elemental metallic substance, the melting point of which was to be measured, is mounted inside the cyclotron in the standard target position. Separate chromel and alumel leads were prepared by melting the end of each wire to form a ball with a diameter equal to 1.5 times that of the wire. These wires were inserted individually into holes drilled into the target substance and were held in place by compressing the metal in a vise until the thermocouple wires were firmly bonded in place. The metal specimen was next mounted in place on the cyclotron target mount, and the thermocouple elements were individually weighted with lead slugs (Fig. 41). The thermocouple was then connected to the usual measuring and recording circuit. As the intensity of the proton beam striking this target was increased, the temperature of the target element was also increased by the proton energy of the beam. The melting point of the target was finally reached by raising the temperature at a rate of about 100 to 200°C per minute. As the temperature reached the melting point, the target no longer supported the weighted thermocouple elements; they became detached, broke the electrical circuit, and registered a discontinuity on the time-temperature record of the measurements. Curves of this type, were measured for lead (m.p. 327.4°C), aluminum (m.p. 659.7°C), and silver (m.p. 960.5°C), and are shown in Fig. 41. In all cases the measured melting point

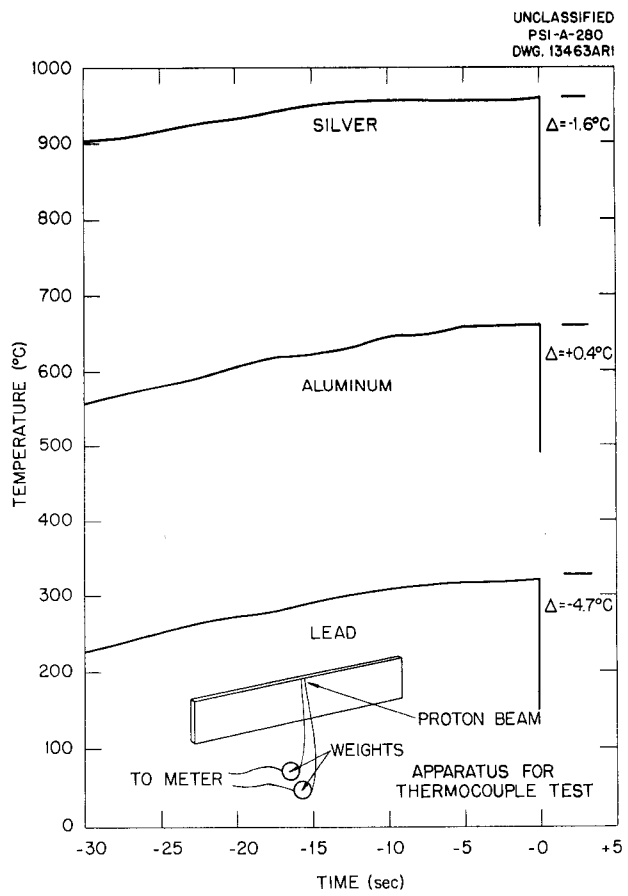

Fig. 41. Thermocouple Accuracy Determination.

was within ±5°C of the accepted value and well within the accuracy of the 30-gage wire as specified by the manufacturer – a precision considered adequate for these experiments.

By using Geiger counting of segmented targets and autoradiography of target foils, it was possible to study the nature of the cyclotron beam as a function of dee-to-dee voltage and magnetic field strength and to measure quantitatively the deflection of the beam as a function of the strength of the magnetic field. An optimum set of parameters thus established made possible an increase of about 50% in specific energy input to the target.

Twenty-four fuel pins were studied in this series – 16 were bombarded with 20-Mev protons and 8 served as control specimens (Table 11). Of the bombarded samples, 5 of the inconel cases melted owing to inadvertent local overheating in an inhomogeneous proton beam. These specimens have doubtful validity and are not considered in this analysis.

To be able to report chemical and metallurgical conclusions with some degree of assurance, it was felt that a statistical approach would eliminate a few of the many variables and would partially compensate for the broad tolerance in some of the experimental aspects. Consequently, results are taken from an analysis of the entire group of samples with no particular emphasis placed upon the unusual behavior of any individual specimen. In the wide band of specific energy inputs (30 to 415 w/cc), results expressed must thus be in terms of a weighted mean, perhaps about 300 w/cc for 1.5 hr, with indicative information on either side of this value. This corresponds to about 45 min in the ARE or about 7 min in the final aircraft reactor. Ruptured fuel pins, because of the obviously excessive temperatures involved, are not included in the evaluations reported here.

It is possible to conclude that the depth of general intergranular corrosion under the integrated proton bombardment of these experiments was not increased within ±50% of that obtained from control samples raised to the same temperature for the same length of time. The corrosion was greater at the bends in the tubing where the radius of curvature had been decreased in fabricating the target for cyclotron bombardment. Probably the minute fissures introduced in the bending process caused the depth of penetration to be greater in this region. A cursory survey of the results would seem to indicate that the depth of this penetration was increased in some cases as a result of bombardment. However, since during bombardment the temperature of parts of the specimen exceeded that of the control fuel pins by 100 to 150°C and the corrosion depends strongly on temperature, the penetration increase probably arose from thermal causes entirely.

Several of the earliest fuel-pin targets gave evidence of grain growth, a property that occurred only once in a control sample. Additionally, the grain-size increase was uniquely localized in each instance in such a manner as to indicate that its occurrence depended upon the change in radius introduced in flattening the originally circular cross section to the modified elliptical section used in the targets (R-effect).

To eliminate the possibility that the effect was a result of radiation, a series of experiments was performed. In the first experiment, samples of the inconel tubing in an as-received condition were heated for 1 hr. A total of eight individual samples

were heated at 100°C-temperature intervals covering the 500 to 1200°C range. Metallurgical examination showed that grain growth was produced under these conditions between 900 and 1000°C and at all temperatures above this value. In a second experiment, tubing samples made from the same stock were reshaped to duplicate the geometry and cold working of the cyclotron target specimens. Results in the range of 500 to 1200°C were the same as for the earlier series.

The grain growth above 900°C in these cold-worked tube sections duplicated the R-effect of the cyclotron series and eliminated the possibility that it was radiation induced. The cause of grain growth in the case of the bombarded samples was taken to be the inhomogeneous cyclotron beam used to bombard the early targets, with consequent poor temperature regulation causing local overheating and grain growth.

The quantitative uranium determinations show that all values (irradiated samples, heat-treated samples, and original batch analysis) lie within ±1% of the mean, well within the accuracy claimed for this analysis. The results were interpreted to indicate no radiation-induced effect on the relative amount of uranium in the eutectic, hence no loss of fluorine. Only one analytical value was outside the 1% range and this was determined by a different technique and is not considered necessarily consistent with other members of the group.

In the case of fluorine, the analytical values without exception lie within 1% of the mean. Consequently, no detectable fluoride decomposition was found to occur as a result of proton bombardment at the rates and durations of these experiments.

Among the trace-quantity elements, no effect on the amount of iron in the eutectic was found arising from heat treatment in the control samples nor was any change observed in the cyclotron irradiated samples.

In agreement with the results of Kertesz,[3] chromium, which seems to be selectively soluble in molten eutectic, showed no additional effect from proton irradiation. Increases from about 15 ppm in the original eutectic mixture to 1000 to 2500 ppm were observed in heat-treated control tubes as well as in the bombarded specimens. Batches of stabilized eutectic with 1000 to 4500 ppm of chromium added showed no different final concentrations, which indicates that perhaps an equilibrium chromium concentration exists in the eutectic.

Analyses indicate less nickel in the control and bombarded fuel pins than was present in the bulk eutectic that filled the tubes. This also agrees with the observations of Kertesz. Whether this condition is a result of plating out of nickel or nickel precipitation followed by incomplete sampling was not apparent from these analyses. Again the net result of the chemical analyses showed no effect that could be attributed to the proton irradiation.

A determination of the effects of radiation upon inconel and type-316 stainless steel containing potassium hydroxide, otherwise identical to the experiments discussed above, has been started. Chemical and metallurgical analyses are to be similar to those in the eutectic series, and bombardments are to be made in the same type of target capsule. Since the specific radiation energy input to the hydroxide in a hydroxide-moderated

---

[3] F. Kertesz, personal communication.

TABLE 11

History of Cyclotron-Bombarded Fuel Pins

(Target: 0.010-in. inconel-encased eutectic mixture of fluorides of uranium, sodium, and potassium)

				TARGET DATA			BOMBARDMENT DATA										METALLURGICAL DATA					CHEMICAL DATA						
PIN NO.	RUN NO.	CYCLOTRON RUN NO.	DATE	EUTECTIC THICKNESS (mils)	MOUNTING	COOLING	ΔT (°C)	WATER FLOW (gal/min)	BEAM CURRENT (μa)	INTEGRATED BEAM CURRENT (μa-hr)	DURATION (hr)	NATURE OF BEAM	TEMPERATURE AT COUPLE (°C)	PROTON ENERGY (Mev)	ENERGY DENSITY (watts/cc)	CONTROL PIN NO.	GENERAL INTERGRANULAR CORROSION (in.)	CORROSION AT BENDS (in.)	GRAIN SIZE EFFECT IN BEAM	OUTSIDE BEAM	METALLURGICAL SAMPLE NO.	U (%)	F (%)	Fe (ppm)	Cr (ppm)	Ni (ppm)	BATCH NO.	STABILIZED
BOMBARDED PINS																												
64	III A	C-46	7-13-51	100	Clamped	Radiation			~2.5	~10	4	?	650-700	20	30	63	0.001	0.002	B-Effect		3124	54.0	28.3	90	1640	120	2	Yes
66	II A	C-45	7-13-51	100	Clamped	Radiation			~2.5	~2.5	1	?	650-700	20	30	67	None observed	None observed	B-Effect	B-Effect	3114	54.08	28.28	130	1510	20	2	Yes
101	IV A	C-47	7-13-51	100	Clamped	Radiation			~2.0	~8	4	?	675-725	20	25	100	0.001	0.002	B-Effect	B-Effect	3126	53.8	28.4	70	1440	50	16	No
305	I C	C-113	8-16-51	100	3/8-in. S.S.	Water	<0.1	14.4	<18	<18	1	Probably peaked	<875	20	<220	103	≤0.001	0.001	None observed	None observed	3364	53.5	28.3	115	1900	68	16	No
306	VIII F	C-159	9-13-51	100	3/8-in. S.S.	Water	0.06	9.8	9.5	9.5	1	Flat	650-700	21.4	240	103	<0.001	<0.001	None observed	None observed	3560	51.4		934	240	<20	16	No
308	IV C	C-116	8-17-51	100	3/16-in. S.S.	Water	0.08	13.2	14	14	1	Probably peaked	650-700	20	170	103	<0.001	≤0.001	None observed	None observed	3365	53.7	28.2	86	1900	80	16	No
311	III C	C-115	8-17-51	100	On copper	Water		14			1	Probably peaked	650-700	20		103	0.001	0.001 dense	None observed	None observed	3366	53.5	28.4	115	1550	340	16	No
481	IV E	C-139	8-30-51	52	On copper	Water	0.15	3.6	9	9	1	1:30	650-700	20	220	484-485	<0.001	~0.004	None observed	None observed	3559	53.5		465	194	543	30	No
483	IV F	C-156	9-12-51	52	On copper	Water	0.18	5.4	16	16	1	1:30	750-800	21.4	415	484-485	0.001	≤0.002	None observed	None observed	3739	53.4	28.4	165	2690	165	30	No
CONTROL PINS																												
63			7-18-51	100							4		700				0.001	*	B-Effect		3127	55.0	28.6	125	1310	25	2	Yes
67			7-17-51	100							1		700				None observed	None observed	None observed	None observed	3113	53.41	28.45	110	1120	<20	2	Yes
100			7-18-51	100							4		700				*	*	None observed	None observed	3128	54.1	28.5	100	1070	20	16	No
103			11-5-51	100							1		675				≤0.001	≤0.001	None observed	None observed	3721	54.4	28.4	100	1240	<15	16	No
484			11-5-51	52							1		675				≤0.001	≤0.001	None observed	None observed	3719	54.4	28.2	130	1910	230	30	No
485			11-5-51	52							1		675				≤0.001	≤0.001	None observed	None observed	3723	54.2	28.2	110	1800	130	30	No
509			11-5-51	52							1		675				≤0.001	≤0.001	None observed	None observed	3722	54.1	28.7	150	1550	120	2	Yes
510			11-5-51	52							1		675				≤0.001	≤0.001	None observed	None observed	3724	53.9	28.6	100	1460	<15	2	Yes
RUPTURED PINS																												
65	I A	C-44	7-12-51	100	Clamped	Radiation			?	?	>1	?	<875	20	?	67	Center		*	*	3125	57.5	27.5	150	2200	55	2	Yes
307	II D	C-123	8-23-51	100	3/16-in. S.S.	Water					Cracked in few min	Probably peaked		20		103	≤0.001	≤0.001	None observed	None observed	3720	54.2	28.4	180	1800	80	16	No
309	I B	C-90	8-9-51	100	3/8-in. S.S.	Water	0.24	8.4	~25	~25	1	Peaked	700-750	20	300	103	<0.001	≤0.001	*	*	3502	54.3	28.6	80	1280	40	16	No
310	II B	C-91	8-9-51	100	3/8-in. S.S.	Water	0.18	8.4	20	20	1	Peaked	600-650	20	240	103	<0.001	<0.001	*	*	3501	53.9	28.6	85	1360	20	16	No
507	V F	C-157	9-13-51	52	On copper	Water	0.05	10.7	9	36	4	1:30	750-800	21.4	230	63	<0.001	~0.003	None observed	None observed	3561	54.4		314	57	207	2	Yes
508	VI F	C-158	9-13-51	52	On copper	Water	0.05	8.1	6.5	6.5	1	Flat	650-700	21.4	170	509-510	<0.001	~0.003	*	None observed	3558	50.8		209	167	<20	2	Yes
BATCH ANALYSIS																												
																								115	15	2070	16	No
																						53.5	28.5	100	<15	1280	27	No
																						54.4	28.3	210	<15	2180	30	No
																								630	1030	30	2	Yes

* Observed but not quantitatively determined.

system is well below that in the fuel substance, it is expected that radiation cooling of the target will be adequate to duplicate reactor radiation densities. Work on the KOH-inconel system is severely limited by the corrosive nature of the hydroxide. It has not been possible to prepare inconel tubes that successfully contain molten potassium hydroxide without excessive corrosion at the crimped portions of the tubing.

A group of targets of KOH-stainless steel have been prepared and bombarded at 635°C for several hours. These samples, together with their controls, await analysis.

X-RAY WORK

G. E. Klein F. A. Sherrill

Additions to the x-ray laboratory during the past quarter include a 3-ft-dia circular-top x-ray table to which a Philips x-ray head and a copper-target diffraction tube have been fitted. The new table is supplied with power from the Hilger unit and may be operated in place of the Hilger tube. The Philips spectrometer, Laue camera, and powder cameras have been adjusted to the Philips tube and can be used whenever constancy of operation is required.

Designs for two back-reflection Laue cameras have been submitted to the shop for construction. The nature of the specimens handled in the laboratory and the volume of work being performed necessitate the new design of the cameras.

The General Electric spectrometer to be used inside the hot cell has been received and bench tests are being conducted prior to installation. Slight modifications in design are indicated by the results of the bench tests.

The work of the x-ray laboratory consists of 80% routine testing and 20% research for other members of the Physics of Solids Institute group. The chemical identification of the components in copper phthalocyanine before and after irradiation, x-ray studies of lithium fluoride and quartz crystals before and after irradiation, and studies of copper single crystals before and after irradiation have been made. These studies are concerned with a change in the mosaic character of the materials, atomic displacement, effects of annealing to remove irradiation effects, and the depth of penetration of irradiation effects.

A study of irradiated copper single-crystal test specimens before and after being subjected to stress is under way. The results will indicate the amount of stress that will produce cold-work effects. Further tests of single-crystal x-ray techniques will show whether any lattice parameter changes take place in irradiated copper specimens.